Modelling of Radio Wave Propagation Using Finite Element Analysis

Kamran Arshad

Thesis submitted to Middlesex University

in partial fulfilment of the requirements

for the degree of

Doctor of Philosophy

School of Computing Science

Middlesex University

London, U.K.

July 2007

Dedication

My late mother who gave it all for us but did not get much in return

To my father who is willing to sacrifice anything for my academic success

AND

To my wife who provided her unconditional support to this cause

ABSTRACT

Fourth generation (4G) wireless communication systems are intended to support high data rates which requires careful and accurate modelling of the radio environment. In this thesis, for the first time finite element based accurate and computationally efficient models of wave propagation in different outdoor and indoor environments has been developed. Three different environments were considered: the troposphere, vegetation and tunnels and wave propagation in these environments were modelled using finite element analysis. Use of finite elements in wave propagation modelling is a novel idea although many propagation models and approaches were used in past.

Coverage diagrams, path loss contours and power levels were calculated using developed models in the troposphere, vegetation and tunnels. Results obtained were compared with commercially available software Advanced Refractive Effects Prediction Software (AREPS) to validate the accuracy of the developed approach and it is shown that results were accurate with an accuracy of 3dB. The developed models were very flexible in handling complex geometries and similar analysis can be easily extended to other environments. A fully vectored finite element base propagation model was developed for straight and curved tunnels. An optimum range of values of different electrical parameters for tunnels of different shapes has been derived.

The thesis delivered a novel approach to modelling radio channels that provided a

fast and accurate solution of radio wave propagation in realistic environments. The results of this thesis will have a great impact in modelling and characterisation of future wireless communication systems.

ACKNOWLEDGEMENTS

All praise and glory goes to Almighty Allah who gave me the courage and patience to carry out this work.

First and foremost gratitude is due to the esteemed university, **Middlesex University** for the award of a research studentship without which it would not have been possible for me to undertake this period of postgraduate study.

My deep appreciation and heartfelt gratitude goes to my Director of Studies Dr Ferdinand Katsriku and Advisor Dr Aboubaker Lasebae for their constant endeavour, guidance and the numerous moments of attention they devoted throughout the course of this research work. Dr Ferdinand Katsriku was always ready to help me and his valuable suggestions made this work interesting and knowledgeable for me. I would particularly like to acknowledge Dr Aboubaker Lasebae in motivating me to apply for a research degree at Middlesex and for his extended academic and non-academic cooperation throughout my stay at London. Working in a friendly and motivating environment was really a joyful and learning experience. Special thanks goes to Ms Gill Whitney and Dr Michael Foster to read my thesis and mark English

language corrections.

I extend my deepest gratitude to all faculty members of School of Computing Science. I would like to acknowledge Dr Orhan Gemikonakli, Dr Glenford Mapp, Dr Robert Ettinger, Prof Richard Comley, Miss Gill Whitney, Dr Muthana Jabbar, Dr Shahedur Rahman, Dr Nawaz Khan, Dr Elke Duncker and many other professors at Middlesex University for their extended support when it mattered most. I am truly thankful to them. I would also like to thank research staff and my fellow colleagues at Middlesex including Claudia Kalay, Frida Attrams, Pia Wallington, Deborah Martin, Esther Cousens, Angie Baird, Winsome Townsend, Joyce, Leigh Kelly, Catherine Riley, Olivia Copper, John Soper, Dominique Jennah-Landi, Eve Sevume, Sue Shaw, Sue Wellstead, Noreen Ahmad, Kathryn Mcanulty, Jackie Dennison, Victoria, Adele Kelly, Louise Sexton, Manuela Rossini, Millie Chen, Sarah Greaves, Maggie Walkowska, Suzie, Sally Barker, Nikki Barker and many more all of them I can not list here.

Family support plays a vital role in the success of an individual. I would like to thank from the core of my heart to my father Arshad Ullah Khan, my brothers Dr Nauman Arshad, Imran Arshad and Zeeshan Arshad and my loving and wonderful wife Mrs Saima Kamran whose support and patience make this task possible. My deepest appreciation and thanks are given to my father-in-law Jalal Uddin Pasha and my mother in-law Razia Jalal for their patience and understanding, without their support it was impossible for me to take this opportunity and pursue my PhD

studies. I also especially like to thank my elder brother Dr Nauman Arshad who always provided all kind of support and tried to make my stay at UK enjoyable. I would like to acknowledge my sister in law Sarah Nauman, Asma and her husband Shiraz for providing me joyful company during my stay at London.

Sincere friendship is the spice of life. Special thanks goes to my fellow PhD colleagues Abu Syeed Shah, Dhawal Thakker, Amala Rajan, Saurabh Bansal, Fatema Sheikh, Michael Foster, Enver Ever, Agozie, Dilli, Yoney Kirsal and many others. They made my work and stay at Middlesex University very pleasant and joyful. My heartfelt thanks to my days old friends Hasib Siddiqui, Abdullah Bin Jarrar, Farhad Jamil, Moin Uddin, Saad Azhar, Amir Siddiqui, Mehmood Minhas, Shahzada Basharat and Waqas Ali. They truly are my great friends, I wish we could be together again. Finally I would like to thank anyone who has helped me directly or indirectly to complete this project.

Contents

Abstract ii

Acknowledgements iv

List of Tables xii

List of Figures xvii

Glossary xviii

1 Introduction 1

1.1 Current Trends in Wireless Communication 1

1.2 Motivation 3

1.3 Research Statement 6

1.4 Structure of the thesis 7

2 Parabolic Equation Method 10

2.1 Introduction 10

2.2 The Parabolic Wave Equation (PWE) 15

2.2.1 Parabolic Equation Propagation Model (PEPM) 16

2.2.2 Parabolic equation method algorithms 21

2.3 Review of Numerical Approximation Techniques 27

2.3.1 Method of Moments 29

2.3.2 Finite Difference Time Domain Method 30

2.3.3 Transmission Line Matrix Method 31

2.3.4 Generalised Multipole Technique 32

2.3.5 Conjugate Gradient Method 32

2.4 Wave Propagation in the Troposphere 33

2.5 Wave Propagation in the presence of Vegetation 35

2.6 Wave Propagation in Tunnels 38

2.7 Summary 43

3 Finite Element Analysis (FEA) 44

3.1 Introduction 44

3.2 Numerical Methods 46

3.3 Basic concepts in finite element analysis 47

3.3.1 Domain Discretisation 48

3.3.2 Interpolation Functions 52

3.3.3 Formulation of the System of Equations 53

3.3.4 Solution of the system of equations 54

3.4 One Dimensional Finite Element Analysis 54

3.4.1 Discretisation and Interpolation 55

3.4.2 Formulation via Galerkin's Method 57

3.4.3 Assembly of Element Matrices 59

3.4.4 Incorporation of Boundary Conditions 62

3.4.5 Solution to the system of equations 64

3.5 Two Dimensional Finite Element Analysis 65

3.5.1 Discretisation and Interpolation 66

3.5.2 Linear Triangular Elements 67

3.5.3 Formulation via Galerkin Method (weak form) 69

3.5.4 Assembly of Element Matrices 71

3.5.5 Incorporation of Boundary Conditions 73

3.5.6 Solution to the system of equations 74

3.6 Finite element programming in Matlab (An Overview) 75

3.6.1 Section of a Typical Finite Element Programs 75

3.7 Summary 78

4 Radio Wave Propagation Modelling using Finite Element Method in the Troposphere **79**

4.1 Introduction 79

4.2 Refractivity and Tropospheric Ducting 81

4.3 Mathematical modelling of wave propagation in the troposphere . . . 83

4.3.1 Earth Flattening Transformation 84

4.3.2 Path Loss and Propagation Factor 85

4.3.3 Boundary Conditions 85

4.3.4 Initial Field 89

4.4 Finite Element Formulation of the Problem 90

4.4.1 Narrow Angle FEM formulation 90

4.4.2 Wide Angle FEM Formulation 94

4.5 Results and Discussions 95

4.5.1 Irregular Terrain and Urban Environment Modelling 110

4.5.2 Results of Wave Propagation in Three dimensional environments 117

4.6 Summary 120

5 Finite Element Formulation of Radio Wave Propagation Modelling in Vegetation Canopies 122

5.1 Introduction 122

5.2 WPEM technique for vegetation 125

5.3 Results and Discussion 128

5.4 Summary 132

6 Wave Propagation Modelling inside Tunnels 134

6.1 Introduction 134

6.2 Parabolic Equation Modelling for Curved Tunnel 138

6.3 Finite Element Formulation of Vectorial Parabolic Equation Model . 143

6.4 Results and Discussions 146

6.4.1 Simulation Parameters 146

6.4.2 Geometry of Tunnel 148

6.4.3 Electrical Parameters and Wall Properties 160

6.4.4 Transmitter Antenna Position 163

6.4.5 Effect of Curvature 164

6.4.6 Effect of Vehicles 165

6.5 Summary 170

7 Conclusion and Further Work **172**

7.1 Conclusions 172

7.2 Further Work 176

Appendix 1: Method of Weighted Residual **178**

Appendix 2: Linear Quadratic Elements **186**

Appendix 3: List of Publications **189**

References **192**

List of Tables

3.1 Connectivity matrix for mesh given in figure 3.6 72

4.1 Reference atmosphere as defined by ITU [1] 83

4.2 Simulation Parameters used to model radio wave propagation in the troposphere 97

6.1 Different Vehicles dimensions used in simulations 148

List of Figures

2.1 Finite Difference Grid for Crank-Nicolson Scheme 26

3.1 Example of an arbitrary shaped tunnel with regions of different material properties 49

3.2 Typical finite element geometries 50

3.3 Linear element with local node numbers 56

3.4 Example of the element assembly process 61

3.5 Linear Triangular Element 68

3.6 Example of sub-division of a two dimensional domain 72

4.1 2D Illustration of Domain 87

4.2 Standard Atmospheric Profile 98

4.3 Direction Convention used in Simulations 98

4.4 Coverage diagram without and with PML at 100MHz 100

4.5 Coverage diagram with of antenna with transmission at 500MHz and 1GHz 102

4.6 Path Loss diagram with transmission at 100MHz and 500MHz 104

4.7 Path Loss vs Range at Receiver Height (100, 500, 1000)MHz 105

4.8 Path Loss Vs Height at 50Km Range at different frequencies 107

4.9 Behaviour of Narrow-angle and Wide-angle PEM at large angles . . . 108

4.10 Coverage Diagrams at low duct intensity profiles at 1GHz 109

4.11 Coverage Diagrams at low duct intensity profiles at 3GHz 110

4.12 Path Loss at receiver height in ducting environment at different frequencies 111

4.13 Staircase representation of terrain 113

4.14 Coverage Diagrams at 100MHz on an irregular terrain 114

4.15 Coverage Diagrams at 100MHz on an irregular terrain 115

4.16 Path Loss in an urban street at 100MHz 115

4.17 Received Power in an urban street at 100MHz 116

4.18 Coverage diagram of antenna with transmission at 30km propagation distance with no duct (all dimensions are in meter) 117

4.19 Coverage diagram of antenna with transmission at 70km propagation distance with no duct (all dimensions are in meter) 118

4.20 Coverage diagram of antenna with transmission at 30km propagation distance with medium intensity duct (all dimensions are in meter) . . 119

4.21 Coverage diagram of antenna with transmission at 30km propagation distance with strong intensity duct 120

5.1 Example of using PE technique in vegetation 127

5.2 Comparison of Propagation Loss calculated by FEM with Tamir Results at 100MHZ 129

5.3 Comparison of Propagation Loss calculated by FEM with Tamir Results at 100MHZ 129

5.4 Comparison of Propagation Loss calculated by FEM with Tamir Results at 100MHZ 130

5.5 Plot of Path Loss variations with Receiver Height at 1000m range . . 131

5.6 Plot of Path Loss variations with Receiver Height at 1000m range . . 132

5.7 Plot of Path Loss variations with Receiver Height at 1000m range . . 133

6.1 Cross section of a curved Tunnel with radius of curvature ρ 140

6.2 Mesh of cross section of tunnel (all dimensions are in meters) 147

6.3 Signal Intensity at the end of rectangular tunnel at 100MHz (all dimensions are in meters) 150

6.4 Signal Intensity at the end of rectangular tunnel at 700MHz (all dimensions are in meters) 151

6.5 Signal Intensity at the end of rectangular tunnel at 3GHz (all dimensions are in meters) 152

6.6 Signal Intensity at the end of arch tunnel at 100MHz (all dimensions are in meters) 153

6.7 Signal Intensity at the end of arch tunnel at 700MHz (all dimensions are in meters) 154

6.8 Signal Intensity at the end of arch tunnel at 3GHz (all dimensions are in meters) 155

6.9 Average Signal Power across straight rectangular tunnel cross section versus tunnel length 157

6.10 Average Signal Power across curved rectangular tunnel cross section versus tunnel length 158

6.11 Average Signal Power across straight arch tunnel cross section versus tunnel length 159

6.12 Average Signal Power across curved arch tunnel cross section versus tunnel length 159

6.13 Average Signal Power at 900MHz for different ϵ_r in rectangular tunnel 160

6.14 Average Signal Power at 900MHz for different σ in rectangular tunnel 161

6.15 Average Signal Power at the end of arch tunnel at 900MHz versus ϵ_r . 162

6.16 Average Signal Power at the end of arch tunnel at 900MHz versus σ . 162

6.17 Plot of power distance dependence on transmit antenna positions . . 163

6.18 Average Power Distribution in an arch tunnel at 900MHz for different curvature radius 164

6.19 Received power level vs. tunnel length in Straight tunnel 166

6.20 Received power level vs. tunnel length in Curved tunnel 166

6.21 Received power level vs. tunnel length in Straight tunnel 167

6.22 Received power level vs. tunnel length in Curved tunnel 168

6.23 Received power level vs. tunnel length in Straight tunnel 169

6.24 Received power level vs. tunnel length in Curved tunnel 170

A1-1 Residual over domain of interest 182

A2-1 Quadratic element with local node numbers 187

Glossary

Abbreviations

4G	Fourth Generation
2D/3D	Two or Three Dimensional
HF	High Frequency
VHF	Very High Frequency
UHF	Ultra High Frequency
ITU	International Telecommunication Union
BW	Bandwidth of Transmitted Signal
FFT	Fast Fourier Transform
IFFT	Inverse Fast Fourier Transform
OFDM	Orthogonal Frequency Division Multiplexing
CDMA	Code Division Multiple Access
PEM	Parabolic Equation Method
PPEM	Parabolic Equation Propagation Model
PWE	Parabolic Wave Equation

SPE	Standard Parabolic Equation
SSPE	Split-step formulation of SPE
FEM	Finite Element Method
BEM	Boundary Element Method
FEA	Finite Element Analysis
GSM	Groupe Spećial Mobile
CIR	Channel Impulse Response
HPOL	Horizontal Polarization
VPOL	Vertical Polarization
FDTD	Finite Difference Time Domain Method
FDFD	Finite Difference Frequency Domain Method
TLM	Transmission Line Matrix Method
GMT	Generalized Multipole Technique
RET	Energy Transfer Theory
PML	Perfectly Matched Layer
GO	Geometric Optics
AREPS	Advanced Refractive Effects Prediction System

Greek Symbols

λ	Wave Length
α	Attenuation constant

k	Wave number
ϵ	Permittivity
σ	Conductivity
Ω	Discretization domain
ω	Frequency in radians per second
e	Element domain
Δx	Step size in propagation direction
Γ	Boundary enclosing domain Ω

Chapter 1

Introduction

1.1 Current Trends in Wireless Communication

In the last decade there has been a rapid growth in mobile and wireless communications. Chandarn [2] reports that a new wireless subscriber signs up every 2.5 seconds. The combination of the flexibility of radio communications with the quality of digital transmission has contributed to the success of these systems. There is no doubt that future wireless systems must support significantly higher data rates than the current systems, for example, Orthogonal Frequency Division Multiplexing (OFDM) systems [3, 4].

A typical mobile radio environment in an urban area has no direct line-of-sight path between the transmitter and the receiver. The environment is so dynamic and the path between the transmitter and the receiver can vary drastically from simple

line-of-sight to one that is severely obstructed by buildings, mountains and trees. Hence, the mobile radio environment places fundamental limitations on the performance of wireless communication systems. So the development and deployment of future mobile communication systems require careful modelling of propagation environments [5].

The phenomena that influence radio wave propagation can generally be described by four basic mechanisms: Reflection, penetration, diffraction, and scattering. For the practical prediction of propagation in a real environment these mechanisms must be described by approximations. This requires a three-stage modelling process: In the first step the real (analogue) terrain has to be digitised yielding digital terrain data. The second modelling step includes the definition of mathematical approximations for the physical propagation mechanisms. Based on the solutions for the basic problems both deterministic and empirical approaches need to be developed for the various environments, which is the third modelling step.

Today's communication systems as well as radars are mostly used within multi-area, multi-sensor, maritime and/or air-based integrated complex systems. The research towards development and performance evaluation of such systems require powerful computer simulation tools. Simulations require ground wave propagation through the atmosphere over a 3D regional digitised terrain map. A site engineer needs to have access in real time to the propagation characteristics between any two selected points, e.g. a transmitter and receiver, which includes terrain profile, vegetation

and atmospheric effects. Although all physical propagation problems are in three dimensions, two dimensional approximations can be used if symmetry in one of the three dimensions exists. It is well accepted to solve atmospheric propagation problems in 2D for a broad frequency range because of the azimuthal symmetry of the earth [6].

1.2 Motivation

The number of mobile telephone users is increasing dramatically as the world sees countries with large populations experience rapid economic growth like China and United Kingdom [7]. This has created a need for increasing the system capacity. These factors have initiated worldwide research for the most efficient and cost effective methods. The development of a mobile telephony system is very complex, and can be broken down into a number of areas. One area of great interest is the behaviour of radio waves during propagation in the radio channel; that is from the transmitting antenna to the receiving antenna. One of the major tasks for a radio communication engineer when designing a communication system is to be able to predict the behaviour of a radio signal from the point of transmission to the receiving point. It is here that the majority of signal degradation occurs and to develop effective transmission methods it is necessary to have an intimate knowledge of what actually happens in the channel. Research into radio channel effects

has generally taken the form of developing a model, obtaining experimental results and then adjusting the model. The use of computer simulation has greatly aided this process, and will continue to do so. Simulation also allows ease of comparison between various models.

To implement a mobile radio system, wave propagation models are necessary to determine propagation characteristics for any arbitrary installation. The predictions are required for a proper coverage planning, the determination of multipath effects as well as interference and cell calculations, which are the basis for the high-level network planning process. In a GSM (Groupe Spećial Mobile) or DCS (Digital Cellular System) system, the high-level network planning process includes for example the frequency assignment and the determination of the base station subsystem parameter set. Similar planning tasks will also exist in third generation systems. The environment where these systems are intended to be installed, are stretching from in-house areas up to large rural areas. Hence wave propagation prediction methods are required to cover the whole range of macro-, micro- and pico-cells including outdoor scenarios and situations in special environments like tunnels.

Other than mobile telephony, radio propagation is at the heart of any wireless communication system. Radio environment obstacles interact with electromagnetic waves in different ways leading to phenomena such as reflection, diffraction and scattering [8]. This results in multipath fading, delay, angular spreads and polarisation cross coupling. A knowledge of propagation mechanisms is required for radio

network planning to ensure the most cost effective deployment of wireless systems. In order to determine the coverage area, to estimate the interference between radio stations in the network and to reach the optimal level for the base station configuration while meeting the expected service level requirements, accurate propagation prediction is needed.

Radio propagation in tunnels has gained increasing interest from cellular network operators. Every new city highway includes some tunnel sections, for example in Austria, 10% of high-priority roads are in tunnels [9]. Because tunnels are confined it is difficult to model the propagation of signals accurately, so there are some simplifications introduced in theoretical studies. The common cell planning concepts are not applicable in tunnels and increasing numbers of researchers in the UK and Europe are turning their attention to this problem [10].

In order to understand the propagation of radio waves in any indoor environment such as a building or a tunnel, it is useful to examine the field distribution throughout the tunnel. To solve for the field distribution a number of factors must be taken into account such as shape and transverse dimension, frequency, direction of polarisation and electrical parameters such as permittivity and conductivity of the surrounding material. Recently, propagation research has begun to concentrate on the characterisation of radio channels in indoor environments such as offices, rooms and tunnels [11].

1.3 Research Statement

Given an operating frequency f, the transmitting antenna height H_0, the 3-dB beam width and the environment profile, the field at a certain range from the transmitting antenna is calculated. The finite element formulation of parabolic equation method (PEM) is used to determine the field in different environments. Although there are several computational techniques for predicting the field at a desired range from the transmitting antenna, including the ray tracing approach and the integral equation method, few offer the computational advantages of the parabolic equation method which can approximate the elliptic operator governing the true wave behaviour by a much simpler parabolic operator that permits marching in range. The PE method has the advantage that all important aspects of propagation such as reflection, refraction and diffraction are included automatically in the formulation. However, the penalty for employing the PE method is that it neglects back scattering[12]. This assumption will not contribute any significant errors for the class of applications considered in this thesis since radiowaves predominantly propagate in the forward direction.

In this research, the finite element method is applied to model radio wave propagation in the troposphere, vegetation and tunnels. The main advantage of using the finite element method for solving propagation problems is that it is more accurate; it gives the distribution of the field in the whole domain in contrast to Finite

Difference Time Domain Method (FDTD) which gives the distribution of fields at nodes. Moreover by using finite elements, any fast varying environment can be easily modelled simply by assigning different parameters to different mesh elements. FEM has previously been shown to be a most accurate and versatile method and well suited to study propagation in optical mediums [13]. This approach is expected to produce results that will enhance the design of future mobile communication systems. Even though there are many propagation models and approaches to solve propagation problems, the use of FEM in outdoor and indoor propagation is a novel idea. A vector field finite element based beam propagation method will be developed for the numerical modelling of electromagnetic waves in wireless systems. The model developed will be tested and implemented in different environmental conditions: wave propagation in the troposphere, in the presence of vegetation and indoor environments like tunnels.

1.4 Structure of the thesis

This thesis is concerned with the application of the finite element method (FEM) to radio wave propagation in different outdoor and indoor environments. The discussion which follows gives an outline of the structure of this thesis beginning with an introduction which is presented in this chapter. This provides an analysis of the basic research idea and a brief review of the research domain.

An extensive review of previously published literature is given in chapter 2. Several methods for propagation analysis are considered including semi-analytical and numerical methods. Some commonly used numerical schemes will be briefly describe in chapter 2. The basics of the parabolic equation model is also presented together with different formulations and solution techniques.

The formulation of the finite element method as a powerful method in the solution of complex problems is presented in chapter 3. This chapter reviews the history and present state of the finite element method as applied to electromagnetic field problems in the radio frequency range. A detailed study of the finite element method along with the use of both linear and second order elements and shape functions is undertaken with a view of developing an algorithm for the propagation analysis of the environments considered in this thesis. Chapter 3 briefly explores the capabilities, limitations and critical comparison of the finite element method with other numerical schemes.

Models of radio wave propagation in the troposphere are indispensable in the design and analysis of wireless communication systems. They are used to predict power and interference levels and analyse other properties of radio links. Chapter 4 covers various aspects of wave propagation in the troposphere. The parabolic equation method is used to model propagation in the troposphere and a finite element based model is presented. Simulation results with discussions are presented in chapter 4.

Chapter 5 is devoted to propagation modelling of electromagnetic waves at VHF

inside a forest by using the finite element method. A finite element formulation of the method is described which can be used with the irregular terrain, multi-layer forest model and range dependant propagation in a forest. Results are compared with the well known Tamir's results [14]. It is shown that the finite element method gives an accurate and computationally efficient solution.

In chapter 6 the application of the finite element method to the analysis of wave propagation in tunnels is described. This chapter discusses propagation in tunnels, describing expected radio frequency strength in various types of tunnels, antenna height and building materials. Radio propagation in a confined environment is much more complicated than propagation in free space. A number of factors affects radio propagation in tunnels. Chapter 6 focuses on mathematical modelling of propagation in tunnels at different radio frequencies using finite element analysis.

Finally chapter 7 concludes the thesis with some suggested future work.

Chapter 2

Parabolic Equation Method

2.1 Introduction

During the past several decades, researchers in the area of applied electromagnetics have been searching for rigorous and efficient models for mathematically describing the problem of electromagnetic propagation in different environments. In order to assess the radio propagation effects for the various indoor and outdoor environments many measurement and experimental studies have been carried out in the past [15]. Channel key parameters needed for wireless system design and the corresponding parameter settings are then derived from the measurements. However, for advanced communication systems it is in general not possible to design a system and judge its performance with the knowledge of the channel key parameters only. A more accurate validation of the performance by means of Monte Carlo simulations is

normally needed [16].

Currently, there are several large-scale propagation path loss models being utilised in commercial cellular communication systems in Europe, America, Asia, and around the world. Some of the popular models include the Okumura model, the Hata model, and the COST-231-Walfish-Ikegami model [17]. These models were developed by measurements and statistical analysis made specifically for frequency coverage between 150MHz and 2GHz, and are typically based on certain environments such as London or New York city. These models provide a reasonable approximation for current cellular communication applications. However, they are complicated and expensive to develop and do not offer the accuracy, computational advantages, and efficiency of models such as the parabolic equation method (PEM), ray methods, etc.

Gladstone and McGeehan [18] described a statistical model of an outdoor mobile channel that is defined using the placement of buildings within the environment. The principles of reflection are used to determine the paths of propagation from the transmitter to the receiver. The path lengths are calculated and that information is used to calculate delays and path strengths. It has been found that the resulting probability distributions model the measured distributions more closely than more basic statistical models such as the Raleigh fading model. It is possible to use a more complete description of the environment over which the propagation is occurring to determine the channel response. Increasing the complexity of the model will have

the effect of increasing the modelling time, and ultimately modelling the channel becomes infeasible as more detail is incorporated into the model.

McKown *et al*, [19] introduced a ray tracing model for an indoor environment that calculates the signal power and delay spread over a specified area of a floor plan for 1.8GHz and 18GHz carrier frequencies. Honcharenko *et al.* [20] took a similar approach using a three dimensional model that incorporates scattering to determine the average signal power over an office floor. Their results are compared to measurements conducted at 900MHz and found to model the distance-power relationship well. However these approaches shares the disadvantages of ray tracing techniques as describe in section 2.4.

For an outdoor mobile channel, Lebherz *et al*, [21] have used a combination of a two dimensional model incorporating the effects of diffraction in the vertical transmitter to receiver plane, and a three dimensional reflection and scattering model that is constructed from an accurate description of the environment. As expected, with a more completely defined model, the resulting simulated channel is closer to the measured channel when compared with simpler models.

Several solutions have been proposed to simulate the radio channel i.e., the Channel Impulse Response (CIR), stored CIR's [22], ray-tracing techniques [23], and stochastic parametric models for the CIR [24]. Stored CIR's incorporate all details of the radio channel. However, this method requires a large storage capacity for the measured reference CIR's and it is also very difficult to find a small set of CIR's that

include all propagation effects and situations encountered in a certain environment. Ray-tracing is a very powerful tool to perform a coverage prediction in a particular environment and to compute the CIR at some specific point in this environment. The main drawbacks of ray-tracing techniques are the need for a precise description of the location which sometimes makes it difficult to translate the results to other situations and the relatively high computational complexity [19].

Numerical methods applied to 3D propagation problems are generally categorised as Integral or Differential equation methods. Integral equation methods result in extremely large, full matrices that need to be inverted to find unknown fields. In addition a rigorous treatment of the inhomogeneous troposphere via an integral equation method is extremely difficult [25]. Alternatively the differential equation method accounts for atmospheric inhomogeneity in a straight forward fashion and results in a sparse matrix system that can be inverted easily using any computer programming language like Matlab.

These methods have now largely been superseded by Parabolic Equation (PE) algorithms, which provide a fast and efficient numerical solution to most propagation problems. The problem of propagation of electromagnetic waves along the surface of the earth based on parabolic equations was originally considered theoretically by Leontovich and Fock [12]. This method was then adapted by various authors for the modelling of wave propagation in the troposphere using numerical techniques [26]-[27]. The PE is based on the solution of the two or three dimensional differential

equation, fitted by homogenous or inhomogeneous refractive profiles [27]. Models based on the parabolic approximation of the wave equation have been used extensively for modelling refractive effects on tropospheric propagation [28]. The biggest advantage of using the PE method is that it gives a full-wave solution for the field even in the presence of range-dependent environments.

Various methods for the solution of the PE have been developed and presented in the literature. Two of the most popular are based on the finite-difference techniques [29], and the split-step Fourier algorithm [30]. Other models for propagation over terrain have also been developed and presented [31, 32]. The most efficient algorithm seems to be the Split Step Solution which employs the Fast Fourier Transform (FFT) to advance the solution over many small range steps. This algorithm has been widely used in many applications [33]. Split-step methods are extremely attractive in literature but they lack flexibility for boundary modelling [27]. Further, if variations of refractive index with height are fast, the error will be greater because in the split-step method error depends on the height variations of refractive index [27]. A brief description of the split step fourier and finite difference methods is given later.

In this chapter, a review of some of the basic techniques used in modelling and simulating the problem of propagation using the parabolic equation method is provided. The discussion begins with the parabolic wave equation formulation as an initial value problem along with its narrow and wide angle versions. A brief review of different numerical approximation techniques in applied electromagnetics

is then provided. An extensive review of literature related to propagation in the troposphere, vegetation and tunnels is also presented.

2.2 The Parabolic Wave Equation (PWE)

The parabolic wave equation is an approximation of the wave equation which models energy propagating in a cone centered on a preferred direction; the paraxial direction. Parabolic equation method is one of the most popular methods for modelling the problem of electromagnetic wave propagation, initially developed for the study of underwater acoustic problems [12, 34] and later extended to different propagation scenarios [27]. The Parabolic Equation Method is based on the assumption that the wave energy propagates predominantly in the forward direction. This assumption is good for low grazing-angle propagation over a terrain or ocean surface where the small backscattered field components can be neglected, as described later in section 2.2.1.

Recent progress in the parabolic equation method allows the efficient modelling of radio wave propagation over irregular terrain, vegetation and urban areas under all weather conditions in two or three dimensions. Using back propagation methods, PEM is also extended for treating electromagnetic scattering problems [35]. A new application for the PEM, radiolocation using inverse diffraction has been investigated in [36]. Also in [37] a new propagation model related to PEM, Huygen's Principle

Model (HPM) has been introduced. The algorithm can be used for radiolocation as well as for rough surface modelling but the accuracy of the algorithm depends on small range steps which in turns produces a large computational burden.

There are two formulations of the parabolic wave equation method: narrow angle and wide angle formulation, both neglect backscatter [27]. Narrow-angle formalism can be solved by the very fast and efficient split-step fourier method; however its accuracy deteriorates for long range propagation problems. The wide-angle can more accurately predict propagation outside the forward region but requires finite difference solution methods. Narrow-angle parabolic approximation was introduced by Leontovich and Fock [12] in the 1940's to treat the problem of diffraction of radiowaves around the Earth. They used the narrow-angle parabolic approximation to determine more simply the well-known Watson [38], Van der Pol and Bremmer [39] results, and then extended the method to more complicated cases involving atmospheric refraction. Malyuzhinets was the first to combine parabolic approximation with geometric optics [40]. The development of the wide-angle PWE method is attributed to different authors who proposed different models [41, 42]. An excellent account of these models can be found in Jensen *et al.* [43].

2.2.1 Parabolic Equation Propagation Model (PEPM)

In PEPM, a $e^{-j\omega t}$ time dependence of the field is assumed, where ω is the frequency in radians per second. Consider a two-dimensional space i.e. space where

the field quantities do not depend on the y-coordinate. For horizontal polarisation, the electric field **E** has one non-zero component E_y, while for vertical polarisation, the magnetic field **H** has one non-zero component H_y. The scalar component Ψ, of the electromagnetic field is governed by the Helmholtz wave equation:

$$\frac{\partial^2\Psi(x,z)}{\partial x^2} + \frac{\partial^2\Psi(x,z)}{\partial z^2} + k_0^2 n^2(x,z)\Psi(x,z) = 0 \tag{2.1}$$

where $\Psi(x,z)$ is the scalar component of the electric or magnetic field depending on polarisation, k_0 is the wave number in vacuum and n is the refractive index. In all type of problems considered in this thesis, variation of refractive index $n(x,z)$ remain slow on the scale of wavelength so equation (2.1) is exact [44]. A reduced function $\Psi(x,z)$ can be associated with paraxial direction x as:

$$\Psi(x,z) = u(x,z)e^{jk_0x} \tag{2.2}$$

The main purpose of using this reduced function is that it is slowly varying at angles close to paraxial direction x. Substituting equation (2.2) in equation (2.1) and simplifying;

$$\frac{\partial^2}{\partial x^2}\{u(x,z)e^{jk_0x}\} + \frac{\partial^2}{\partial z^2}\{u(x,z)e^{jk_0x}\} + k_0^2 n^2(x,z)\{u(x,z)e^{jk_0x}\} = 0$$

$$\frac{\partial}{\partial x}\{u(x,z)(jk_0e^{jk_0x}) + e^{jk_0x}.\frac{\partial u(x,z)}{\partial x}\} + \frac{\partial^2}{\partial z^2}\{u(x,z)e^{jk_0x}\} + k_0^2 n^2(x,z)\{u(x,z)e^{jk_0x}\} = 0 \tag{2.3}$$

$$(jk_0)^2 ue^{jk_0x} + jk_0e^{jk_0x}\frac{\partial u(x,z)}{\partial x} + e^{jk_0x}\frac{\partial^2 u(x,z)}{\partial x^2} + jk_0e^{jk_0x}\frac{\partial u(x,z)}{\partial x} + e^{jk_0x}\frac{\partial^2 u(x,z)}{\partial z^2} + k_0^2 n^2(x,z)u(x,z)e^{jk_0x} = 0 \tag{2.4}$$

yields,

$$\frac{\partial^2 u(x,z)}{\partial x^2} + j2k\frac{\partial u(x,z)}{\partial x} + \frac{\partial^2 u(x,z)}{\partial z^2} + k_0^2(n^2(x,z)-1)u(x,z) = 0 \qquad (2.5)$$

The next step is to introduce the famous paraxial approximation, i.e.

$$|\frac{\partial^2 u(x,z)}{\partial x^2}| \ll |j2k_0\frac{\partial u(x,z)}{\partial x}|$$

and hence reduce (2.5) to the familiar standard parabolic equation (SPE) in two dimension space given by,

$$j2k_0\frac{\partial u(x,z)}{\partial x} + \frac{\partial^2 u(x,z)}{\partial z^2} + k_0^2(n^2(x,z)-1)u(x,z) = 0 \qquad (2.6)$$

where x is the propagation direction and z is the transverse direction.

The above parabolic equation may be derived using a more general operator technique [43]. For the sake of completeness, this method is outlined for cartesian coordinates. Again consider (2.1) and rewrite it in the following form:

$$[p^2 + k_0^2 Q^2]\Psi = 0, \qquad (2.7)$$

where,

$$p = \frac{\partial}{\partial x}, \qquad Q = \sqrt{n^2(x,z) + \frac{1}{k_0^2}\frac{\partial^2}{\partial z^2}}$$

With the assumption that the refractive index is slowly varying in x, the operators p and Q approximately commute, i.e.

$$pQ \cong Qp$$

and equation (2.7) may be written in the following factorised form:

$$(p + jk_0Q)(p - jk_0Q)\Psi = 0 \tag{2.8}$$

The equation represented by the first bracketed factor of (2.8) is the one governing the backward-propagating wave, while that represented by the second factor is the one governing the forward-propagating wave. Consider the forward wave equation,

$$p\Psi = jk_0Q\Psi$$

or

$$\frac{\partial \Psi}{\partial x} = jk_0\sqrt{n^2(x,z) + \frac{1}{k_0^2}\frac{\partial}{\partial z^2}}\Psi \tag{2.9}$$

For the sake of simplicity assume,

$$\alpha = n^2(x,z) - 1, \qquad \gamma = \frac{1}{k_0^2}\frac{\partial^2}{\partial z^2}, \qquad q = \alpha + \gamma \tag{2.10}$$

and the square-root operator Q defined in (2.6) as,

$$Q = \sqrt{1+q} \tag{2.11}$$

Using Taylor series,

$$\sqrt{1+q} = 1 + \frac{q}{2} + \frac{q^2}{8} + ... \tag{2.12}$$

The narrow-angle PWE is obtained by keeping only the first two terms in the series defined by (2.12)

$$Q \cong 1 + \frac{q}{2} = 1 + \frac{1}{2}(n^2(x,z)(x,z) - 1) + \frac{1}{2k_0^2}\frac{\partial^2}{\partial z^2} \tag{2.13}$$

Putting (2.13) into (2.9),

$$\frac{\partial \Psi}{\partial x} = jk_0[1 + \frac{1}{2}(n^2(x,z) - 1) + \frac{1}{2k_0^2}\frac{\partial^2}{\partial z^2}]\Psi \tag{2.14}$$

Again if field Ψ can be written in the form given by equation (2.2) and substituting it in equation (2.14) the same standard narrow-angle parabolic equation as given in equation (2.6) can be obtained. Similarly a parabolic equation in cylindrical coordinates can be developed by assuming azimuthal symmetry as shown in [45]. Before proceeding to wide angle PWE, it is important to restate the approximations upon which equation (2.6) was based. These are:

- Backscatter is negligible
- Far field approximation
- In inhomogeneous media, $n^2(x,z)$ must be varying slowly in the range coordinate x or in the direction of predominant wave propagation. This assumption was needed to arrive at the factorized equation (2.7) above.

The simplest approximation of equation (2.1) is obtained either by using paraxial approximation or using the first-order Taylor expansion of the square root function, which yields the standard parabolic equation (SPE). The SPE is extremely useful for solving long range propagation problems, however, its limitations are due to its bad behaviour at large propagation angles. For a plane wave propagating at angle

α from the horizontal, the error is proportional to [27]:

$$\frac{1}{k_0^2}\left|\frac{\partial^2 u}{\partial z^2}\right| = \sin^2\alpha \tag{2.15}$$

Hence the error is proportional to $\sin^4\alpha$, going from 10^{-7} for an angle of 1^o to 10^{-3} for an angle of 10^o and over 10^{-2} for an angle of 20^o; which clearly shows that SPE is a narrow-angle approximation of the parabolic wave equation. For propagation problems, involving large propagation angles a more accurate expansion of operator Q is required. The very first thing that comes to mind is to include more terms in the expansion of the operator Q defined in eqution (2.12). But, unfortunately, including more terms in the expansion produces instability in numerical schemes. An alternate method is to approximate the square-root operator using rational function approximations of the form [46],

$$\sqrt{(1+q)} \cong \frac{a_0 + a_1 q}{b_0 + b_1 q} \tag{2.16}$$

where the coefficients are choosen to meet a given criteria [47]. However, the resulting wide-angle PWE can no longer be solved using the efficient split-step Fourier algorithm and requires some more elaborate methods [27].

2.2.2 Parabolic equation method algorithms

Various methods for the solution of the PE have been developed and presented to date; two of them are very popular in the literature. One uses finite-difference tech-

niques [29], and the other uses the split-step fourier algorithm [30]. Both methods are described briefly in this section and for a detailed study refer to [27].

These methods march the propagating field from the transmitter to the receiver over range increment Δx. Another PE model for propagation over terrain has been developed by Marcus [31], incorporating a hybrid finite-difference/surface Greens function. Two PE terrain models currently exist that use the split-step algorithm. One is by McArthur [48], and the other was developed by Ryan [32]. The most efficient algorithm seems to be the split step solution which employs the Fast Fourier Transform (FFT) to advance the solution over small range steps. The algorithm has been widely used in many applications [28]. More specifically, using the split step Fourier method, Barrios [49] treated horizontally inhomogeneous environments and a terrain model respectively. Craig and Levy [28] applied the split step solution to assess radar performance under multipath and ducting conditions. Split-step methods are extremely attractive in the literature but they lack flexibility for boundary modelling [27]. Further, if the variations of refractive index with height are fast error will be greater because in the split-step method error depends on the height variations of refractive index [27]. The Finite Different Method (FDM) on the other hand, enforces the terrain boundary condition in the spatial domain and therefore treats irregular terrain in a more straightforward fashion. Here, a brief overview of split-step fourier method and finite difference method is presented, for detailed reading refer to [27].

Split-step formulation of SPE (SSPE)

Consider the standard parabolic equation as defined in equation (2.6) and written as,

$$\frac{\partial u(x,z)}{\partial x} = \underbrace{\frac{jk_0}{2}}_{\delta}\left[\underbrace{\frac{1}{k_0^2}\frac{\partial^2}{\partial z^2}}_{A} + \underbrace{(n^2(x,z)-1)}_{B}\right]u(x,z) \tag{2.17}$$

Equation (2.17) can not be solved using simple fourier techniques if the refractive index $n(x,z)$ is varying with both the vertical and propagation direction x. The concept of SSPE is to separate the term containing the refractive index n. Assume initially that refractive index is a function of height z, then the solution of (2.17) can be expressed as:

$$u(x+\Delta x, z) = e^{\delta(A+B)}.u(x,z) \tag{2.18}$$

The main goal is that the two terms in the exponent are split into a product of exponents containing only A and B. While there are many possibilities, the simplest split is given by,

$$S = e^{\delta A}e^{\delta B}$$

However, if the refractive index n depends on height z, the two operators A and B will not commute because

$$\frac{\partial^2\{(n(z)^2-1)u(x,z)\}}{\partial z^2} \neq \left(n(z)^2-1\right)\frac{\partial^2 u}{\partial z^2}$$

But if the variations of refractive index are small with respect to height then the error incurred by splitting the exponential remains small. Therefore with the split-

step fourier method one of the main assumptions is that variations of refractive index with height should be small. To calculate the error, a commutator can be defined as:

$$[A, B] = AB - BA \tag{2.19}$$

Error E caused by the split is,

$$E = e^{\delta A} e^{\delta B} - e^{\delta(A+B)} \tag{2.20}$$

By expanding the exponentials using Taylor's series, error E can be written as a function of range step Δx. The dominant term of the error function is given as

$$\frac{k_0^2}{8}(\Delta x)^2[A, B]$$

Thus in the split-step fourier solution of the standard parabolic equation the error is a function of refractive index variations with height and range step size. For split S as defined above the solution at range step $x + \Delta x$ is given as,

$$u(x + \Delta x, z) = e^{\delta B}.\{e^{\delta A}.u(x, z)\} \tag{2.21}$$

If refractive index n depends on range as well as height then the refractive index operator B must be defined as an integral,

$$B = \frac{1}{\Delta x} \int_x^{x+\Delta x} n(\zeta, z) d\zeta$$

which can be approximated as

$$B = n(x + \frac{1}{2}\Delta x, z)$$

Comments about operators: Operator B is straightforward but the main difficulty is to construct the exponential operator A to simplify the computations. With complex irregular boundaries and refractive index variations it is a complex task. By eliminating the original exponential operator, the problem of the refractive index variations can be eliminated but the problem of boundary modelling still remains.

Finite Difference formulation of SPE

In this section, Crank-Nicolson type finite-difference implementations of SPE is presented. Assume that the lower boundary is located at $z = 0$ and upper boundary is at $z = z_{max}$, Consider an integration grid which is fixed in the vertical direction but not in range, so that it can adapt to terrain shape. Let,

$$z_j = j\Delta z, \qquad j = 0, N$$

be the vertical points and assume $x_0, ..., x_m, ...$ be the integration ranges. Consider a mid-point as shown in figure 2.1,

$$\xi_m = \frac{x_{m-1} + x_m}{2} \tag{2.22}$$

The main aim of the finite difference method is to write all terms of the differential equation involving differential operators at point (ξ_m, z_j) which involves only values of function say u at the corners of adjacent rectangles as shown in figure 2.1. The central finite difference approximation of the first derivative of u in range is given

as,

$$\frac{\partial u}{\partial x}(\xi_m, z_j) = \frac{u(x_m, z_j) - u(x_{m-1}, z_j)}{x_m - x_{m-1}} \tag{2.23}$$

Similarly the second order derivative in height is approximated as,

$$\frac{\partial^2 u}{\partial z^2}(\xi_m, z_j) = \frac{u(\xi_m, z_{j+1}) + u(\xi_m, z_{j-1}) - 2u(\xi_m, z_j)}{\Delta z^2} \tag{2.24}$$

The error in (2.23) and (2.24) is of the order of $(\Delta x_m)^2$ and $(\Delta z)^4$ respectively [27]. Equation (2.24) only makes sense if all the points are inside the integration domain which means this equation can not be applied to a boundary where j is either 0 or N. Some additional equations are needed to incorporate boundary conditions.

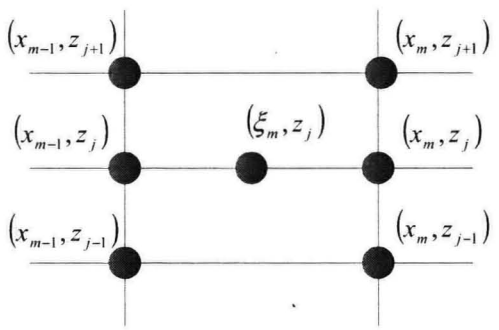

Figure 2.1: Finite Difference Grid for Crank-Nicolson Scheme

Consider again the standard parabolic equation (SPE) as defined in equation (2.6),

$$j2k\frac{\partial u(x,z)}{\partial x} + \frac{\partial^2 u(x,z)}{\partial z^2} + k_0^2(n^2(x,z) - 1)u(x,z) = 0 \tag{2.25}$$

Substitute equations (2.23) and (2.24) in (2.25),

$$\begin{aligned} j2k_0\frac{u(x_m, z_j) - u(x_{m-1}, z_j)}{x_m - x_{m-1}} &+ \frac{u(\xi_m, z_{j+1}) + u(\xi_m, z_{j-1}) - 2u(\xi_m, z_j)}{\Delta z^2} \\ &+ k_0^2(n^2(\xi_m, z_j) - 1)u(\xi, z_j) = 0 \end{aligned} \tag{2.26}$$

Now approximate u at range x_m by averaging values at ranges x_{m-1} and x_m. Let,

$$u_j^m = u(x_m, z_j) \tag{2.27}$$

$$b = j4k_0\frac{\Delta z^2}{\Delta x} \tag{2.28}$$

$$a_j^m = k_0^2(n^2(\xi_m, z_j) - 1)\Delta z^2 \tag{2.29}$$

And substituting these values in equation (2.25) gives,

$$u_j^m(-2 + b + a_j^m) + u_{j+1}^m + u_{j-1}^m = u_j^{m-1}(2 + b - a_j^m) - u_{j+1}^{m-1} - u_{j-1}^{m-1} \tag{2.30}$$

for $j = 1, ...N - 1$ yields $N - 1$ linear equations. To complete systems one must add additional equations for boundaries as stated before. One advantage of finite difference schemes is they normally yield sparse type matrices which are fast to invert using computer programming.

2.3 Review of Numerical Approximation Techniques

Many problems in radio wave propagation normally involve solving one or two partial differential equations subject to boundary constraints, for example the parabolic equation method discussed in section 2.2. Very few practical problems can be solved without the aid of a computer. Nowadays, antenna and microwave engineers rely heavily on computer techniques to analyse propagation problems, and to design efficient wireless systems.

Computer methods for analysing propagation problems can be divided into two categories: *analytical* and *numerical* techniques. Analytical techniques make some assumptions about the geometry of the region in order to apply a closed form solution of the problem. Numerical techniques attempt to solve fundamental field equations directly, subject to the boundary constraints posed by the geometry. Analytical techniques can be a useful tool when the important electromagnetic interactions of the configuration can be anticipated. However, most problems of interest are simply too unpredictable to be modelled using this approach. Numerical methods have come to occupy a major role in the field of applied electromagnetism [50]. Although the theoretical tools behind such methods have been available for many years, the true birth of computational electromagnetics can be traced to the 1960's shortly after the advent of the first mainframe computer. The current level of activity and interest in computational electromagnetics may be gauged by examining the lists of papers presented at technical conferences [51].

A number of different numerical techniques for solving propagation problems are available. Each numerical technique is well-suited for the analysis of a particular type of problem. This section has outlined several general numerical modelling techniques that have been used to analyse different electromagnetics problems with some success.

2.3.1 Method of Moments

The method of moments or simple moment method is a technique for solving complex integral equations by reducing them to a system of linear equations. The method of moments employs a technique called the method of weighted residuals. For further details about the method of residuals refer to any standard text on the subject for example [52]. Harrington [53] was responsible for popularising the term *method of moments* in the field of electrical engineering.

The moment method technique is used for analysing a variety of important electromagnetic radiation problems. General purpose moment method codes are particularly efficient at modelling wire antennas or wires attached to large conductive surfaces. They are widely used for antenna and electromagnetic scattering analysis. Several non-commercial general purpose moment method computer programs are available [54].

The method of moments requires calculating only boundary values, rather than values throughout the space defined by partial differential equation. Boundary element formulations typically give rise to fully populated matrices which require large storage requirements and more computation time. By contrast finite element matrices are sparse matrices requiring less storage requirements and can be easily manipulated as will be described in chapter 3.

2.3.2 Finite Difference Time Domain Method

The Finite-Difference Time-Domain (FDTD) method, as first proposed by Yee in 1966 [55], is a simple and elegant way to discretise the differential form of Maxwells equations. Yee used an electric field **E** grid which was offset both spatially and temporally from a magnetic field **H** grid to obtain update equations to yield the present fields throughout the computational domain in terms of the past fields. The update equations are used in a leap-frog scheme to incrementally march the **E** and **H** fields forward in time. Despite the simplicity and elegance of Yees algorithm, it did not receive much interest immediately after its publication. The lack of attention might have been due to the high computational cost of the day as well as to some of the limitations inherent in the original publication (such as the inability to model an open problem for any significant period of time). However, as the shortcomings of the original FDTD implementation were alleviated and the cost of computing fell, the interest in the FDTD method began to increase.

The Finite Difference Time Domain method is a direct solution of Maxwell's time dependant curl equations,

$$\nabla \times \mathbf{E} = -\mu \frac{\partial \mathbf{H}}{\partial t} \tag{2.31}$$

$$\nabla \times \mathbf{H} = \sigma \mathbf{E} + \mu \frac{\partial \mathbf{E}}{\partial t} \tag{2.32}$$

It uses simple central-difference approximations to evaluate the space and time derivatives [56, 57]. The FDTD method is a simple time stepping procedure and the

inputs are time-sampled analog signals. The region being modelled is represented by two interleaved grids of discrete points. One grid contains the points at which the magnetic field is evaluated, while the second grid contains the points at which the electric field is evaluated. For further details of FDTD, and how to apply FDTD to various electromagnetic problems refer to [57].

The significant disadvantage of this technique, is that the problem size can get too large for some configurations. Another major disadvantage of the FDTD method is that it gives the **E** or **H** field at some specific points on grid.

2.3.3 Transmission Line Matrix Method

The transmission line matrix method is quite similar to the FDTD method in terms of its capabilities, but its approach is unique. Like FDTD, analysis is performed in the time domain and the entire region of the analysis is grided. Instead of interleaving **E** field and **H** fields grids however, a single grid is established and the nodes of this grid are interconnected by virtual transmission lines.

Nevertheless, both the TLM and FDTD techniques are very popular and widely used [56, 58]. TLM method require significantly more computer memory per node, but it does a better job of modelling complex boundary geometries. This is because both **E** and **H** are calculated at every boundary node.

Advantage of using TLM method are similar to those of the FDTD method. The disadvantages of the FDTD method are also shared by this technique. The pri-

mary disadvantage is that voluminous problems that must use a fine grid requiring excessive amounts of computations.

2.3.4 Generalised Multipole Technique

The Generalised Multipole Technique (GMT) is another popular technique for analysing electromagnetic problems [59]. It is a frequency domain technique that is based on the method of weighted residuals similar to the Method of Moments. However, this method is unique in that the expansion functions are analytical solutions of the fields generated by sources (multipoles) located some distance away from the surface where the boundary condition is being enforced. Placing the multipoles requires a great deal of skill which is the main disadvantage of this method.

Over the last twenty years, the GMT has been applied to a variety of EM configurations including dielectric bodies [60], obstacles in waveguides [61], and scattering from perfect conductors [62].

2.3.5 Conjugate Gradient Method

The conjugate gradient method is another technique based on the method of weighted residuals [63]. It is conceptually very similar to the conventional moment method technique. Nevertheless, there are two features that generally distinguish this technique from other moment methods. The first has to do with the way in which the weighting functions are utilised. The second involves the method of solving the sys-

tem of linear equations [64]. The conventional moment method technique generally employs a Guass-Jordan method or another direct solution technique, while, the conjugate gradient method utilises an iterative solution procedure. This procedure called the method of conjugate gradients can be applied to the system of equations or it can be applied directly to the operator equation [64]. The conjugate gradient method shares the advantages and disadvantages with the method of moments.

2.4 Wave Propagation in the Troposphere

Radio coverage in the troposphere has been a challenging problem for many years [65]. An approach for tropospheric propagation modelling was developed by Baumgartner [66] and later improved by Shellman [67] and is normally known as Waveguide Model or Coupled Mode Technique. The main disadvantage of coupled mode techniques lie in the complexity of the root finding algorithms and large computational demands, especially when higher frequencies and complicated ducting profiles are involved.

In the past, emphasis was mainly given to geometrical optics [68]. These methods provide a general geometrical description of ray families, propagating through the troposphere. Ray tracing methods present many disadvantages; for example the radiowave frequency is not accounted for and it is not always clear whether the ray is trapped by the specific duct structure [69].

Researchers in wave propagation have been searching for efficient mathematical models for describing the problem of electromagnetic propagation in the troposphere. Numerous methods are available for predicting electromagnetic wave propagation in the atmosphere [70, 71]. However, the presence of vertical refractivity stratification in the atmosphere complicates the application of some methods. To model refractivity variations in the horizontal as well as vertical direction, geometric optics, coupled-mode analysis, or hybrid methods have been employed [68].

The solution of electromagnetic propagation problems in the terrestrial domain is a complicated matter. Three-dimensional variations in refraction and terrain make the full vector problem extremely difficult to solve in a reasonable time. If one chooses to simplify the problem by assuming symmetry in one or more of the coordinate directions, the vector problem can be decoupled into scalar problems [72]. However the solution of two dimensional scalar problems is still difficult for realistic environments. Some approximations and numerical schemes for the solution are used to reduce the solution of the full two-way equation to one-way equation. The benefits of one-way propagation are the simple numerical implementation of range dependencies in the medium and the avoidance of prohibitive numerical aspects of solving elliptic equations associated with implementing two range-dependant boundary conditions. One of the most reliable and widely used techniques in the literature is the parabolic equation (PE) method, initially developed for the study of underwater acoustic problems and later extended to tropospheric propagation [26]. This method has

emerged as a tool of choice in the study of environmental effects on radio wave propagation. The PE is based on the solution of the two dimensional differential parabolic equation, fitted by homogenous or inhomogeneous refractive profiles, as described in section 2.2. Models based on the parabolic approximation of the wave equation have been used extensively for modelling refractive effects on tropospheric propagation [28, 33] in the last decade. The biggest advantage to using the PE method is that it gives a full-wave solution for the field in the presence of range-dependent environments.

2.5 Wave Propagation in the presence of Vegetation

The large number of mobile users has resulted in network planners increasing capacity by locating transmitting antennas at heights lower than surrounding trees and buildings [73]. In planning a communication link, quantitative knowledge of the excess transmission loss suffered by the radio waves due to the presence of foliage is essential. Trees act as an obstacles and affect radio waves by depolarisation, absorptions and scattering [74]. The depolarisation, scattering and absorption need to be accounted for in radio planning tools to improve accuracy and optimum use of the scarce radio spectrum. Previous studies showed that trees influenced the received signal level by directly providing an additional attenuation and indirectly by

scattering, which resulted in lateral contribution to the received signal [75].

Because of high attenuation rates, direct wave propagation is not possible in the presence of vegetation over large distances and high frequencies. In the HF-UHF range where both the transmitter and receiver are inside the foliage, radio signals can propagate over relatively large distances. This peculiar behavior is explained by Tamir, defining certain types of surface waves known as lateral waves [76].

Several methods to model vegetation for propagation analysis have been presented in the literature [76, 77]. Empirical [78], semi-empirical [79] and analytical [75] models are available in literature, mainly aimed at characterising the effects of vegetation and calculation of path losses. The main advantage of empirical models such as COST 235 [80], ITU-R [78] is their mathematical simplicity and ease of use, while the drawback is their dependance on specified measured data and failure to relate the physical processes involved. Dependence of system parameters for these models e.g. frequency, angle of arrival, etc. are usually determined through regression curves fitted to measured data.

Semi-empirical models [79] were formulated to give best fits to measured data. These methods are relatively easy to apply are new and formulated using measured data. One of the drawbacks of such models lies in the inclusion of an inverse relationship between excess attenuation and the signal frequency. This appears to contradict other models as well as the observed behavior of measured attenuation data [81].

Analytical models such as Geometrical and Uniform theory of diffraction [82], Ra-

diative Energy Transfer Theory (RET) [83], Full Wave Solutions [84] provide more insight into the physical processes involved in radiowave propagation through vegetation. Out of these RET has been found to offer a highly effective vegetation attenuation and scatter model which can be applied in a variety of radio path geometries and frequencies. They normally require the use of numerical analysis methods to provide solutions to the complex mathematical formulations [85].

The lossy dielectric slab model is one popular method for the determination of wave propagation in an area with vegetation [77]. The valid range of frequencies which can be used with the lossy dielectric slab method are from 20 to 200MHz, however, for propagation along the horizon it can be used at higher frequencies [74]. Tamir [86] pointed out that, above 200MHz, these slab models are poor because vegetation cannot be regarded as a homogenous medium with dimensions of the order of vegetation.

Recently, a four layered model has been widely adopted and was used effectively for analysing the propagation mechanism in a forest environment [87, 88]. Two lossy dielectric layers placed over a semi-infinite ground plane are used to represent the canopy layer and trunk layer of the forest, respectively. This is an attempt to take into account the vertical non-homogeneities of the forest. At UHF frequencies the most appropriate method is the four layer model, which can be used with frequencies upto 2GHz [89]. The use of dyadic Green's functions for the analysis of the electromagnetic wave propagation in semi-infinite media was described by [90] and

a generalisation of these functions for the case of an $N-$layered medium yields an expression for the coefficients of the scattered dyadic Green's functions in multi-layered medium [91]. Unfortunately, the integral representation of the solution is very complicated such that considerable efforts is required before numerical computations can be obtained [92].

2.6 Wave Propagation in Tunnels

Fading of electromagnetic signals in tunnels is a well known fact and the first attempt to explain it can be traced back to the 1920's. Wave propagation in tunnels is not a new subject and much work has been done in the past. Initial studies concentrated on the use of leaky cables or antennas set at a distance of 10-20 cm from the wall, which are widely used to provide relatively uniform coverage over a tunnel [93]. The basic principle of radiating cables has been described in many papers and books, working either above or below the tunnel cut-off frequency [94]. Their bandwidth is generally equal to one octave and by adjusting the slot configuration it is even possible to extend this band. However, the attenuation in tunnels increases at high frequencies and any improvement can be obtained only by installing cables of large diameters which leads to prohibitive cost and weight [95]. Leaky feeders are expensive, susceptible to interference and require regular maintenance. Further the use of leaky cables requires prior access to the tunnel in order to install the cable

and related infrastructure. But in metro tunnels sometimes a radiating cable is the only solution because of limited installation space.

Different kinds of antenna solutions are normally used in road tunnels [96], because in road tunnels installation of antennas is easy and radiating cable is usually more expensive. The maximum distance between antennas in tunnels should be calculated to optimise tunnel installation cost. During the 1960's various research projects were started in Europe to study the use of radio in mine tunnels. By 1980 the topic was quite mature and all tunnel research was summarised in [94] which is still the only one on this topic and contains an extensive bibliography.

Many theoretical studies and practical approaches have been conducted on radio wave propagation characteristics in tunnels. Previous experimental studies of radio wave propagation characteristics in tunnels were concentrated on finding the optimal frequency band for minimum attenuation. The results shows that the optimum band seems to be between 1-2 GHz [9]. Modal analysis [97] and Geometrical Optics (GO) [98] are two major theoretical approaches for modelling of wave propagation in tunnels.

In [98] Mahmoud and Wait considered models to predict the propagation of both modes and rays in a rectangular tunnel. They produce models using ray theory and produce rays by the method of stationary phase. They compared results of modal analysis and ray theory and introduced wall roughness with a simple model that modifies the Fresnel coefficients in the specular direction. In all models proposed by

Mahmoud and Wait they assumed the walls of the tunnel were perfectly conducting. In [99] the same authors considered curved rectangular waveguides with the broad walls imperfectly conducting.

Based on the modal theory a theoretical model has been proposed by Emslie *et al.* [100] taking in account the similarity between a tunnel and an electromagnetic waveguide. Emslie was the first to consider different propagating modes in rectangular lossy tunnels. For smaller tunnels and low frequencies the tunnel dimensions are only a few times the wavelength of the radio signal. In this scenario, the modal approach is simpler to use and more accurate. However the modal theory based model is only effective if a limited number of modes dominate, a rare case in actual tunnels. Modal theory was later extended to curved waveguides (adiabatic mode theory) and has been presented in [101]. Although adiabatic mode theory suggests one to study radio wave propagation in realistic tunnels, it is not always convenient for practical applications because of computational efficiency [102]. Recently using the modal approach propagation around corners in tunnels and urban streets canyons were modelled [103].

In GO based models, propagation is achieved using direct ray and a number of reflected rays from tunnel walls. The ray tracing method approximates RF propagation as multiple rays originating from the source and reflecting off and/or diffracting around objects in the region of interest. Analysis using geometrical optics is difficult at long ranges due to the large number of rays and it breaks down in caustic re-

gions. Caustics are regions where multiple rays are focused and the assumptions of ray tracing are violated [104]. While reasonable numerical results can be obtained by calculating wave amplitude by using calculated ray density, this approach requires excessive computational resources [105]. The ray approximation works best at short wavelengths, typically less than characteristic object size. Further, the GO based model is restricted to empty straight tunnels and thus have limitations.

In early 1990's Mariage *et al.* applied ray optics and uniform theory of diffraction to propagation in rectangular road tunnels [106]. Nilsson *et al.* also used rays to derive an estimate of the ray attenuation in a curved 10×5m road tunnel [107]. This paper also includes experiments done by the Norwegian company Telenor. Based on the ray models of Mahmoud and Wait, Lienard and Degauque made theoretical calculations for a straight tunnel [108]. One of the important observation they made in their paper is that the signal amplitude versus distance between the transmitter and receiver can be divided into two zones. One zone is in the vicinity of transmitter where a large number of modes are present and the second zone is at a larger distance where lower order modes become dominant and attenuation per unit length becomes much smaller.

Another ray tracing method is described in [109] in which a bundle of rays were used to represent each physical wave. Each bundle of rays was traced to a receiver position where reception sphere determined which rays are intercepted by the receiver. Experimental verification of this approach were carried out in the Berlin subway

system and is also provided in this paper.

Multi-path propagation modelling may also be used for predicting radio channels in tunnels [110]. The traditional channel model is unable to represent the real propagation characteristics of a radio wave and so cannot be used directly to predict the propagation properties in a tunnel. For the multi-path model, it is extremely important to know the multi-path distances and hence the time delays of each path. An algorithm has been proposed for calculating multi-path distances in simple rectangular tunnel [111] in 2003. Some statistical radio prediction models are also available in the literature for tunnels but they require a large set of measurements to tune the propagation model [105].

Recently, Dudley studied models for propagation in lossy circular tunnels [112]. He developed expressions for the electric field and presented the numerical results for the field intensity both as a function of axial distance and radial distance. The main shortcoming of this work is that it is only for smooth tunnel walls and not the more realistic situation of rough wall tunnels. Pao investigated statistical properties of wave propagation in straight rough tunnels last year but assumes a perfectly conducting boundary at the rough wall/air interface [113].

Actual tunnels have vehicles most of the time hence for future development of mobile communication systems, the study of propagation characteristics inside tunnels with vehicles is a must. A number of measurements have been carried out to study the influence of vehicles inside tunnels see, e.g. [114]. The influence of the vehi-

cles was studied either in moderate traffic conditions [115] or by considering only an individual vehicle passing a fixed link established in a tunnel [96]. To the author's knowledge, only a few analytical investigations (e.g. [116]) have been done on propagation characteristics in non hollow tunnels.

2.7 Summary

An extensive review of literature related to radio wave propagation in general and wave propagation in the troposphere, vegetation and tunnels has been presented in this chapter. The Parabolic Equation Method is one of the most popular methods for modelling of electromagnetic wave propagation and is described in detail. Narrow and wide angle formulations were given with a brief description of algorithms used for the solution of PEM. A critical review of numerical schemes used for electromagnetic modelling was also presented.

Chapter 3

Finite Element Analysis (FEA)

3.1 Introduction

Numerical methods have come to occupy a major role in the field of applied electromagnetism. Although the theoretical fundamentals of such methods have been available for many years, the true birth of computational electromagnetism can be traced to the 1960's after the invention of first mainframe computer. The finite element method was first outlined in 1942 by Courant [117]. Finite Element Methods are widely used by civil and mechanical engineers to analyse material and structural problems. Its application to electronic engineering only began in 1969, when a finite element solution of the classical waveguide mode problem was published in a special issue of the Italian journal, Alta Frequenza [118]. Finite elements were soon applied also to integral operators in both electrostatic and antenna problems [119].

Electrical engineers use finite element method to solve complex, nonlinear problems in magnetics and electrostatics.

Until recently, however very little practical modelling of 3-dimensional electrostatic radiation problems was performed to use this technique. Practical 3-dimensional problems require more computation than 2-dimensional problems which seems to be the reason why researchers were reluctant using this method in past. However, in recent years, an increasing availability of computer resources coupled with a desire to model more complex electromagnetic problems has resulted in a wave of renewed interest in finite element methods for solving EM propagation problems.

In the past, the finite element method has been used to solve complex engineering problems including structural analysis in the aircraft industry, heat transfer, fluid flow, and mass transport. In recent years it has found application in many areas including electromagnetic field problems. The finite element method has established itself as one of the most powerful and accurate methods for solving problems associated with the sophisticated integrated optical waveguides and microwave devices being developed today. The versatility of the method allows elements of various shapes to be used to represent an arbitrary cross-section. Each element could also be of a different material type and shape.

The basic idea of the finite element method is to divide the region of interest into a large number of finite elements or sub-regions. These elements may be one, two or three-dimensional. The idea of representing a given domain as a collection of

discrete elements is not new, it is recorded that ancient mathematicians estimated the value of π by representing the circle as a polygon with a large number of sides. This chapter describes the basic steps in the finite element method. A complete one and two dimensional analysis of the method is provided which forms the basis of the rest of the material in this thesis.

3.2 Numerical Methods

In the last two decades, numerical methods have been widely used in electromagnetics due to the availability of faster and cheaper computer power. These methods are concerned with finding numerical solutions to the Helmholtz's wave equation derived from Maxwell's equations. In many instances, a choice has to be made between a numerical method and an approximate method where the choice is dependent on the level of accuracy required. For the accurate characterisation of 3-D environments, a fully numerical method such as the finite difference or the finite element method is required.

A numerical method is in simple terms, a technique which converts the infinite degrees of freedom of an unknown analytical solution to a finite set of unknowns which can then be solved computationally. The finite element method (FEM) is one such numerical technique for solving, with a high degree of accuracy, complicated boundary value problems. There are some general texts on numerical methods for

applied electromagnetism in which the finite element method is treated, although such methods are usually introduced through static or quasi-static potentials [120]. Two important finite element formulations are variational and weak formulations. Weak formulations are based on the method of weighted residual and is the technique used in this thesis; variational methods will hence not be discussed further. Variational formulation depends on existence of a variational principle while method of weighted residual starts directly from differential equations and can be use in all types of problems. Method of weighted residual is described in detail in Appendix 1.

3.3 Basic concepts in finite element analysis

The finite element method is a domain discretisation technique and can be interpreted from either a physical or mathematical standpoint. The first step in finite element analysis is to divide the configuration into a small number of small elements. The major advantage that finite element method have over other methods stems from the fact that the electrical and geometric properties of each element can be defined independently. This permits the problem to be setup with a large number of small elements in regions of complex geometry and fewer large elements in relatively open regions. Thus it is possible to model configurations that have complicated geometries and many arbitrarily shaped dielectric regions in a relatively

efficient manner.

As stated earlier, the finite element method is a numerical procedure for obtaining solutions to boundary value problems. The main principle of the method is to replace an entire continuous domain by a number of subdomains in which an unknown function is represented by simple interpolation functions with unknown coefficients. So, an original boundary value problem with an infinite number of degrees of freedom is converted into a problem with a finite number of degrees of freedom. Then a system of equations is obtained by applying either Ritz variational or Galerkin procedures, and finally a solution of the boundary value problem is achieved by solving the system of equations.

Commercial finite element codes [121, 122] are available that have graphical user interfaces and can determine the optimum placement of node points for a given geometry automatically. Specific implementation of three dimensional electromagnetic finite element codes are described in a PhD dissertation by Maile [123, 124]. Silvester and Ferrari [52] have written an excellent text on this subject for electrical engineers. The main steps of finite element analysis are described in the next subsection.

3.3.1 Domain Discretisation

Domain discretisation is one of the most important steps in finite element analysis. Domain discretisation affects the computer storage requirements, the computation

time and accuracy of the numerical results. An entire domain, say Ω is divided into a number of small domains say Ω^e called *finite elements* or simply *elements*. Elements can be small where geometric details exist and much larger otherwise. In each finite element, a simple (normally linear) variation of the field quantity is assumed. The corners of the elements are called nodes. The goal of the finite element analysis is to determine the field quantities at the nodes. These elements can be of various shapes such as triangles and rectangles thus enabling the use of an irregular grid for a complex waveguide structure see figure 3.1. The method can therefore be easily

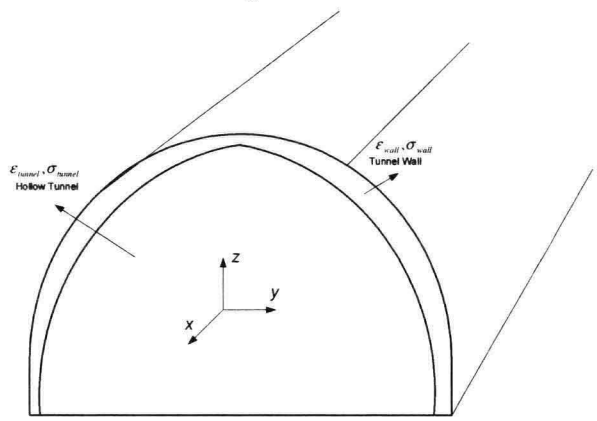

Figure 3.1: Example of an arbitrary shaped tunnel with regions of different material properties

used to analyse problems with steep variations of the field and can be adapted quite readily to anisotropic and inhomogeneous problems. The accuracy of the method could be systematically increased by increasing the number of elements. The method does not rely on the Galerkin method for its establishment, it could be established by the used of the variational method.

Element Attributes

In the finite element method , elements are isolated by discretisation and localisation steps. The procedure involves the separation of elements from their neighbours by disconnecting the nodes, followed by referral of the element to a convenient local coordinate system. In terms of computer programming, a function or subroutine can be written that constructs by suitable parametrisation all elements of one type rather than writing a new code for each element type. Figure 3.2 shows typical finite element geometries in different dimensions.

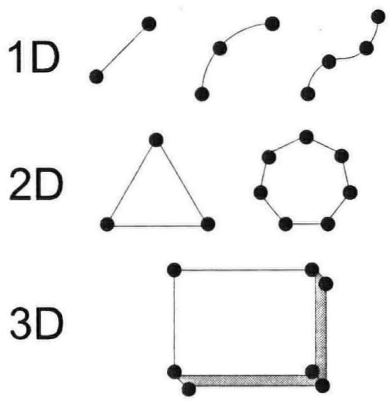

Figure 3.2: Typical finite element geometries

Dimensionality

Elements may has dimensionality of one, two or three space dimensions. There are also special elements with zero dimensionality, such as lumped springs or point masses. However, dimensionality can be extended if necessary, e.g. a 1D element

can be used to build a model in 2D or 3D space.

Nodes

Each element have corner points called *nodal points* or simply *nodes* as shown in figure 3.2. Nodes serve two purposes: definition of element geometry and home for degree of freedom. Nodes are usually located at the corners or end points of elements but in some higher order elements nodes are also placed on sides or faces as well as possibly the interior of elements.

Geometry

The geometry of an element is usually defined by the placement of nodal points. Most elements used in practice have simple geometries. In one dimension, elements are usually straight lines and in two dimension they are usually triangular or quadrilateral shape.

In most finite element solutions, the problem is formulated in terms of the unknown function u at nodes associated with the elements. For example, a linear element has two nodes one at each endpoint and a triangular element has three nodes one at each vertex. For computer implementation it is necessary to describe these nodes. A complete description of a node for a computer program contains its coordinate values, local number and global number. The local number of a node indicates its position in the element, whereas the global number specifies its position in the entire

system.

Domain discretisation is a completely separate step from the other finite element method steps. Many well-developed finite element packages have the capability of subdividing an arbitrarily shaped line, surface and volume into the corresponding elements and also provide optimized global numbering [125].

3.3.2 Interpolation Functions

The next step in finite element analysis is the selection of an interpolation function that provides an approximation of the unknown solution within an element domain Ω^e. Interpolation functions are normally selected to be a polynomial of first, second or higher order. In an element domain Ω^e, unknown approximate solution u can be expressed as,

$$\begin{aligned} u^e &= \sum_{j=1}^{n} N_j^e u_j^e \\ &= \{N^e\}^T \{u^e\} \end{aligned} \tag{3.1}$$

where e denotes the eth element and n is the number of nodes in the element. ${N_j}^e$ is the interpolation function also called the shape function for node j. Two important characterstics of interpolation functions are that their summation is always equal to 1 and they are only non-zero within the elements and outside the elements they vanish.

3.3.3 Formulation of the System of Equations

The next step in finite element analysis is to formulate the system of equations. The most widely used methods to formulate system of equations are the Ritz variational [117] and Galerkin methods [126]. In this thesis, the Galerkin method for the formulation of equations is used so Ritz variational methods will not be discussed further. The Galerkin method is based on a weighted residual method and is described in Appendix 1. The Galerkin method formulation yields a system of equations and number of equations that depend on system degrees of freedom.

Assembly

After formulating element equations for each element using either the Ritz or Galerkin method, the next step is assembly. Assembly is a process to sum all element equations to form a system of equations for the whole system. Before solving a system of equations for a specific solution, required boundary conditions need to be applied.

Boundary Conditions

There are two kinds of boundary conditions that are often encountered: One is Dirichlet boundary conditions which prescribe unknown u at the specified boundary and the other is Neumann boundary condition which requires the normal derivative of u to vanish at the boundary. Sometimes for exact modelling some other types of boundary conditions are required as discuss in chapter 4.

3.3.4 Solution of the system of equations

Solving the system of equations is the final step in finite element analysis. The resulting equations are either deterministic or eigenvalue types of equations. In electromagnetics, deterministic systems are usually associated with scattering, radiation and other problems where there exists a source or excitation. On the contrary, eigenvalue types are usually associated with source free problems. Normally the resulting matrices are very large and require some specific methods for solution.

3.4 One Dimensional Finite Element Analysis

After introducing the basics of finite element analysis now a simple one dimensional boundary value problem using the finite element method is described. Consider a simple boundary value problem along with boundary conditions defined as:

$$\frac{\partial^2 u}{\partial z^2} + b = 0, \quad \text{for} \quad 0 \leq z \leq z_{max} \tag{3.2}$$

$$u|_{z=0} = p \tag{3.3}$$

$$\left[\alpha \frac{\partial u}{\partial z} + \gamma u\right]_{z=z_{max}} = q \tag{3.4}$$

where p, α, γ and q are known parameters of functions. Equation (3.3) is usually referred to as a boundary condition of the first kind or a Dirichlet condition, whereas equation in (3.4) is referred to as a boundary condition of the third kind. For boundary condition of the second kind or Neumann condition, $\gamma = 0$. In this

section the basic steps of finite element analysis outlined in chapter 1 and in section 3.3 are followed to formulate the solution.

3.4.1 Discretisation and Interpolation

Given the problem as defined in equation (3.2)

$$\nabla^2 u + b = 0 \tag{3.5}$$

as the governing equation defined within domain $0 \leq z \leq z_{max}$, where u is the electric or magnetic field component depending on polarity and ∇^2 is a Laplacian operator defined as,

$$\nabla^2 = \frac{\partial^2}{\partial x^2} + \frac{\partial^2}{\partial y^2} + \frac{\partial^2}{\partial z^2} \tag{3.6}$$

in three dimensions. However for the present case it is simply defined as $\nabla^2 = \frac{\partial^2}{\partial z^2}$. In the finite element method the first step is to divide entire solution domain $(0, z_{max})$ into small subdomains, which in this case will be short line segments. Assume l^e is the length of the e^{th} element and the total number of elements are M so $e = 1, 2, 3, ..., M$. Further let z_i with $i = 1, 2, 3, ..., N$ denote the position of the i^{th} node with $z_1 = 0$ and $z_N = z_{max}$. Now to adopt a general procedure consistent with two and three dimensional systems it is necessary to adopt a local numbering system in the formulation. As a convention, assume e is used to denote a quantity with a local number as its subscript, while for all other quantities the subscript is a global number.

The second step of the finite element analysis is to select an interpolation function and for simplicity and purpose of understanding assume linear functions first.

Linear Elements

Consider an element e as shown in figure 3.3. Within an element e, trial function

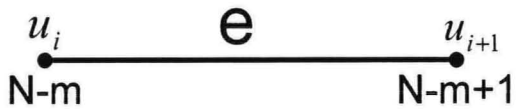

Figure 3.3: Linear element with local node numbers

or interpolation function is approximated as,

$$u^e(x) = a + bz \tag{3.7}$$

where a and b are the constants to be determined. For linear elements, there are two nodes per element so at node $N - m$ the value of the interpolation function is u_i and at node $N - m + 1$ value of interpolation function is u_{i+1}. Putting these values in equation (3.7) yields,

$$\begin{aligned} u_i^e &= a + bz_i \\ u_{i+1}^e &= a + bz_{i+1} \end{aligned} \tag{3.8}$$

Now solve two equation defined in (3.8) for a and b, and substitute back in equation (3.7),

$$u^e(z) = \sum_{j=1}^{2} N_j^e(z) u_j^e \tag{3.9}$$

Where N_1^e and N_2^e are called basis functions or shape functions given by,

$$N_1^e(z) = \frac{z_2^e - z}{z_2^e - z_1^e}$$
$$N_2^e(z) = \frac{z - z_1^e}{z_2^e - z_1^e} \tag{3.10}$$

For convergence of the solution, the shape function N_j^e must satisfy certain conditions:

1. the interpolation function u^e and its derivative must include certain terms
2. the interpolation function u^e must be continuous at the interface of two adjacent elements.

The first of the two conditions is also known as the completeness condition and is simple to satisfy provided complete polynomial expressions are used in each element. The second of the two conditions is called the compatibility condition. First order elements are the most fundamental and first order polynomials are used with them but higher order elements are used with higher order polynomials. Similar analysis for linear quadratic elements is described in Appendix 2.

3.4.2 Formulation via Galerkin's Method

According to the Galerkin method, the residual for a given approximate solution u is,

$$R = \frac{\partial^2 u}{\partial z^2} + b \tag{3.11}$$

and thus the weighted residual for an element e can be written as,

$$R_i^e = \int_{z_i}^{z_{i+1}} N_i^e R\, dz \qquad \text{i=1,2} \tag{3.12}$$

Putting equation (3.11) in (3.12) yields,

$$R_i^e = \int_{z_i}^{z_{i+1}} N_i^e \left(\frac{\partial^2 u}{\partial z^2} + b \right) dz \tag{3.13}$$

For weak formulation of (3.13) use integration by parts,

$$R_i^e = \int_{z_i}^{z_{i+1}} \left(-\frac{\partial N_i^e}{\partial z} \frac{\partial u}{\partial z} + N_i^e b \right) dz - N_i^e \frac{\partial u}{\partial z}\Big|_{z_i}^{z_{i+1}} \tag{3.14}$$

Now for linear elements substitute equation (3.9) into (3.14) gives,

$$R_i^e = \sum_{j=1}^{2} u_j^e \int_{z_i}^{z_{i+1}} \left(-\frac{\partial N_i^e}{\partial z} \frac{\partial N_j^e}{\partial z} \right) dz + \int_{z_i}^{z_{i+1}} N_i^e b\, dz - N_i^e \frac{\partial u}{\partial z}\Big|_{z_i}^{z_{i+1}} \tag{3.15}$$

where shape functions N are given by (3.10). Similarly for quadratic elements, summation starts from $j = 1$ to 3 and shape functions are defined as given in appendix 2. Equation (3.15) can be written in matrix form as,

$$\{R^e\} = [K^e]\{u^e\} + \{b^e\} - \{g^e\} \tag{3.16}$$

where,

$$\begin{aligned} \{b^e\} &= \int_{z_i}^{z_{i+1}} N_i^e b\, dz \\ \{g^e\} &= N_i^e \frac{\partial u}{\partial z}\Big|_{z_i}^{z_{i+1}} \end{aligned} \tag{3.17}$$

In this, $\{u^e\} = [u_i^e, u_{i+1}^e]^T$ and,

$$K_{ij}^e = \int_{z_i}^{z_{i+1}} -\frac{\partial N_i^e}{\partial z} \frac{\partial N_j^e}{\partial z}\, dz \tag{3.18}$$

It should be noted that $[K^e]$ is symmetric and analytically given by,

$$[K^e] = \begin{bmatrix} \frac{1}{l^e} + \frac{l^e}{3} & -\frac{1}{l^e} + \frac{l^e}{6} \\ -\frac{1}{l^e} + \frac{l^e}{6} & \frac{1}{l^e} + \frac{l^e}{3} \end{bmatrix} \tag{3.19}$$

For quadratic elements matrix $[K^e]$ can be defined as,

$$[K]^e = \begin{bmatrix} \frac{7}{3l^e} + \frac{2l^e}{15} & -\frac{8}{3l^e} + \frac{1}{15} & \frac{1}{3l^e} - \frac{l^e}{30} \\ -\frac{8}{3l^e} + \frac{1}{15} & \frac{16}{3l^e} + \frac{8l^e}{15} & -\frac{8}{3l^e} + \frac{l^e}{15} \\ \frac{1}{3l^e} - \frac{l^e}{30} & -\frac{8}{3l^e} + \frac{1}{15} & \frac{7}{3l^e} + \frac{2l^e}{15} \end{bmatrix} \tag{3.20}$$

where l^e is the length of element e.

3.4.3 Assembly of Element Matrices

With the elemental equations given in (3.18), the system of equations can be formed by summing it over all elements, so for M elements,

$$\{R\} = \sum_{e=1}^{M} \{R^e\} = \sum_{e=1}^{M} ([K^e]\{u^e\} + \{b^e\} - \{g^e\}) = \{0\} \tag{3.21}$$

which can be written as,

$$[K]\{u\} + \{b\} - \{g\} = \{0\} \tag{3.22}$$

Now, suppose if the domain consists of M elements, then for the first element, matrix $[K^1]$ can be calculated using equation (3.19) or (3.20) depending on the type of elements used. If we define matrix $[K]$ as,

$$[K^e] = \begin{bmatrix} K_{11}^{(e)} & K_{12}^{(e)} \\ K_{21}^{(e)} & K_{22}^{(e)} \end{bmatrix} \tag{3.23}$$

So for M elements, expand matrix $[K^e]$ and $\{u^e\}$ into $M \times M$ matrix and $M \times 1$ vector. For example, for the first element $[K^{(1)}]$ and $\{u^{(1)}\}$ can be given as,

$$[K^{(1)}] = \begin{bmatrix} K_{11}^{(1)} & K_{12}^{(1)} & \dots \\ K_{21}^{(1)} & K_{22}^{(1)} & \dots \\ \vdots & \vdots & \vdots \end{bmatrix} \tag{3.24}$$

and,

$$\{u^{(1)}\} = \begin{pmatrix} u_1^{(1)} \\ u_2^{(1)} \\ \vdots \end{pmatrix} \tag{3.25}$$

The product of equation (3.24) and (3.25) gives,

$$[K^{(1)}]\{u^{(1)}\} = \begin{pmatrix} K_{11}^{(1)}u_1^{(1)} + K_{12}^{(1)}u_2^{(1)} \\ K_{11}^{(1)}u_1^{(1)} + K_{12}^{(1)}u_2^{(1)} \\ \vdots \end{pmatrix} \tag{3.26}$$

For the second element equation (3.26) can be formulated as,

$$[K^{(2)}]\{u^{(2)}\} = \begin{pmatrix} 0 \\ K_{11}^{(2)}u_1^{(2)} + K_{12}^{(2)}u_2^{(2)} \\ K_{11}^{(2)}u_1^{(2)} + K_{12}^{(2)}u_2^{(2)} \\ \vdots \end{pmatrix} \tag{3.27}$$

and repeat the same steps for all M elements. Finally adding this product $[K^{(e)}]\{u^{(e)}\}$ for all elements yields,

$$\sum_{e=1}^{M}[K^{(e)}]\{u^{(e)}\} = \begin{pmatrix} K_{11}^{(1)}u_1^{(1)} + K_{12}^{(1)}u_2^{(1)} \\ K_{21}^{(1)}u_1^{(1)} + K_{22}^{(1)}u_2^{(1)} + K_{11}^{(2)}u_1^{(2)} + K_{12}^{(2)}u_2^{(2)} \\ \vdots \end{pmatrix} \tag{3.28}$$

Now for linear elements, according to the global and local node number convention, $u_1^{(1)} = u_1$, $u_2^{(1)} = u_1^{(2)} = u_2$ and so on as shown in figure 3.4. So from equation (3.28),

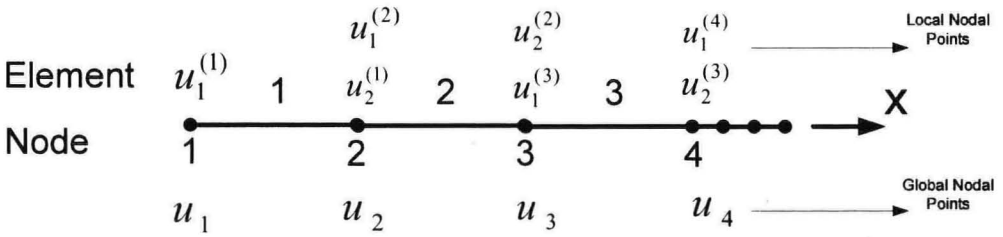

Figure 3.4: Example of the element assembly process

$$\sum_{e=1}^{M}[K^{(e)}]\{u^{(e)}\} = \begin{pmatrix} K_{11}^{(1)}u_1 + K_{12}^{(1)}u_2 \\ K_{21}^{(1)}u_1 + \left(K_{22}^{(1)} + K_{11}^{(2)}\right)u_2 + K_{12}^{(2)}u_3 \\ \vdots \end{pmatrix} \tag{3.29}$$

or it can be rewritten as,

$$\begin{aligned} \sum_{e=1}^{M}[K^{(e)}]\{u^{(e)}\} &= \begin{bmatrix} K_{11}^{(1)} & K_{12}^{(1)} & 0 & 0 & \dots \\ K_{21}^{(1)} & K_{22}^{(1)} + K_{11}^{(2)} & K_{12}^{(2)} & 0 & \dots \\ 0 & K_{21}^{(2)} & K_{22}^{(2)} + K_{11}^{(3)} & K_{12}^{(3)} & \dots \\ \vdots & \vdots & \vdots & \vdots & \vdots \end{bmatrix}\{u\} \\ &= [K]\{u\} \end{aligned} \tag{3.30}$$

where $\{u\} = \{u_1, u_2, u_3, \ldots\}^T$.

Similarly, vector $\{b\}$ is given as,

$$\sum_{e=1}^{M} \{b^{(e)}\} = \begin{pmatrix} b_1^{(1)} \\ b_2^{(1)} + b_1^{(2)} \\ b_2^{(2)} + b_1^{(3)} \\ \vdots \end{pmatrix} \tag{3.31}$$

So the system of equations can be written in a more compact way like this,

$$[K]\{u\} = \{b\} \tag{3.32}$$

3.4.4 Incorporation of Boundary Conditions

Before the system of equations is ready to solve, there is a need to impose boundary conditions on it.

Dirichlet boundary condition

Dirichlet boundary conditions as defined in equation (3.3), $u|_{x=0} = p$ can be accomplished by setting,

$$K_{11} = 1, \qquad b_1 = p, \qquad K_{1j} = 0 \qquad j = 2, 3, 4, ..., N$$

Defining these parameters the system of equations defined in (3.32) becomes,

$$\begin{bmatrix} 1 & 0 & 0 & 0 & \dots \\ K_{21} & K_{22} & K_{23} & K_{24} & \dots \\ K_{31} & K_{32} & K_{33} & K_{34} & \dots \\ \vdots & \vdots & \vdots & \vdots & \end{bmatrix} \begin{pmatrix} u_1 \\ u_2 \\ u_3 \\ \vdots \end{pmatrix} = \begin{pmatrix} p \\ b_2 \\ b_3 \\ \vdots \end{pmatrix} \tag{3.33}$$

After applying boundary condition the system is no longer symmetric. This is no longer desirable because symmetry is a very important property that can be exploited to reduce computer simulation time. To restore symmetry equation (3.33) can be further modified as,

$$\begin{bmatrix} 1 & 0 & 0 & 0 & \dots \\ 0 & K_{22} & K_{23} & K_{24} & \dots \\ 0 & K_{32} & K_{33} & K_{34} & \dots \\ \vdots & \vdots & \vdots & \vdots & \end{bmatrix} \begin{pmatrix} u_1 \\ u_2 \\ u_3 \\ \vdots \end{pmatrix} = \begin{pmatrix} p \\ b_2 - K_{21}p \\ b_3 - K_{31}p \\ \vdots \end{pmatrix} \tag{3.34}$$

So symmetry has been restored without affecting the solution to the system.

Third kind or Neumann boundary condition

Consider equation (3.22), assembly of $[K]$ and $\{b\}$ matrices were already discussed, now consider boundary element vector $\{g\}$.

$$\sum_{e=1}^{M}\{g^{(e)}\} = \begin{pmatrix} g_1^{(1)} \\ g_2^{(1)} + g_1^{(2)} \\ g_2^{(2)} + g_1^{(3)} \\ \vdots \end{pmatrix} \tag{3.35}$$

For one dimensional analysis, the boundary is only at the first and last element, therefore, $\{g\}$ has only two nonzero elements:

$$\{g\} = \begin{pmatrix} -\alpha \frac{\partial u}{\partial z}\Big|_{z=0} \\ \vdots \\ \alpha \frac{\partial u}{\partial z}\Big|_{z=z_{max}} \end{pmatrix} \tag{3.36}$$

For a general problem with N nodes,

$$g_1 = -\alpha \frac{\partial u}{\partial z}\Big|_{z=0} \tag{3.37}$$

$$g_N = \alpha \frac{\partial u}{\partial z}\Big|_{z=z_{max}} \tag{3.38}$$

and $g_i = 0$ for $i = 2, 3, .., N-1$.

3.4.5 Solution to the system of equations

After formulating the problem, the final step of the finite element method is to solve the system of unknowns u_i $(i = 1, 2, 3, ..., N)$. The system of equations form is a

symmetric tridiagonal one, i.e., the matrix has non zero elements K_{ii}, $K_{i,i-1}$ and $K_{i,i+1}$. This formulation yields very large matrices but they are sparse matrices which can be solved efficiently using a computer.

3.5 Two Dimensional Finite Element Analysis

The finite element method is more popular in two dimensional spaces, where the mathematical models of most physical problems are usually so complicated that an analytical or close-form solution is not available. In this thesis finite element analysis was applied for two dimensional tropospheric problems and tunnels. For basic understanding of two dimensional finite element analysis a general two dimensional boundary value problem using a simple linear triangle elements is considered.

Consider a general two dimensional boundary value problem, defined by a second order differential equation as,

$$\nabla^2 u + b = 0 \qquad \text{(y,z)} \in \Omega \tag{3.39}$$

where Ω is the domain and for two dimensional problems operator ∇^2 is given as,

$$\nabla^2 = \frac{\partial^2}{\partial y^2} + \frac{\partial^2}{\partial z^2}$$

The boundary conditions to be considered are given as,

$$u = p \qquad \text{on} \qquad \Gamma_1 \tag{3.40}$$

and

$$\left(\frac{\partial u}{\partial y}\hat{y} + \frac{\partial u}{\partial z}\hat{z}\right).\hat{n} + \gamma u = q \qquad \text{on} \qquad \Gamma_2 \tag{3.41}$$

where $\Gamma = (\Gamma_1 + \Gamma_2)$ denotes the boundary enclosing area Ω, $\hat{n}$ is the outward normal vector coming out from the boundary and γ and q are unknown parameters associated with boundary.

3.5.1 Discretisation and Interpolation

Similar to 1D finite element analysis the first step is to divide whole domain Ω into a number of two dimensional elements. The most commonly used and simple two dimensional elements are triangular elements, which are used in this thesis. A basic requirement for the discretisation is that there should be no overlap and no gap between elements. A good discretisation for triangular elements satisfy the following criteria[52]:

1. Avoid generating narrow elements or triangles having small inner angles.

2. Generate small elements which gives a more accurate solution but increases computational burden, so it is necessary to keep the number of elements to a minimum for a desired accuracy.

In the case of triangular elements, each element is connected with three nodes so a separate set of integers for identification is needed. In this case, there are three

different numbers - the global node number, the local node number and the element number - so it is easy to introduce a $3 \times M$ integer array called a connectivity array. This integer includes all information concerning the numbering of elements and nodes. Along with the connectivity array, another array is needed which relates the segments coincident with boundary with their nodes. This array will be used to facilitate the incorporation of boundary conditions. For Dirichlet boundary conditions, a vector is needed that stores the global numbers of the nodes residing on boundary.

3.5.2 Linear Triangular Elements

After discretisation of the domain Ω, it is necessary to approximate the unknown function u within each element e. If linear triangular elements are assumed the trial or interpolation function within each element is approximated as,

$$u^e(x, y) = a + by + cz \tag{3.42}$$

where a, b and c are constant coefficients to be determined and e denotes element number $e = 1, 2, 3..., M$. For a linear triangular element, there are three nodes located at vertices of the triangle as shown in figure 3.5. In the finite element method it is standard practice that nodes are numbered counterclockwise by numerals 1, 2 and 3 with the corresponding values of u denoted by u_1^e, u_2^e and u_3^e, as shown in figure

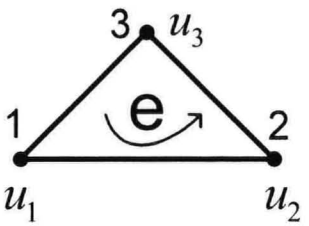

Figure 3.5: Linear Triangular Element

3.5. Enforcing equation (3.42) at the three nodes of element e gives,

$$\begin{aligned} u_1^e &= a + by_1 + cz_1 \\ u_2^e &= a + by_2 + cz_2 \\ u_3^e &= a + by_3 + cz_3 \end{aligned} \tag{3.43}$$

where y_j^e and z_j^e with $j = 1, 2, 3$ denote the coordinate values of the jth node in the eth element. Solve equation (3.43) for a, b and c and putting values back in equation (3.42). This gives,

$$u^e(y, z) = \sum_{j=1}^{3} N_j^e(y, z) u_j^e \tag{3.44}$$

where N_j^e is the shape function and is given by,

$$N_j^e(y, z) = \frac{1}{2\Delta^e} \left(a_j^e + b_j^e + c_j^e\right) \qquad j = 1, 2, 3 \tag{3.45}$$

in which,

$$\begin{aligned} a_1^e &= y_2^e z_3^e - z_2^e y_3^e, & b_1^e &= z_2^e - z_3^e, & c_1^e &= y_3^e - y_2^e \\ a_2^e &= y_3^e z_1^e - z_3^e y_1^e, & b_2^e &= z_3^e - z_1^e, & c_2^e &= y_1^e - y_3^e \\ a_3^e &= y_1^e z_2^e - z_1^e y_2^e, & b_3^e &= z_1^e - z_2^e, & c_3^e &= y_2^e - y_1^e \end{aligned} \tag{3.46}$$

and

$$\Delta^e = \frac{1}{2}\begin{vmatrix} 1 & y_1^e & z_1^e \\ 1 & y_2^e & z_2^e \\ 1 & y_3^e & z_3^e \end{vmatrix} \tag{3.47}$$

is the area of eth element. Two important properties of element shape functions N_j^e are:

1. It can be easily shown from (3.45), (3.46) and (3.47) that interpolation function have the property,

$$N_i^e(y_j^e, z_j^e) = \delta_{ij} = \begin{cases} 1 & i = j \\ 0 & i \neq j \end{cases} \tag{3.48}$$

2. The second important feature of the shape functions is that it vanishes when the observant point (y, z) is on the element side opposite to the jth node. Therefore, the value of u^e at an element side is not related to the value of u at the opposite node, but rather, it is determined by the values at the two endpoints of its associated side. This feature guarantees continuity of the solution across the element side.

3.5.3 Formulation via Galerkin Method (weak form)

By applying the Galerkin method the residual associated with equation (3.39) is,

$$R = \frac{\partial^2 u}{\partial y^2} + \frac{\partial^2 u}{\partial z^2} + b \tag{3.49}$$

and thus the weighted residual for the element e according to the Galerkin method is,

$$R_i^e = \iint_{\Omega^e} N_i^e R \, dy \, dz \tag{3.50}$$

Substituting equation (3.49) in (3.50) yields,

$$R_i^e = \iint_{\Omega^e} N_i^e \left[\frac{\partial^2 u}{\partial x^2} + \frac{\partial^2 u}{\partial z^2} + b \right] dy \, dz \tag{3.51}$$

Now using integration by parts (weak formulation) equation (3.51) yields,

$$R_i^e = - \iint_{\Omega^e} \left[\frac{\partial N_i^e}{\partial y} \frac{\partial u}{\partial y} + \frac{\partial N_i^e}{\partial z} \frac{\partial u}{\partial y} \right] dy \, dz + \iint_{\Omega^e} N_i^e b \, dx \, dy - \oint_{\Gamma^e} N_i^e D.\hat{n}^e \, d\Gamma \tag{3.52}$$

where Γ^e denotes the contour enclosing Ω, $\hat{n}^e$ is the outward unit vector normal to Γ^e and

$$D = \left(\frac{\partial u}{\partial y} \hat{y} + \frac{\partial u}{\partial z} \hat{z} \right) \tag{3.53}$$

Substituting equation (3.44) in (3.53) yields the elemental equation for element e,

$$R_i^e = \sum_{j=1}^{3} \iint_{\Omega^e} - \left[\frac{\partial N_i^e}{\partial y} \frac{\partial N_j^e}{\partial y} + \frac{\partial N_i^e}{\partial z} \frac{\partial N_j^e}{\partial z} \right] u_j^e \, dy \, dz + \iint_{\Omega^e} N_i^e b \, dy \, dz - \oint_{\Gamma^e} N_i^e D.\hat{n}^e \, d\Gamma \tag{3.54}$$

which can be written in matrix form as,

$$\{R^e\} = [K^e]\{u^e\} + \{b^e\} - \{g^e\} \tag{3.55}$$

where the elements in $[K^e]$ are given by,

$$K_{ij}^e = - \iint_{\Omega^e} \left[\frac{\partial N_i^e}{\partial y} \frac{\partial N_j^e}{\partial y} + \frac{\partial N_i^e}{\partial z} \frac{\partial N_j^e}{\partial z} \right] dy \, dz \qquad \text{i,j=1,2,3} \tag{3.56}$$

and those in vector $\{b^e\}$ and $\{g^e\}$ are,

$$b_i^e = \iint_{\Omega^e} N_i^e b \, dy \, dz \qquad \text{i=1,2,3} \tag{3.57}$$

$$g_i^e = \oint_{\Gamma^e} N_i^e D.\hat{n}^e \, d\Gamma \qquad \text{i=1,2,3} \tag{3.58}$$

3.5.4 Assembly of Element Matrices

After calculating thee element matrices and vectors the next step is to sum all element matrices and vectors for all M elements using the stationary condition that the sum of weighted residuals must be zero.

$$\{R^e\} = 0$$

So from equation (3.55),

$$\sum_{e=1}^{M} ([K^e]\{u^e\} + \{b^e\}) = 0 \tag{3.59}$$

remember that boundary condition matrix will be incorporated in the next step. Assume $[K] = \sum_{i=1}^{M}[K^e]$ and $\{b\} = \sum_{i=1}^{M}\{b^e\}$ equation (3.59) can be written in a compact form,

$$[K]\{u\} + \{b\} = \{0\} \tag{3.60}$$

Now to assemble matrix $[K]$ start with a $t \times t$ null matrix, where t is the total number of nodes in the system. Than add individual element matrices $[K^{(1)}]$, $[K^{(2)}]$, $[K^{(3)}]$, ... $[K^{(M)}]$ to the null matrix $[K]$ or in a more concise way the augmented matrices for the elements to $[K]$. To illustrate it in a simple way assume $M = 4$ with

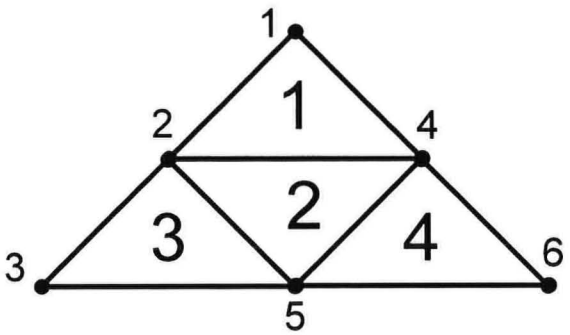

Figure 3.6: Example of sub-division of a two dimensional domain

$t = 6$ as shown in figure 3.6. The connectivity array for this mesh can be given in table 3.1: Elements can be numbered in any way as long as they are numbered

e	n(1,e)	n(2,e)	n(3,e)
1	2	4	1
2	5	4	2
3	3	5	2
4	5	6	4

Table 3.1: Connectivity matrix for mesh given in figure 3.6 ; Obviously, this table is not unique.

counterclockwise. Now, let us consider $K_{11}^{(1)}$ first. Referring to table 3.1, $n(1,1) = 2$, which means that the first local node of the first element corresponds to the second second global node. Since $K_{11}^{(1)}$ relates intersection of this node to itself, it can be added to K_{22}. Next consider $K_{12}^{(1)}$ and again refer to table 3.1 it should be noted that $n(2,1) = 4$, so $K_{12}^{(1)}$ can be simply added to K_{24}. So in short, K_{ij}^{e} can be added to $K_{n(i,e),n(j,e)}$. So following this procedure, adding elemental matrices $[K^{(1)}]$, $[K^{(2)}]$,

$[K^{(3)}]$ and $[K^{(4)}]$ to $[K]$, yields following system matrix,

$$[K] = \begin{bmatrix} [K_{33}^{(1)}] & [K_{31}^{(1)}] & 0 & [K_{32}^{(1)}] & 0 & 0 \\ [K_{13}^{(1)}] & [K_{11}^{(1)}] + [K_{33}^{(2)}] + [K_{33}^{(3)}] & [K_{31}^{(3)}] & [K_{12}^{(1)}] + [K_{32}^{(2)}] & [K_{31}^{(2)}] + [K_{32}^{(3)}] & 0 \\ 0 & [K_{13}^{(3)}] & [K_{11}^{(3)}] & 0 & [K_{12}^{(3)}] & 0 \\ [K_{23}^{(1)}] & [K_{21}^{(1)}] + [K_{23}^{(2)}] & 0 & [K_{22}^{(1)}] + [K_{22}^{(2)}] + [K_{33}^{(4)}] & [K_{21}^{(2)}] + [K_{31}^{(4)}] & [K_{32}^{(4)}] \\ 0 & [K_{13}^{(2)}] + [K_{23}^{(3)}] & [K_{21}^{(3)}] & [K_{12}^{(2)}] + [K_{13}^{(4)}] & [K_{11}^{(2)}] + [K_{22}^{(3)}] + [K_{11}^{(4)}] & [K_{12}^{(4)}] \\ 0 & 0 & 0 & [K_{23}^{(4)}] & [K_{21}^{(4)}] & [K_{22}^{(4)}] \end{bmatrix} \tag{3.61}$$

By using a similar procedure, matrix $\{b\}$ can be assembled as,

$$\{b\} = \begin{pmatrix} b_3^{(1)} \\ b_1^{(1)} + b_3^{(2)} + b_3^{(3)} \\ b_1^{(3)} \\ b_1^{(1)} + b_2^{(2)} + b_3^{(4)} \\ b_1^{(2)} + b_2^{(3)} + b_1^{(4)} \\ b_2^{(4)} \end{pmatrix} \tag{3.62}$$

3.5.5 Incorporation of Boundary Conditions

Dirichlet boundary conditions can be applied in exactly the same way as for the 1D problem, however for the incorporation of the third kind boundary conditions defined in equation (3.41), consider vector $\{g\}$ as given in (3.55), for the mesh shown

in figure 3.6,

$$\{g\} = \begin{pmatrix} g_3^{(1)} \\ g_1^{(1)} + g_3^{(2)} + g_3^{(3)} \\ g_1^{(3)} \\ g_1^{(1)} + g_2^{(2)} + g_3^{(4)} \\ g_1^{(2)} + g_2^{(3)} + g_1^{(4)} \\ g_2^{(4)} \end{pmatrix} \tag{3.63}$$

Using the expression of $\{g_i\}$ given in (3.57) and noting that N_i^e vanishes at the element side opposite node i and internal elements do not contribute to $\{g\}$, only those terms residing on geometry have nontrivial contributions. The final expressions for $\{g\}$ can be written on boundary segments s and $s+1$ as [127]:

$$g_i = b_2^s - \sum_{j=1}^{2} K_{2j}^s u_j^s + b_1^{s+1} - \sum_{j=1}^{2} K_{1j}^{s+1} u_j^{s+1} \tag{3.64}$$

where K_{ij}^s and b_i^s are the same as defined in (3.56) and (3.57) respectively.

3.5.6 Solution to the system of equations

Once the system of equations is assembled and boundary conditions are incorporated, they are ready to solve for unknowns u_i with $i = 1, 2, 3, ..., N$. Many methods are available to solve the system of equations, categorized as direct or iterative methods. In this thesis, only direct methods are considered and the system of equations is solved using Matlab solver using sparse matrix techniques.

3.6 Finite element programming in Matlab (An Overview)

Matlab is an interactive software which is widely used in various areas of engineering and scientific applications. The power of Matlab is represented by the length and simplicity of the code. For example, one page of matlab code may be equivalent to many pages of other computer language source codes. Matlab is a useful tool for vector and matrix manipulations. The finite element method is a well defined candidate for which Matlab can be very useful as a solution tool.

A simple two dimensional finite element program in Matlab need only be a few hundred lines of code whereas in Fortran or C++ one might need a few thousand. It should be noted that the built-in Matlab functions are already compiled and are extremely efficient and should be used as much as possible. Keeping the slow down due to the interpretive nature of Matlab in mind, one programming construct that should be avoided at all costs is the for loop, especially nested for loops. These can make a Matlab programs run time orders of magnitude longer than may be needed, especially in finite element programming where large size of matrices are used. Often for loops can be eliminated using Matlab's vectorised addressing.

3.6.1 Section of a Typical Finite Element Programs

A typical finite element program consists of the following sections.

1. Define constants and allocate space for larger matrices
2. Generate mesh using some meshing algorithm or software
3. Calculate nodal and element connectivity matrices
4. Calculate element matrices and vectors for every element
5. Assemble element matrices and vectors into system matrices and vectors
6. Enforce boundary conditions
7. Solve the matrix equation for the primary nodal variables
8. Compute secondary variables (if any) and quantities
9. Plot and/or print desired results

Input Data

Major input parameters for finite element analysis program are:

- total number of nodes in the system,
- total number of elements in the system,
- coordinates of each node,
- type of all elements,
- governing equation and boundary conditions

Determination of the total nodes and number of elements are directly related with a mesh. Meshes can either be generated manually in Matlab or using some commercial mesh generation matlab codes [125]. Type of element determines the number of nodes per element as well as how many degrees of freedom for each node of the element. It is possible to define different types of element in this case this information is needed for every type of element. The node coordinates are stored in the nodal coordinate matrix. Another data structure is defined in which coordinates of each node is stored. These two matrices are linked with each other. Element definitions are stored in the element connectivity matrix. This is a matrix of node numbers where each row of the matrix contains the connectivity of an element. It should be noted that element connectivities are all ordered in a counter-clockwise fashion, if this is not done then some Jacobian's will be negative and thus cause the system matrix to be singular, which is obviously wrong.

In the finite element method boundary conditions are used to either form a force vector (natural or Neumann) or to specify the value of an unknown field on a boundary (essential or Dirichlet). In either case a definition of boundary is needed. Two more vectors are needed to define constraints nodes and their values. In the case of flux boundary conditions, an additional element matrix is added in the element equations as described earlier in section 3.4.4.

Assembly of Element Matrices and Vectors

After having defined all element nodes and their respective coordinates, element vectors and matrices need to be calculated. Element matrices and vectors can be calculated based on Galerkin weak formulation or variational principles of system equations. Once these matrices and vectors are computed, they need to be assembled into the system matrix and vector. To this end information on where the element matrix and vector are to be located in the system matrix and vector is needed. For this purpose another array is defined which contains this information.

3.7 Summary

This chapter has considered the general formulation of the finite element method. Various aspects of the implementation of the method have been considered including domain discretisation, shape functions and Galerking formulation. This chapter describes 1D and 2D finite element solutions of a simple boundary value problem. Finally an overview of finite element programming using Matlab is given. This chapter forms the basis of the work described in subsequent chapters of this thesis.

Chapter 4

Radio Wave Propagation Modelling using Finite Element Method in the Troposphere

4.1 Introduction

The troposphere which forms the lowest layer of atmosphere extends from the earth's surface upto several km. Long range electromagnetic wave propagation in the near-horizon direction is mainly dependant on the spatial distribution of refractive index which in turn, depends on pressure, temperature and water vapours in air [128]. Spatial distribution of refractive index in the air affects the propagation of electromagnetic waves in the troposphere. The path of the wave is bent and this bending

depends on the fluctuation of the vertical gradient of refractivity. The tropospheric refractive index is frequency independent so the lower parts of the atmosphere affect the radiowave propagation in a wide frequency range, from VHF to optical frequencies, whereas, abnormal environmental conditions can end up to ducting phenomena as describe later in section 4.2.

The modelling of radio wave propagation through the troposphere has been extensively studied, and nowadays a great number of reliable models are in use, for reference see chapter 2. Solution of electromagnetic propagation problems in the lower part of atmosphere is a complicated matter. Variations in refraction and terrain make the solution of the full vector problem extremely difficult. The problem can be simplified by assuming symmetry in one or more of the coordinate directions, the vector problem then can be uncoupled into two scalar problems [72]. In this thesis the parabolic approximation method is used to simplify the solution of wave propagation in the troposphere and then solve by using the finite element method. A method to model tropospheric electromagnetic wave propagation where the refractivity is a function of height is presented in this chapter using the finite element method (FEM). The versatility and accuracy of the FEM as compared with other methods in the solution of EM wave propagation problems in certain areas such as photonic device design has been well established [13, 129]. In this thesis finite element analysis is extended to the solution of parabolic approximation in the troposphere. Using the finite element method the solution is computed at some initial

range and then advanced in the propagation direction using the marching algorithm. Vertical tropospheric profile characteristics are assigned to every mesh element, while the solution advances in small variable range steps, each excited by solution of the previous step.

The remainder of this chapter is organised as follows; brief description of refractivity and ducting in the troposphere is first presented. A model of wave propagation in the troposphere along with earth flattening transformation is described with its finite element formulation. Both narrow and wide angle versions of the parabolic equation is considered with boundary conditions and initial field distribution. Finally, results and discussions are presented along with a summary.

4.2 Refractivity and Tropospheric Ducting

The lower part of the troposphere affects radio wave propagation in a number of ways. Among them a special case is clear air propagation mechanisms related to the refractive index variations caused by temperature and water vapour changes. Spatial changes of refractive index is larger with height than with range and generally the range variations can be neglected [130].

For practical purposes, the real measurements are replaced by different modified refractivity profiles, which account for the average behaviour of refractive index profiles. To a very good approximation, the real part of the radio refractive index

is given by Debye formula [128],

$$n = 1 + 77.6 \times 10^{-6} \frac{p}{T} + 0.373 \frac{e}{T^2} \tag{4.1}$$

where p is the atmospheric pressure in millibar, e is the water vapor pressure in millibars and T is the temperature in Kelvin.

Near the earth's surface its value is close to unity and hence a more practical value, the refractivity is normally used [1];

$$N = 10^6 \times (n - 1) \tag{4.2}$$

$$= N_0 \times e^{-z/h_0} \tag{4.3}$$

where N_0 is the refractivity at sea level and z is the height above sea level in kilometers. Refractivity is defined in N-units. Refractivity gradient is one of the important parameters used to define different meteorological conditions and is defined as $\frac{\partial N}{\partial z}$. Under standard atmospheric conditions as defined by the ITU the value of refractivity gradient is -39.6 N-units/km. The nonstandard troposphere conditions cause anomalous propagation called anaprop; that is, rays bend upward (subrefraction) or downward (superrefraction or ducting) to the earth surface in a way that is different from the standard. This leads to highly variable propagation conditions which significantly affects a radio propagation link. Effects of refractive gradients on ray bending can be approximated as [15]:

$$\rho = -\frac{1}{\partial n / \partial z} \tag{4.4}$$

Tropospheric ducting occurs when the gradient $\frac{\partial N}{\partial z} < -157$ N-units/km, allows only waves above the cut off point to propagate [27]. The main cause of ducting is abrupt changes in refractive index of the medium. Standard atmosphere parameters are defined in table 4.1.

Parameter	Value(s)
Refractivity at sea level, N_0	315 N-units
Reference Hight, h_0	0.136 km
Refractivity gradient, $\frac{\partial N}{\partial z}$	-39.6 N-units/km

Table 4.1: Reference atmosphere as defined by ITU [1]

4.3 Mathematical modelling of wave propagation in the troposphere

The efficacy of the PEM in solving tropospheric propagation problems is well known [33]. A detailed description of the parabolic equation method has already been presented in chapter 2. The following analysis starts from the standard parabolic equation (SPE) in 2 dimensions as given in equation 2.6:

$$j2k_0\frac{\partial u(x,z)}{\partial x} + \frac{\partial^2 u(x,z)}{\partial z^2} + k_0^2(n^2(x,z)-1)u(x,z) = 0 \tag{4.5}$$

where k_0 is the free space wavenumber, $u(x,z)$ is the unknown electric or magnetic field depending on polarization and $n(x,z)$ is the refractive index of the troposphere.

4.3.1 Earth Flattening Transformation

In long-distance propagation scenarios, the effect of the Earth's curvature must be considered. To this end, although the final numerical calculations are conducted in a cartesian coordinate system, the problem is normally formulated in a spherical coordinate system (r, ϕ, θ), with the origin located at the earth's center. An earth flattening transformation is then used to map the resulting equations onto a cartesian coordinate system. The simplified PE problem is formulated in terms of a scalar parabolic equation governing the field components E_y for horizontal and H_y for vertical polarisation. With this approximation solution is valid at low heights, provided if refractive index is replaced with modified refractive index $m(x, z)$ using conformal transformation [27].

$$m(x, z) = n(x, z)\left(1 + \frac{z}{R}\right) \tag{4.6}$$

where R is the radius of earth. Modified refractivity M is given as,

$$M = (m - 1) \times 10^6 \tag{4.7}$$

and is expressed in M-units. After substituting equation (4.6) in (4.5), it becomes,

$$j2k_0\frac{\partial u(x, z)}{\partial x} + \frac{\partial^2 u(x, z)}{\partial z^2} + k_0^2\left(n^2(x, z) - 1 + \frac{2z}{R}\right)u(x, z) = 0 \tag{4.8}$$

The wave propagation model based on PE as defined in equation (4.8) is subject to a terrain boundary condition, which represents the relationship that must hold between the field $u(x, z)$ and terrain (e.g. ground). Note from equation (4.8) that

the earth curvature enters only through the $\frac{2z}{R}$ term; if this term is ignored, the equation (4.8) describes propagation over a flat earth.

4.3.2 Path Loss and Propagation Factor

In tropospheric radiowave propagation, results are normally expressed in terms of path loss or propagation factor. According to the International Telecommunications Unit (ITU), path loss $L(x,z)$ is defined as the ratio between the power radiated by the transmitting antenna and the power which would be available at the receiving antenna if there were no losses in the radio frequency circuit [1]. Path loss and propagation factors are normally expressed in decibels. Path loss in terms of the transformed PE field $u(x,z)$ is given by [27]:

$$L(x,z) = -20\log|u(x,z)| + 20\log(4\pi) + 10\log\left(R\sin\frac{x}{R}\right) - 30\log(\lambda) \tag{4.9}$$

where λ is the wavelength. Propagation factors F is given as,

$$F(x,z) = 20\log|u(x,z)| - 10\log(x) - 10\log(\lambda) \tag{4.10}$$

Both path loss L and propagation factor F are expressed in decibels.

4.3.3 Boundary Conditions

In the two dimensional tropospheric propagation problem, there are two boundaries, one at the starting height, $z = z_{min}$ which in fact is the Earths surface at height

0, and at the maximum altitude considered, $z = z_{max}$. The bottom boundary of the domain in radiowave propagation problems is physical ground often assumed as perfectly conducting ground or represented by a surface boundary impedance condition. Although the perfectly conducting ground model is adequate for many applications, it is not universally applicable. A more accurate model is required for ground wave propagation to consider different parameters of ground including its permittivity ϵ and conductivity σ. The top boundary is a computational artifact needed to limit the integration domain in height.

Perfectly Matched Layer

When numerical propagation simulations are performed, infinite propagation domains cannot be realised and the size of the propagation domain must be truncated. This is accomplished numerically by implementing absorbing boundary conditions or Perfectly Matched Layer (PML) on the upper boundary at $z = z_{max}$ in 2D analysis and on the upper and on two vertical sides of the propagation domain in the case of 3D PEM analysis. The perfectly matched layer has to be applied to reduce the effects of any possible reflections and allow for the propagation of the signal. The domain in the 2D case is illustrated in figure 4.1. The propagation model defined in equation (4.8) is an ordinary differential equation in range x and we can solve it as an initial value problem with respect to x i.e. an initial condition is needed at initial range $x = 0$. In other words initial distribution of the electric or magnetic

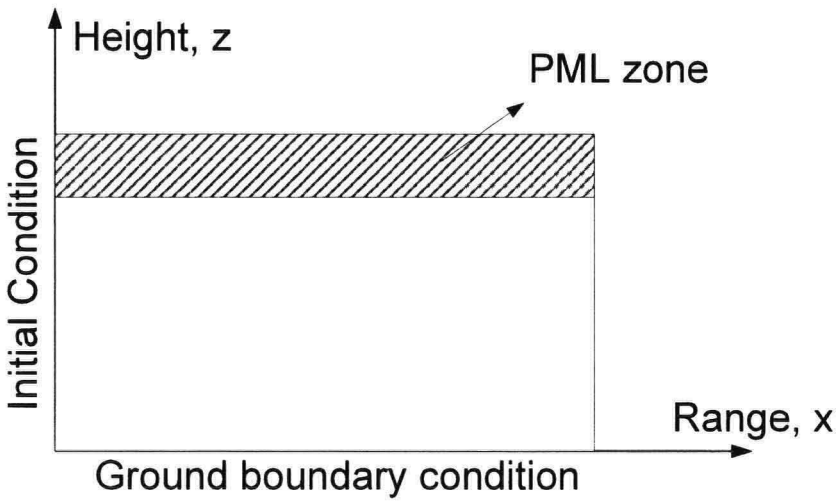

Figure 4.1: 2D Illustration of Domain

field is required.

At the top of the domain, a perfectly matched layer (PML) zone is assumed to terminate the grid as shown in figure 4.1. PML is a relaxation zone with a specified number of layers or grid points where the solution can be efficiently damped. In order to incorporate the perfectly matched layer an additional term is added to equation (4.8) which will act as damping factor to give [131],

$$j2k_0\frac{\partial u(x,z)}{\partial x}+\frac{\partial^2 u(x,z)}{\partial z^2}+k_0^2\left(n^2(x,z)-1+\frac{2z}{R}\right)u(x,z)+jk_0\bar{\eta}u(x,z)=0 \quad (4.11)$$

$\bar{\eta}$ is varied only in the PML zone and outside the zone it will be zero. So outside the PML zone equation (4.11) will become (4.8). In short,

$$\begin{cases} \bar{\eta}=0 & \text{when } z\leq z_b \\ \bar{\eta}>0 & \text{when } z>z_b \end{cases}$$

where z_b is the threshold height, the PML zone starts for $z > z_b$. Many methods

have been proposed to calculate the damping coefficient $\bar{\eta}$ in the literature [132]. One simple approach to implement PML is to calculate the damping coefficient η_0 in the first PML layer then the damping coefficient in ith layer is given by,

$$\eta_i = \eta_0 \frac{\gamma^{i-1}}{h_i} \tag{4.12}$$

where γ is a constant and h_i is the thickness of ith PML layer. Quantity η_0 can be calculated by an empirical type of formula,

$$\eta_0 = log\frac{1}{R}.\frac{c}{D} \tag{4.13}$$

where R is the reflection coefficient, D is the thickness of the PML zone and c is some typical velocity. However, it should be noted that the formula for calculating $\bar{\eta}$ is empirical and in the literature it is stated that numerical experimentation is needed in order to obtain a reasonable damping of the field [133].

Surface Impedance Boundary Condition

An impedance type of boundary condition is used to account for the finite conductivity of the surface of the earth. The entrance boundary conditions are expressed by the equation [26]:

$$\left[\frac{\partial u(x,z)}{\partial z} + qu(x,z)\right]_{z=z_{max}} = 0 \tag{4.14}$$

where,

$$q = q_v = \frac{jk_0}{\sqrt{\varepsilon_r - j60\sigma\lambda}} \tag{4.15}$$

$$q = q_h = jk_0\sqrt{\varepsilon_r - j60\sigma\lambda} \tag{4.16}$$

for vertical and horizontal polarisation respectively. ε_r is the complex relative permittivity and σ is the conductivity of ground whereas λ is the wavelength of the radio waves in meters.

4.3.4 Initial Field

Source modelling capabilities have been developed in this section to model accurately pattern and the altitude of a transmitting antenna. Starting or initial field simulate the field of any antenna. In this thesis a normalised gaussian pattern is used in which the initial field $u(0, z)$ can be written as [134],

$$u(0, z) = [A(z - H_0) - \bar{A}(z + H_0)] \tag{4.17}$$

where H_0 represents the antenna height and bar denotes complex conjugate. The Fourier transform of $A(z)$ is given as,

$$a(\zeta) = e^{-\zeta^2 w^2/4}, \tag{4.18}$$

where w is defined as,

$$w = \frac{\sqrt{2 \ln 2}}{k_0 \sin \frac{\theta_{bw}}{2}} \tag{4.19}$$

In equation (4.19), $\sin \frac{\theta_{bw}}{2}$ is the sine of 3dB beamwidth. The same antenna pattern is also used in commercially available refractive effects prediction software AREPS [135]. So the inverse Fourier transform of equation (4.18) can be calcu-

lated as:

$$A(z) = \sqrt{\frac{2}{w}}\, e^{\frac{-2\pi z^2}{w}} \tag{4.20}$$

So from equation (4.17) the initial field is given as,

$$u(0,z) = \sqrt{\frac{2}{w}} \left(e^{\frac{-2\pi(z-H_0)^2}{w}} - e^{\frac{-2\pi(\bar{z}+H_0)^2}{w}} \right) \tag{4.21}$$

4.4 Finite Element Formulation of the Problem

In this section the finite element formulation of the model is developed using concepts built in chapters 2 and 3. Both formulations of the parabolic equation will be considered: narrow angle as well as wide angle formulation.

4.4.1 Narrow Angle FEM formulation

The analysis to follow starts from the parabolic approximation model defined in equation (4.8), where z is transverse direction represents height and x represents the range direction using the beam propagation marching algorithm. Field $u(x,z)$ is propagating in range direction x. By applying the FEM, the domain $z_{min} \leq z < z_{max}$ is divided into a number of small elements and within each element e the domain is defined as $\bar{z}$. By using a suitable interpolation function $u^e(z)$ within each element domain $\bar{z}$ the interpolation function can be written as,

$$u^e(z) = \begin{bmatrix} H_1 & H_2 \end{bmatrix} \{u\} \tag{4.22}$$

where H_1 and H_2 are basis functions or shape functions and for linear elements they are defined by equation (3.10). For quadratic elements shape functions are given in appendix 2. To simplify the analysis a shape function vector $\{N\}$ is defined as,

$$\{N\} = \begin{bmatrix} H_1 & H_2 \end{bmatrix} \tag{4.23}$$

Assume w as a weighting function, so the weighted residual of equation (4.8) for an element e is given as,

$$\int_{\bar{z}} w.j2k_0 \frac{\partial u^e(x,z)}{\partial x}\, d\bar{z} + \int_{\bar{z}} w.\frac{\partial^2 u^e(x,z)}{\partial z^2}\, d\bar{z} + \int_{\bar{z}} w.k_0^2 \left(n^2(x,z) - 1 + \frac{2z}{R}\right) u^e(x,z)\, d\bar{z} = 0 \tag{4.24}$$

By using the Galerkin method,

$$w = \{N\}^T = \begin{bmatrix} H_1 \\ H_2 \end{bmatrix} \tag{4.25}$$

Using a weak formulation of the Galerkin method and substituting equation (4.25) in (4.24) yields,

$$\int_{\bar{z}} j2k_0 \{N\}^T\{N\} \frac{\partial\{u\}}{\partial x}\, d\bar{z} - \int_{\bar{z}} \{\acute{N}\}^T\{\acute{N}\}\, d\bar{z}\{u\} + k_0^2 \int_{\bar{z}} \{N\}^T\{N\} \left(n^2 - 1 + \frac{2z}{R}\right)\{u\}\, d\bar{z} = 0 \tag{4.26}$$

It should be noted that the equation (4.26) is defined for an element e such that $e \neq \{1, M\}$ where M is the total number of elements. For the boundary elements another term incorporating boundary conditions should be added in equation (4.26).

In equation (4.26), $\{\acute{N}\}$ is defined as,

$$\{\acute{N}\} = \frac{\partial\{N\}}{\partial z}$$

Define two matrices $[M]$ and $[K]$,

$$[M] = \sum_e \int_{\hat{z}} \{N\}^T\{N\}\, d\hat{z} \tag{4.27}$$

$$[K] = \sum_e \int_{\hat{z}} \left(k_0^2 \left[n^2 + \frac{2z}{R} \right] \{N\}^T\{N\} - \{N\}^T\{N\} - \{\acute{N}\}^T\{\acute{N}\} \right) d\hat{z} \tag{4.28}$$

Note that matrices $[M]$ and $[K]$ are not element matrices, they are infact the summation of all the element matrices over the whole domain. Now consider equation (4.26) for the whole domain $z_{min} \leq z < z_{max}$ and substitute $[K]$ and $[M]$ it becomes,

$$j2k_0[M]\frac{\partial\{u\}}{\partial x} + [K]\{u\} - k_0^2[M]\{u\} = 0 \tag{4.29}$$

Finite Element Algorithms

Equation (4.29) can be solved numerically using one of a variety of methods. Most of the solution methods rely on range stepping algorithms where the range x is divided into a succession of discrete steps. Instead of seeking a solution over the entire domain, approximate solutions are sought at the defined steps starting with an initially known solution at zero range i.e. $x = 0$. The solution at the ith step is computed from a recurrence relation, that is an algebraic equation that relates the solutions at two or more successive steps. All of these methods depends on approximating derivatives the same as the finite difference methods descried in

section 2.2.2. In such a scheme, the finite element method is used in the transverse direction while the finite difference method is used in the axial direction. In a number of methods the Crank-Nicolson method is used because of its stability and accuracy.

Crank-Nicolson method The first order x derivative of the field $u(x,z)$ can be approximated at range instant $\left(x+\frac{\Delta x}{2}\right)$ like,

$$\frac{\partial u}{\partial x}\Big|_{x+\frac{\Delta x}{2}} = \frac{\{u\}^{x+\Delta x}-\{u\}^{x}}{\Delta x} \tag{4.30}$$

and field $u(x,z)$ at range $\left(x+\frac{\Delta x}{2}\right)$ is given by,

$$\{u\}\Big|_{x+\frac{\Delta x}{2}} = \frac{\{u\}^{x+\Delta x}+\{u\}^{x}}{2} \tag{4.31}$$

Put equation (4.30) and (4.31) in equation (4.29) at some intermediate range $\left(x+\frac{\Delta x}{2}\right)$ yields,

$$-j2k_0[M]\frac{\{u\}^{x+\Delta x}-\{u\}^{x}}{\Delta x} = \left([K]-k_0^2[M]\right)\left[\frac{\{u\}^{x+\Delta x}+\{u\}^{x}}{2}\right] \tag{4.32}$$

which can be written in a simplified form as,

$$[A]\{u\}^{x+\Delta x} = [B]\{u\}^{x} \tag{4.33}$$

where $[A]$ and $[B]$ are given as,

$$[A] = -j4k_0[M]-\Delta x\left\{[K]-k_0^2[M]\right\} \tag{4.34}$$

$$[B] = -j4k_0[M]+\Delta x\left\{[K]-k_0^2[M]\right\} \tag{4.35}$$

is the final formulation of the propagation equation in the troposphere.

4.4.2 Wide Angle FEM Formulation

For the wide angle finite element formulation of PE consider the wide angle parabolic equation with earth flattening transformation,

$$\frac{\partial^2 u(x,z)}{\partial x^2} + j2k_0\frac{\partial u(x,z)}{\partial x} + \frac{\partial^2 u(x,z)}{\partial z^2} + k_0^2\left(n^2(x,z) - 1 + \frac{2z}{R}\right)u(x,z) = 0 \quad (4.36)$$

Using the same procedure as for the narrow angle FEM formulation of PE, choose an interpolation function and then by using the weak formulation of Galerkin method, matrix equation for the system can be defined as,

$$[M]\frac{\partial^2\{u\}}{\partial x^2} + j2k_0[M]\frac{\partial\{u\}}{\partial x} + [K]\{u\} - k_0^2[M]\{u\} = \{0\} \quad (4.37)$$

where matrices $[M]$ and $[K]$ are defined in equation (4.27) and (4.28) respectively. Rewrite equation (4.37) as,

$$j2k_0[M]\frac{\partial\{u\}}{\partial x} = -\frac{[K] - k_0^2[M]}{1 + \frac{1}{j2k_0}\frac{\partial}{\partial x}}\{u\} \quad (4.38)$$

Using the Pade approximation [46],

$$\frac{\partial}{\partial x} \approx \frac{1}{j2k_0}\left\{[K] - k_0^2[M]\right\} \quad (4.39)$$

Substituting equation (4.39) in (4.38). After simplification it gives,

$$j2k_0[M]\frac{\partial\{u\}}{\partial x}\left\{4k_0^2[M] - [K] + k_0^2[M]\right\} + 4k_0^2[M]\left\{[K] - k_0^2[M]\right\}\{u\} = \{0\}$$

which can be further simplified as,

$$-j2k_0\left\{[M] - \frac{[K] - k_0^2[M]}{4k_0^2}\right\}\frac{\partial\{u\}}{\partial x} = [K]\{u\} - k_0^2[M]\{u\} \quad (4.40)$$

Define $[\tilde{M}]$ as,

$$[\tilde{M}] = [M] - \frac{[K] - k_0^2[M]}{4k_0^2} \tag{4.41}$$

equation (4.39) will become,

$$-j2k_0[\tilde{M}]\frac{\partial\{u\}}{\partial x} = [K]\{u\} - k_0^2[M]\{u\} \tag{4.42}$$

which is the same as equation (4.29) with matrix $[M]$ replaced with $[\tilde{M}]$ in the first term. So at range step $x + \frac{\Delta x}{2}$ equation (4.42) can be written as,

$$-j2k_0[\tilde{M}]\frac{\partial\{u\}}{\partial x}\Big|_{x+\frac{\Delta x}{2}} = \left\{[K] - k_0^2[M]\right\}\{u\}^{x+\frac{\Delta x}{2}} \tag{4.43}$$

Again using the Crank-Nicolson approximation scheme, defined in equation (4.30) and (4.31),

$$-j2k_0[\tilde{M}]\frac{\{u\}^{x+\Delta x} - \{u\}^x}{\Delta x} = \left([K] - k_0^2[M]\right)\left[\frac{\{u\}^{x+\Delta x} + \{u\}^x}{2}\right] \tag{4.44}$$

which can be written in a simplified form as,

$$\Big\{-j4k_0[\tilde{M}] - \Delta x\big\{[K] - k_0^2[M]\big\}\Big\}\{u\}^{x+\Delta x} = \Big\{-j4k_0[\tilde{M}] + \Delta x\big\{[K] - k_0^2[M]\big\}\Big\}\{u\}^x \tag{4.45}$$

4.5 Results and Discussions

In this section results for 2D and 3D finite element solutions of the parabolic equation method will be presented. Coverage diagrams and path loss diagrams are calculated

at different frequencies and under different environmental conditions. Initially start with standard atmospheric conditions and then consider some abnormal conditions yielding ducting phenomenon in the troposphere. In this section, coverage diagrams, path loss contours and different power plots at receiver height and different values of ranges will be investigated.

To demonstrate the efficacy of the present approach a number of simulations were carried out with various frequencies and media profiles. In all of the simulations the following assumptions were made unless stated otherwise. A transmitting antenna of height $H_0 = 150$m above sea level with a 3dB-beam width $\theta_{\text{bw}} = 2^\circ$ and vertical polarisation of the propagating wave is assume. Gaussian beam patterns as describe in section 4.3.4 were used because they have excellent numerical properties as well as providing a good representation for paraboloid dish antennas [27]. The wide angle formulation of the parabolic equation method is used in simulations until stated otherwise. The natural infinite domain of the troposphere can not be realised so perfectly matched layer is used along with boundary conditions as described in section 4.3.3. Transverse direction is assumed to be along z axis while propagation direction is x throughout in simulations, as shown in figure 4.3. Other simulation parameters use in this section are summarised in table 4.5.

Quadratic type line finite elements are used for better accuracy with length of $\lambda/10$ until stated otherwise. Different values of range step Δx were picked somewhere in between 25 and 180m. If a smaller Δx is choosen, the computation takes longer and

Parameter	Value(s)
Tx Antenna Height	150m
Tx Antenna Gain	43.5dB
Rx Antenna Height	150m
Antenna 3dB bandwidth	2°
Ground Conductivity	0.01mho/m
Ground Permittivity	15
PML zone	300m
No. of PML Layers	3
Reflection Coefficient in PML	10^{-4}
Damping Factor	0.5
Tropospheric Duct Height	300
Antenna Polarisation	Horizontal or Vertical
Frequency of Waves	100MHz - 3GHZ

Table 4.2: Simulation Parameters used to model radio wave propagation in the troposphere

more computational resources will be needed. On the other hand for a larger Δx, the computation is accelerated but some significant atmosphere changes might be missed and more error will occur in the simulation results. Therefore, Δx should be optimally choosen accordingly for each problem. However, it is possible to choose Δx and element size having variable lengths in one simulation.

Figure 4.2 shows the dependence of refractivity on height under standard atmospheric conditions as defined by the International Telecommunications Union (ITU). Atmospheric conditions can be entered into the computer program as profiles of refractivity-height data where refractivity N is related to refractive index n as $N = (n - 1) \times 10^6$ (see section 4.2). From the way the program accepts environmental data it is clear that any measured environmental data can easily be entered

into program without any extra computational burden. In cases where horizontally inhomogeneous conditions needs to be modelled, different refractivity profiles can be entered at several ranges, and the program can perform linear interpolation in range and height for use at intermediate calculation positions. Modelling ground

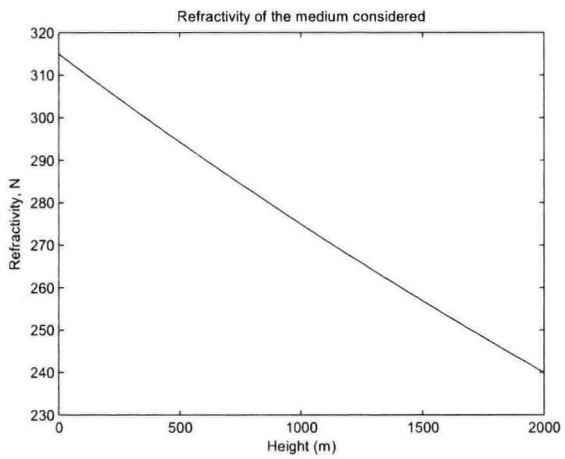

Figure 4.2: Standard Atmospheric Profile

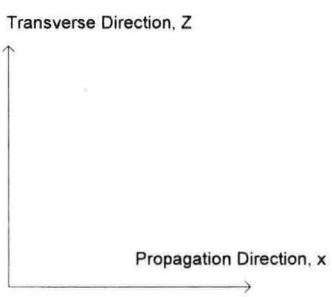

Figure 4.3: Direction Convention used in Simulations

wave propagation for upward propagated waves is a challenging signal processing task. As discussed earlier in section 4.3.3 the upper boundary should be truncated for proper termination of grid or domain. This can be accomplished numerically

by implementing an absorbing boundary condition on the upper boundary or using a perfectly matched layer (PML) as described in section 4.3.3. Effective absorption within PML block depends on the number of PML layers and artificial PML medium parameters. Figure 4.4 presents the coverage diagram of transmitting antenna operating at 100MHz for standard atmospheric conditions with and without PML.

As can be seen from figure 4.4 without the implementation of PML the waves get reflected from the upper boundary however; when a perfectly matched layer (PML) boundary is implemented these reflections are eliminated.

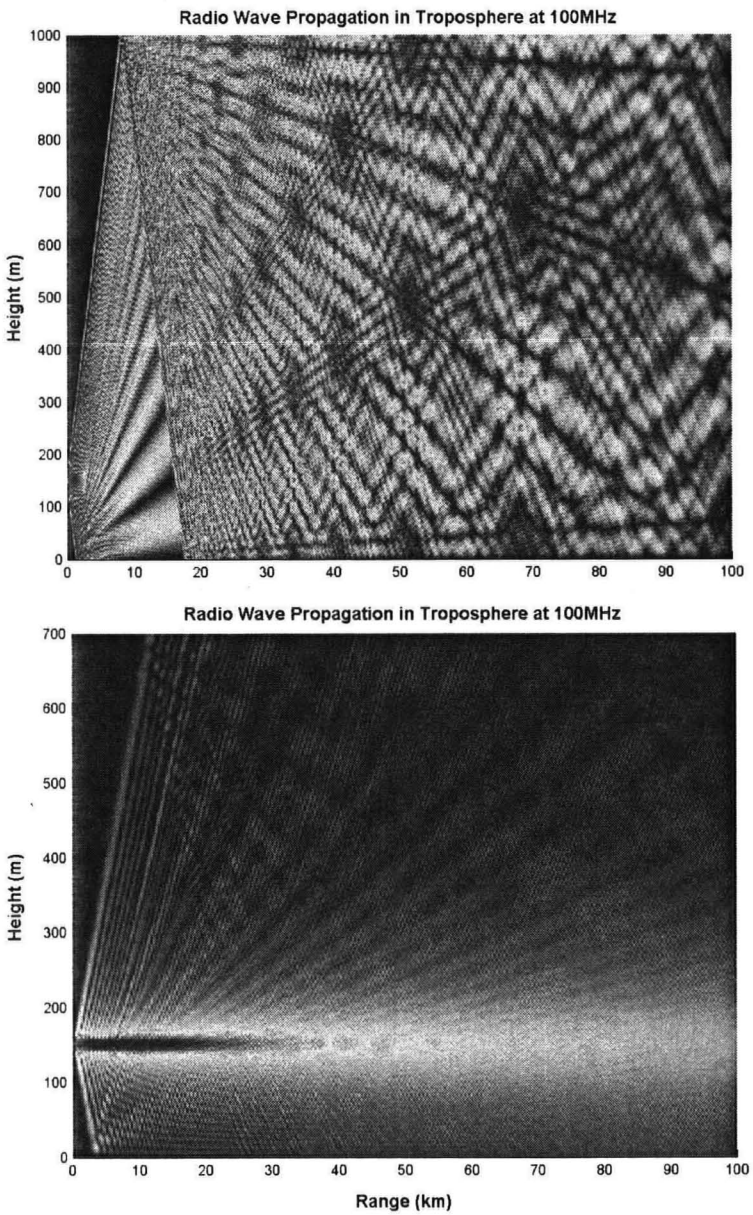

Figure 4.4: Coverage diagram without and with PML at 100MHz

One advantage of the FEM over other methods such as the ray tracing techniques, is that one can incorporate frequency through the wavenumber $k = \frac{2\pi}{\lambda}$ in the simulations. Figure 4.5(a) and 4.5(b) shows the coverage diagram of a transmitting antenna at 500MHz and 1GHz. It can be quite clearly seen, that this diagram is different from that of figure 4.4 at 100MHz. A ray tracing technique would have produced exactly the same results.

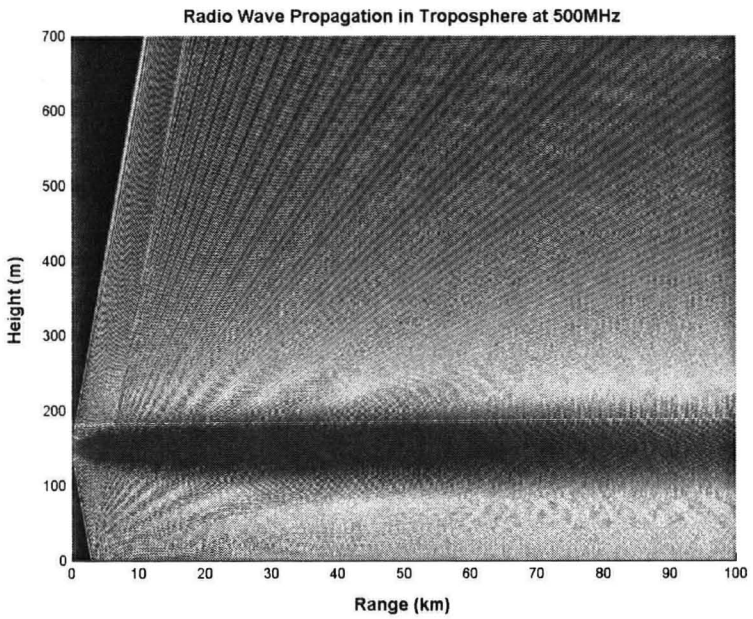

(a) 500MHz

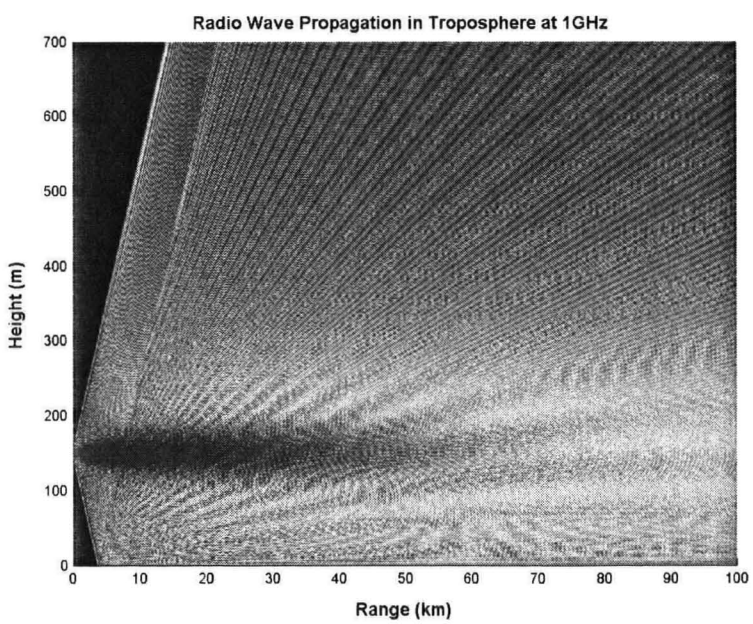

(b) 1GHz

Figure 4.5: Coverage diagram with of antenna with transmission at 500MHz and 1GHz

Path loss is also computed at various frequencies in the lowest part of the troposphere and range-height displays are shown in figures 4.6(a) and 4.6(b). These results show how the path loss changes with height and range at different frequencies. In order to demonstrate it more clearly path loss is plotted versus range at receiver height. To validate the proposed approach results were compared to those obtained by a commercially available software package Advanced Refractive Effects Prediction System (AREPS) [135]. The Advanced Refractive Effects Prediction System (AREPS) program computes and displays a number of tactical decision aids for the assessment of electromagnetic system performance. The internal propagation model used by AREPS is the Advanced Propagation Model (APM). This is a hybrid model that consists of four sub models: flat earth, ray optics, extended optics and split-step parabolic equation. However AREPS has its own limitations, a good discussion about AREPS limitations is given in [136]. From figure 4.7(a) to 4.7(c) an excellent agreement in results can be shown and error in path loss values is less than 3dB. For comparison, the FEM results are offset by 5dB for clarity. Path loss at receiver height increases with range at all frequencies and almost a similar pattern is observed.

Path loss versus height at 50km range is plotted in figure 4.8 at various frequencies. Note the interference that resulted from the reflection of the lower end of the main beam. At 50km from the transmitting antenna it is clear that path loss increases with increasing frequency. A fluctuating behaviour of path loss is observed with

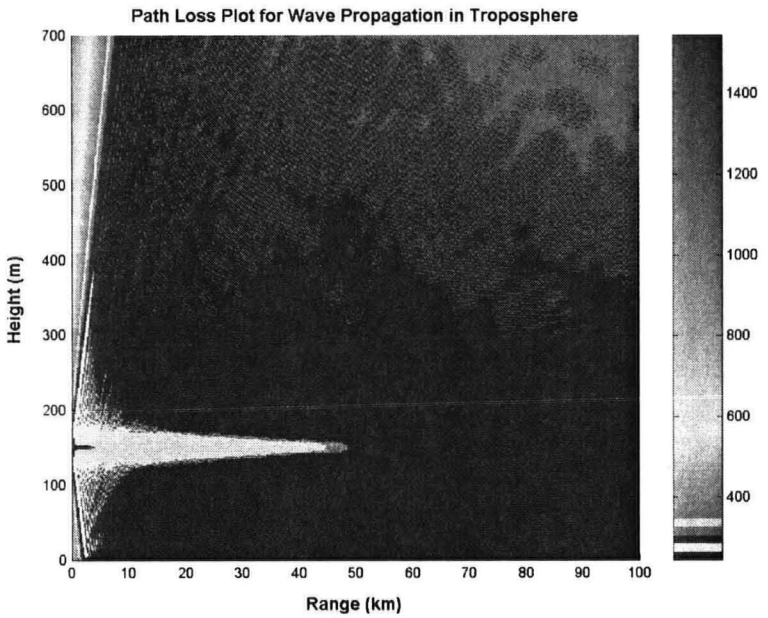

(a) 100MHz

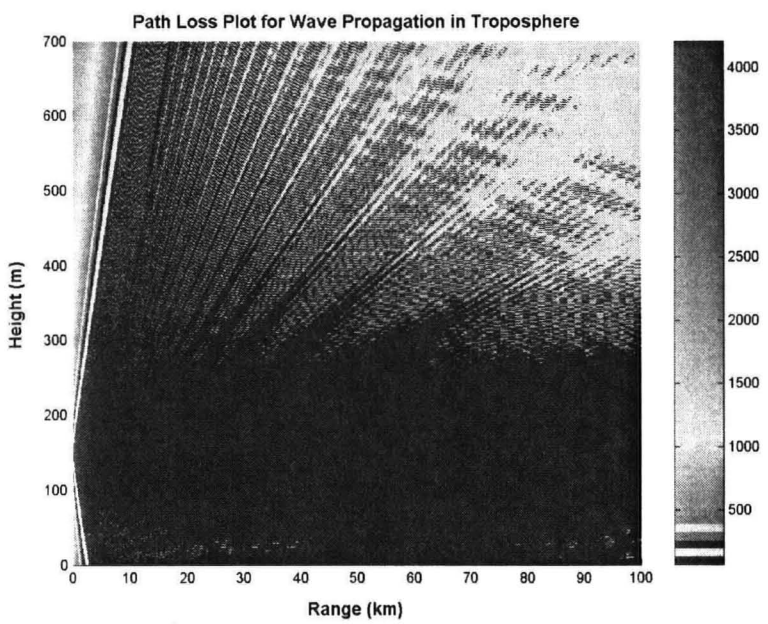

(b) 500MHz

Figure 4.6: Path Loss diagram with transmission at 100MHz and 500MHz

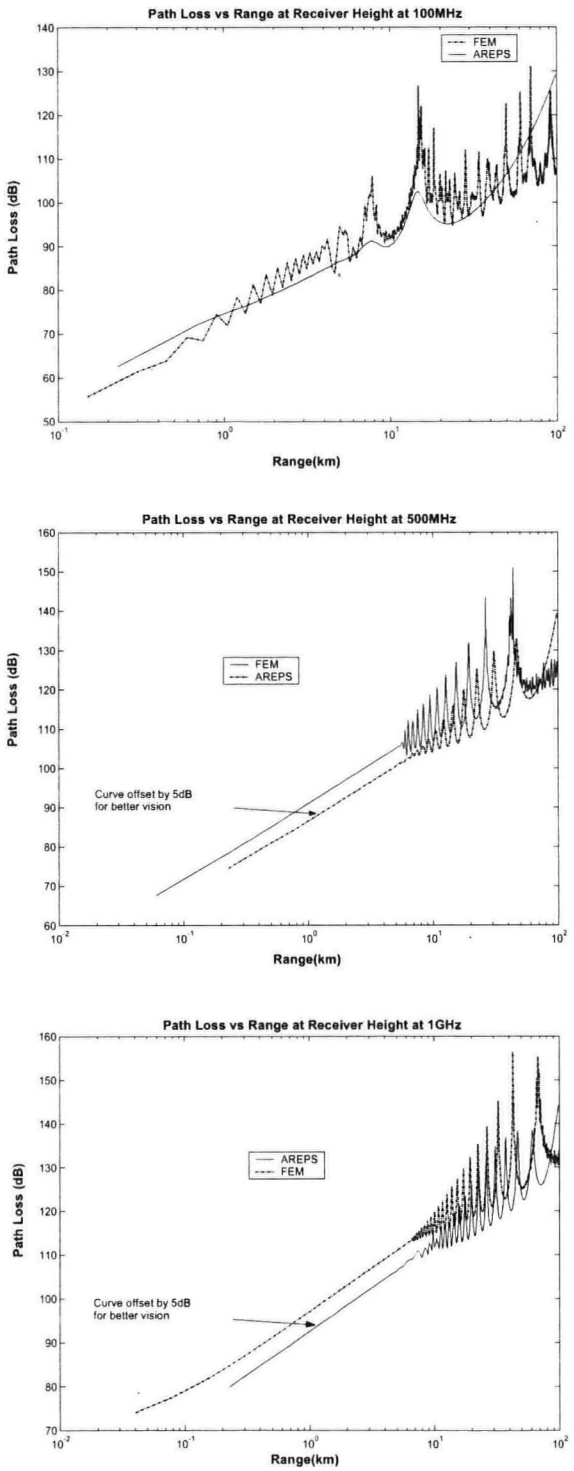

Figure 4.7: Path Loss vs Range at Receiver Height (100, 500, 1000)MHz

height and the number of nulls increases with frequency.

Figures 4.9(a) and 4.9(b) shows the path loss at receiver height for large propagation angle at 100MHz using narrow angle and wide angle formulation of PE. Results are compared with free space loss in both cases. For small propagation angles, narrow angle and wide angle finite element formulation of PEM produces almost the same results. However at large propagation angles, the narrow angle formulation of PEM generate errors while the wide angle FEM-PEM gives accurate results.

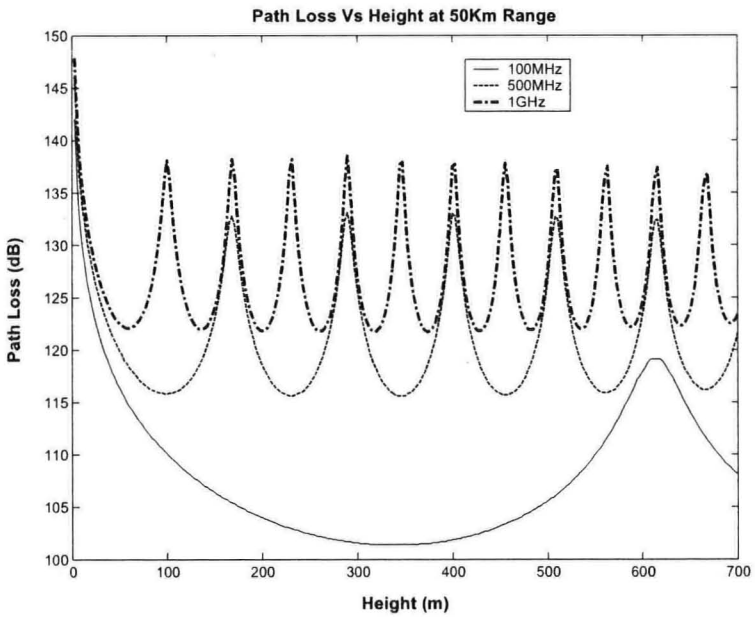

Figure 4.8: Path Loss Vs Height at 50Km Range at different frequencies

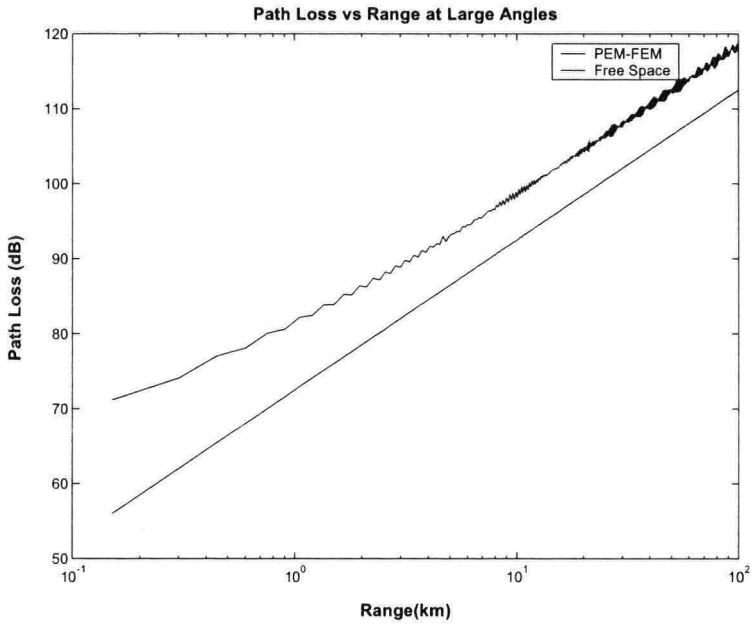

(a) 100MHz

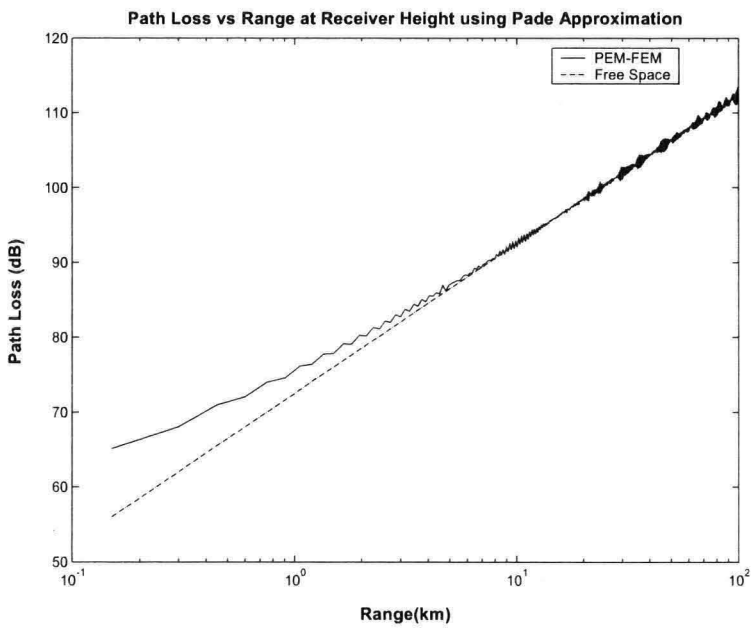

(b) 100MHz

Figure 4.9: Behaviour of Narrow-angle and Wide-angle PEM at large angles

From the above discussion, it can be seen easily that waves propagate undisturbed through the tropospheric medium. In figures 4.10 and 4.11 a bilinear surface ducting profile is included starting from sea level to an altitude of 300m. Standard atmospheric conditions over this altitude were also assumed, while the duct intensity was set to -1N-units/m. Results also shows trapping mechanism at 1GHz and 3GHz, it is clear that a duct of sufficient intensity is capable of capturing the whole energy at 3GHz. At low frequencies even a high intensity duct is unable to divert waves into the duct but at 3GHz waves are almost completely trapped between sea level and duct height.

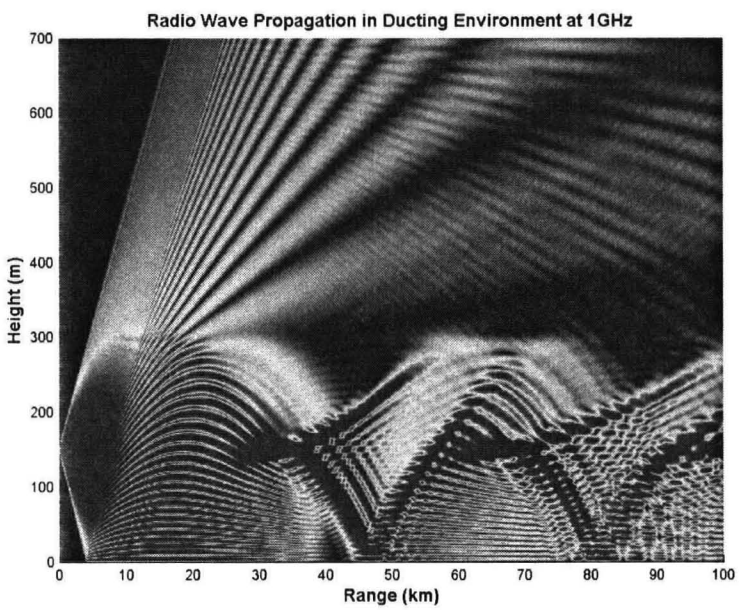

Figure 4.10: Coverage Diagrams at low duct intensity profiles at 1GHz

Figure 4.12 shows path loss at receiver height in the presence of a surface duct. To understand the effect of frequency on path loss in the presence of a duct different

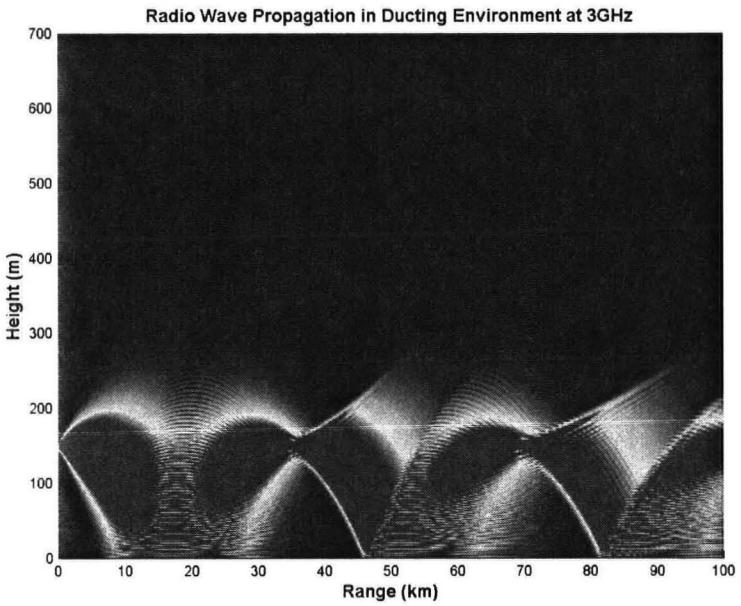

Figure 4.11: Coverage Diagrams at low duct intensity profiles at 3GHz

frequencies in the range of 100MHz to 5GHz were considered. In consistence with previous results, path loss increases with frequency even in the presence of a surface duct. However it should be noted from figure 4.12 that the increase in path loss in far field of the antenna for higher frequencies is more as compare to lower frequencies. For example, at a 50km range, the difference in path loss at 100MHz and 500MHz is about 18dB while at the same range the difference in path loss between 1GHz and 3GHz is only about 3dB.

4.5.1 Irregular Terrain and Urban Environment Modelling

Accurate modelling of radio waves over irregular terrain and especially in an urban environment is crucial for the planning of cellular communications in cities. Many

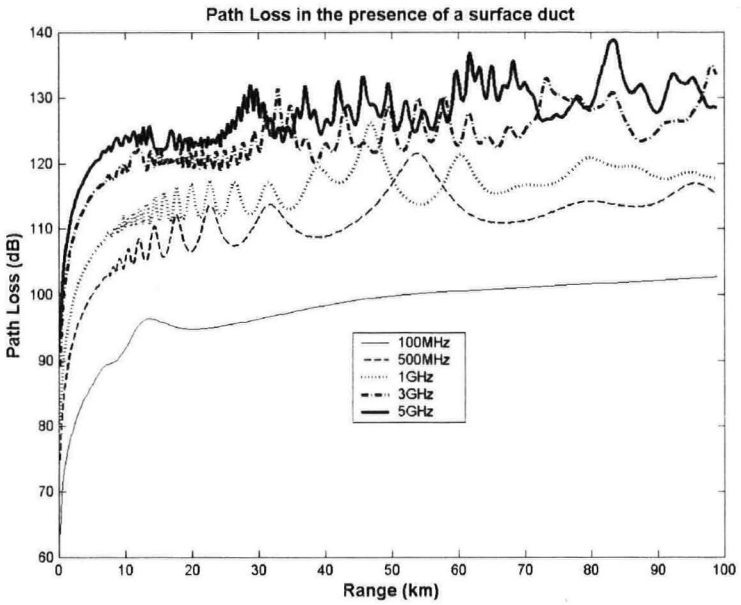

Figure 4.12: Path Loss at receiver height in ducting environment at different frequencies

existing prediction models are based on a simplified Deygout solution for multiple knife-edge diffraction [137]. An important class of propagation models over the irregular terrain is based on the integral equation formulation which in general can be simplified by using a paraxial approximation [138]. In contrast to these methods, the parabolic equation method model combines the effect of terrain diffraction and atmospheric refraction [49] while remaining straightforward to implement.

Finite element formulation of the parabolic equation method using terrain profiles is simple and straightforward. As in the case of refractivity profiles, at each range step Δx the program requires a refractivity profile as a function of height. However if refractivity is not changing along the range then a single refractivity profile is

sufficient. The terrain profile is entered in much the same way as refractivity profiles. All that is required is the series of data points corresponding to height versus range to describe terrain. The simplest and most effective technique models terrain as a sequence of horizontal steps, and is called the staircase method. In this thesis the staircase method was used to model terrain, however other approaches are discussed in detail in [27].

Staircase terrain modelling In staircase terrain modelling , terrain is divided into a number of stairs as shown in figure 4.13 and terrain height is provided as an input to the program for each range step. On each step, the field is propagated in usual way, applying the appropriate boundary conditions at the ground. When terrain height changes, corner diffraction is ignored and the field is simply set to zero on vertical terrain facets. For the case of uphill, when terrain goes up, the field at range step $x + \Delta x$ can be calculated using the following sequence of operations:

- propagate the field on the horizontal segment ignoring the presence of the vertical boundary, this is consistent with the paraxial approximation which neglects backscatter;
- truncate the field by setting it to zero on the uphill segment; this is consistent with the assumption that the ground does not support propagation.

If the terrain goes down the sequence of operations is as follows:

- propagate the field on the horizontal segment ignoring the presence of the vertical boundary and neglect backscatter due to corner diffraction
- pad the field by setting it to zero on the downhill segment.

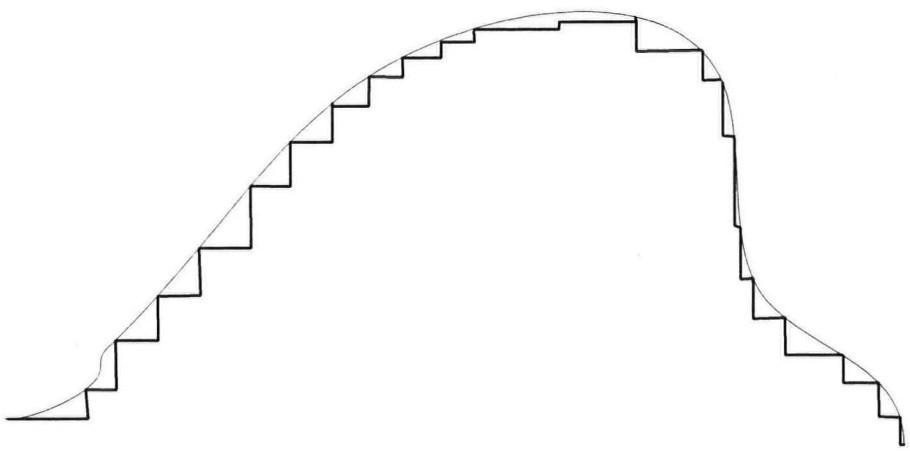

Figure 4.13: Staircase representation of terrain

If the terrain is really a staircase this model is very accurate but for smooth terrain there is an error because the boundary conditions on sloping facets are not properly accounted for. However, this error can be reduced by choosing small range steps.

In generating results for terrain modelling, two different scenarios are choosen. In the first scenario, an irregular terrain is assumed and two random terrain profiles are generated while in the second case, a street in an urban area is considered. Three buildings of arbitrarily heights are placed on the street and the span of the street is assumed to be 50m. Figure 4.14 and 4.15 shows coverage diagrams in the presence of irregular terrain generated by using the *rand* function in Matlab. For an urban

environment radiating antenna is assumed to radiate at 25m while the receiving antenna is at 10m. Three buildings of different heights and widths are assumed along the street. For the sake of simplicity it has been assumed that the building surfaces are perfectly conducting.

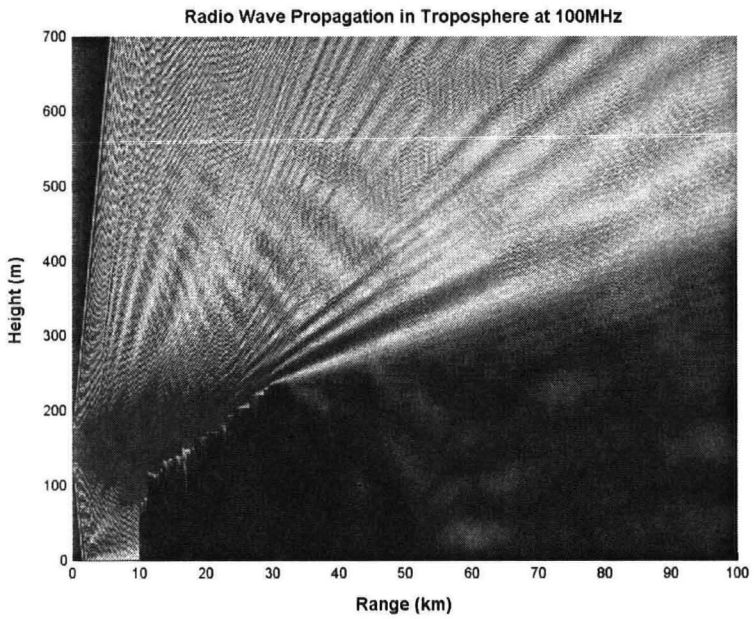

Figure 4.14: Coverage Diagrams at 100MHz on an irregular terrain

Figure 4.16 and 4.17 show the path loss calculated by the PE method and received power at receiver height respectively. Diffraction of waves along the edges of building is quite clear in figure 4.16. Buildings of variable heights are choosen to show the effect of shadowing as seen in figure 4.16. Behind the large building the strength of signal is very low and obviously inside buildings received power is very low (ideally zero) as shown in figure 4.17.

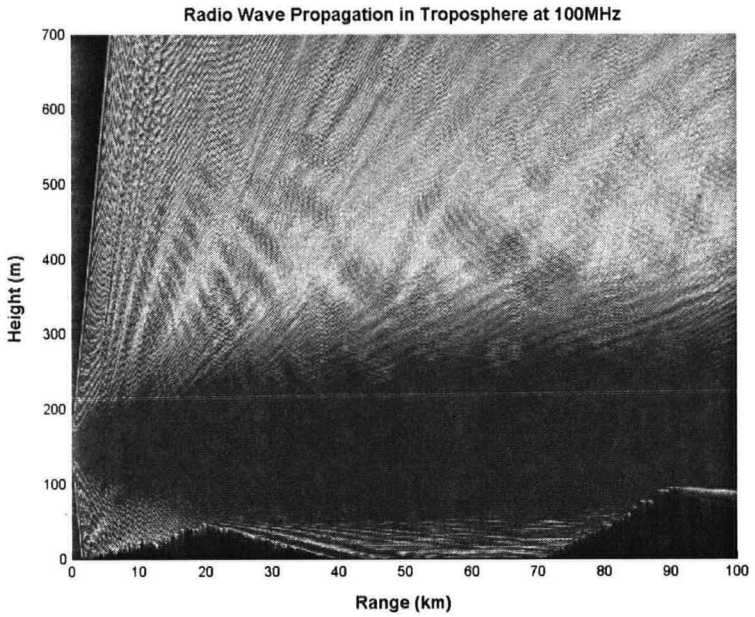

Figure 4.15: Coverage Diagrams at 100MHz on an irregular terrain

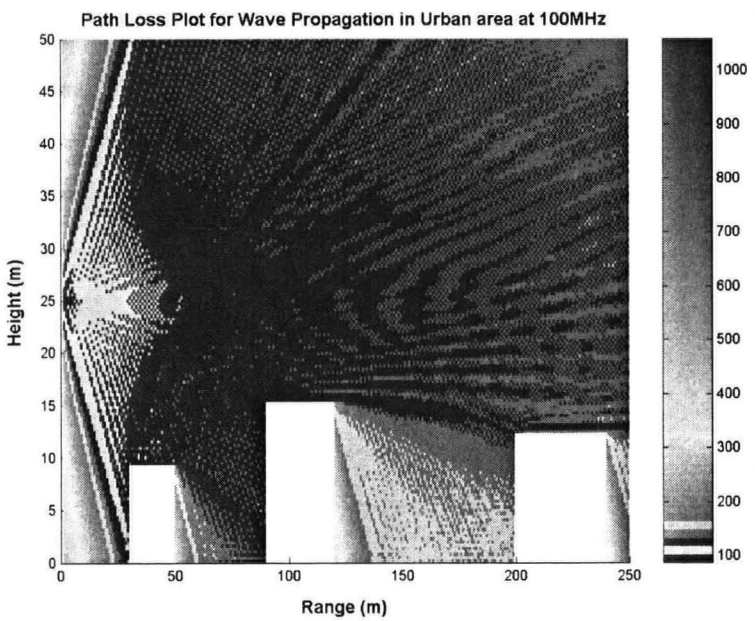

Figure 4.16: Path Loss in an urban street at 100MHz

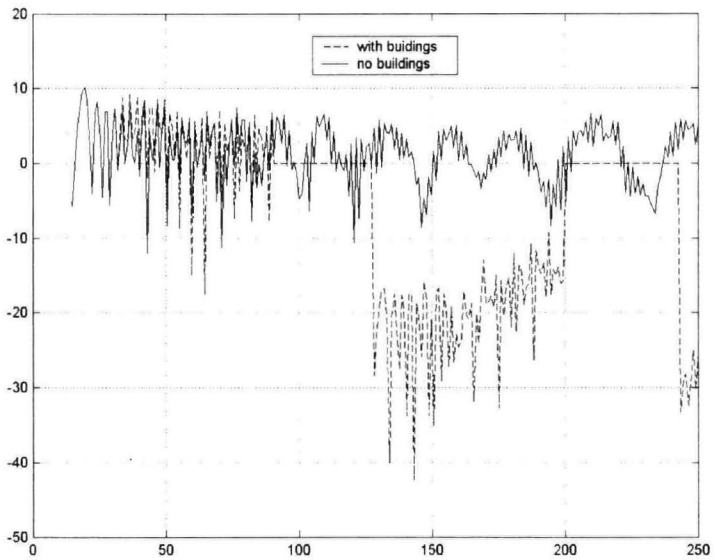

Figure 4.17: Received Power in an urban street at 100MHz

4.5.2 Results of Wave Propagation in Three dimensional environments

The properties of a 3D atmosphere vary as a function of three spatial variables (x, y, z) while the height and slopes of a 2D terrain vary as a function of two spatial variables (x, z) namely range and height. The same concepts can be extended to 3D propagation analysis of waves in the troposphere. Figure 4.18 represents the contour diagram of a transmitting antenna at 100MHz under standard atmospheric conditions at 30km from the antenna.

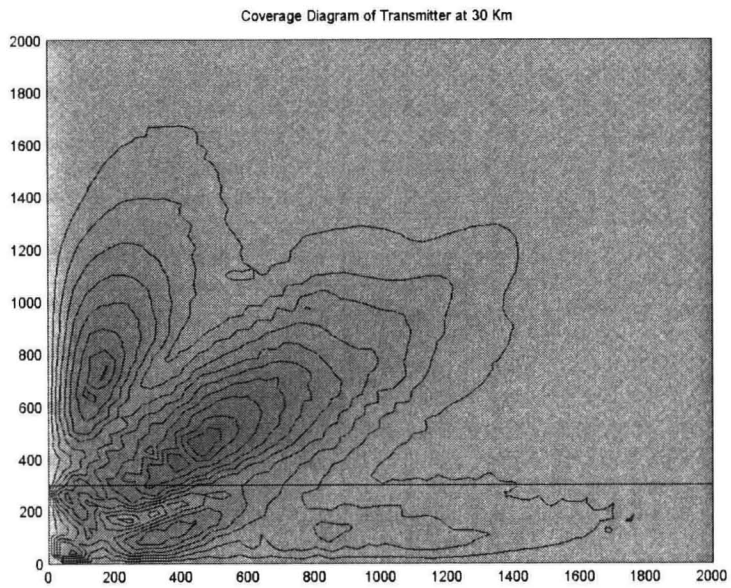

Figure 4.18: Coverage diagram of antenna with transmission at 30km propagation distance with no duct (all dimensions are in meter)

From the above results, it can be seen that as the waves propagate through the tropospheric medium in the absence of ducting, the energy lobe spreads. At a distance

of 30km (figure 4.18) it is more confined then at a distance of 70km (figure 4.19). In these simulations a single refractivity profile was used as given in [1], however different refractivity profiles can be entered at different stages and the computer program can perform linear interpolations in all three dimensions for use at the intermediate calculation positions. In these simulations, a refractivity gradient of -39.4 N-units/km is assumed everywhere. This constant gradient is an approximation of the usual exponential profile and is valid for altitudes under several thousand meters. In all cases, results are generated by assuming a propagation step of $\Delta x = 0.18$km.

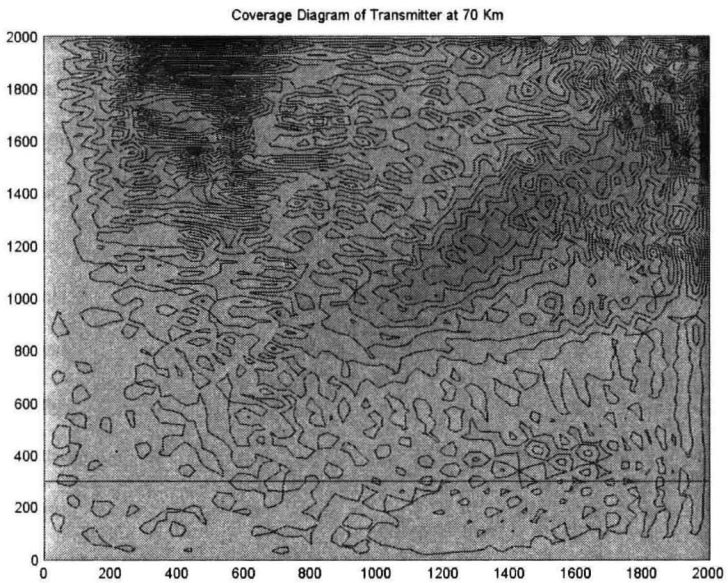

Figure 4.19: Coverage diagram of antenna with transmission at 70km propagation distance with no duct (all dimensions are in meter)

Figure 4.20 to 4.21 shows the use of a bilinear surface ducting profile, starting from

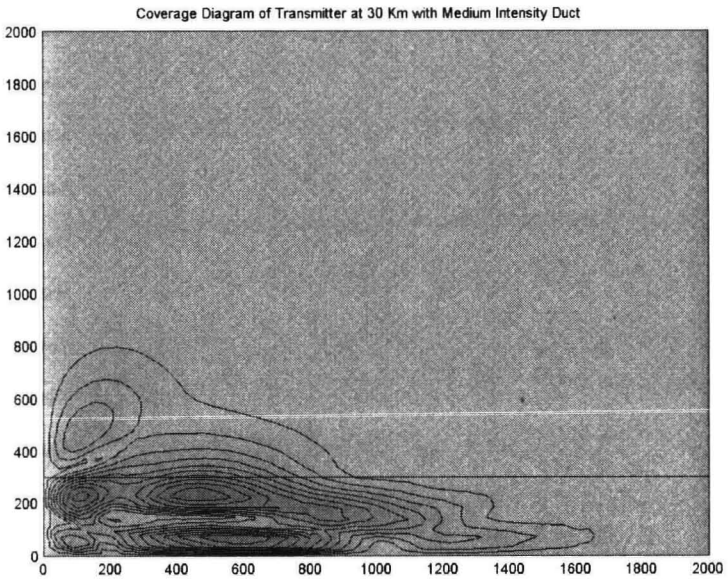

Figure 4.20: Coverage diagram of antenna with transmission at 30km propagation distance with medium intensity duct (all dimensions are in meter)

sea level to an altitude of $300m$. Standard atmospheric conditions over this altitude were also assumed. These illustrate the trapping mechanism and it is clear that as ducting intensity increases, a greater amount of the propagating energy is restricted inside the duct region. By comparing, corresponding diagrams with and without a duct, its quite obvious that a sufficient amount of energy is trapped inside the duct. In these simulations two different cases were considered, a medium intensity duct shown in figure 4.20 the case of a strong duct shown in figure 4.21.

From the diagrams it can be seen that the higher the duct intensity profile the more confined is the field. This will be a great advantage in applications where the transmitter and receiver both reside inside the duct. In this case the receiver will

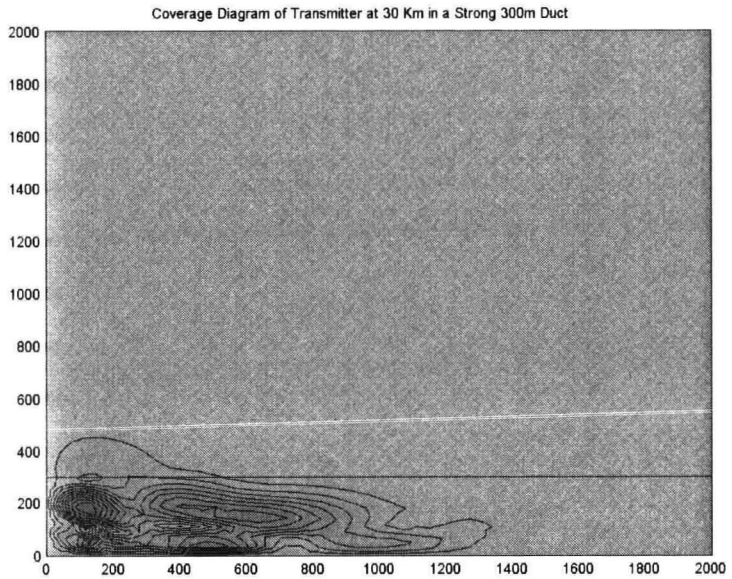

Figure 4.21: Coverage diagram of antenna with transmission at 30km propagation distance with strong intensity duct

capture maximum energy from the medium and the probability of error reduces.

4.6 Summary

A computationally efficient and accurate method has been proposed to model three dimensional tropospheric radio wave propagation in the presence of height-dependent nonstandard environmental conditions using a finite element approach. A brief introduction of the troposphere is given first and then modelling of wave propagation is presented in this chapter. A finite element formulation of narrow and wide angle version of the parabolic approximation is given with emphasis of its matlab implementation. Results are presented and it can be seen that the method is flexible and

can be used with complex geometries. The refractive index is independent between consecutive range steps, giving the ability to include inhomogeneous tropospheric profiles. In these cases, the method response can be directly adjusted to the refractivity variations, by properly modifying the size of the finite elements and the range step. Modelling in the presence of irregular terrain and on urban streets is also presented in this chapter.

Chapter 5

Finite Element Formulation of Radio Wave Propagation Modelling in Vegetation Canopies

5.1 Introduction

It is a well known fact that a radio channel sets limits for present and future wireless communication systems [51]. Propagation algorithms that determine path loss and broadcast signal coverage are essential for planning wireless networks for cellular mobile and for designing fixed terrestrial and satellite communication services. There is a widespread anticipation that customer demands for wireless communication systems will continue to expand in the foreseable future. The large number

of users especially mobile users, has resulted in network planners increasing system capacity by locating transmission antennas at heights lower than surrounding trees and buildings [73]. Vegetation obstructing or close to the line-of-sight propagation path causes radiowave absorption, scattering, diffraction and depolarisation [74]. For successful network planning and basic system design propagation algorithms that determine the path loss and signal coverage are critical to successful deployments.

To date much attention has been directed at frequencies close to the (Groupe Spéciale Mobile) GSM band and the (Digital Cellular System) DCS-1800 bands. At these frequencies, attenuation due to vegetation is considered as one of the dominant effects influencing radio propagation in rural and suburban areas [139]. Accurate modelling of the propagation of microwaves and millimeter waves through tree foliage, generally requires an accurate electromagnetic description of the tree geometry, including its branches and leaves, valid over a wide range of frequencies. Because of the complex physical processes arising from the prediction models involved, approximate prediction models appropriately validated are very useful to radio system planners and designers.

It has been proved that like the troposphere, the parabolic equation method can model radio wave propagation in vegetation [140]. The calculations may take into account the radius of the Earth and terrain effects whereas the polarisation of the propagating radiowaves is implemented on the surface boundary conditions. The most widely used technique for the solution of parabolic equation is the split-step

fourier method which has been successfully applied to analyse the propagation problem in vegetation [45]. However there are some serious drawbacks of the split step Fourier method when used in analysing wave propagation in vegetation. The error in the split-step Fourier method is a function of the derivatives of refractive index squared and horizontal distance [35]. In the presence of vegetation, variations in refractive index may be much larger in comparison with the troposphere, for example, variations of refractive index at the air-canopy boundary. In that case, the split-step Fourier method gives high error rates. Further the split step method is not computationally efficient as at every range step, method the calculates Fourier and inverse Fourier transforms. Recently, Holm [141] presented a good comparison between models based on the parabolic equation method and geometric theory of diffraction, and finally showed that vegetation could be modelled accurately by parabolic equation method rather than the Geometric Theory of Diffraction (GTD). In this thesis the finite element method is applied to the solution of a wide angle formulation of the parabolic equation method. Further, it can include all of the pertinent information available for the propagation path, including terrain profile, terrain permittivity and conductivity and vegetation features. In order to ensure that all the rays effective in wave propagation in the presence of vegetation canopy are taken into consideration, the wide angle formulation of the parabolic equation is used and for numerically accurate results the finite element method is employed to solve the parabolic equation.

The remainder of this chapter is organised as follow. In section 5.2, radio wave propagation inside vegetation and its modelling by WPEM is discussed. Section 5.3 discusses results finally section 5.4 concludes this chapter.

5.2 WPEM technique for vegetation

Military communication inside forests is always of importance for every nation and country, therefore it is important to understand how such environments affect the conditions for wave propagation. Penetrable (transmission) and non-penetrable (diffraction) obstacles between transmitter and receiver seriously degrade the propagation conditions. Diffraction effects in vegetation are normally modelled by using Geometric Theory of Diffraction(GTD)[142]. Semi-transparent obstacles in the form of trees or forests are more difficult to deal with because they allow partial transmission through the object as well as diffraction around or over them. GTD is a ray based technique, which means that to apply it in the presence of vegetation one has to trace all transmitted rays through obstacles also, which significantly increase the complexity of algorithm.

For the case of a homogenous vegetation layer of uniform thickness on flat ground, Tamir has established a set of approximate equations for the electric field as mentioned in chapter 2 [76]. For both the antennas within the forest layer, this method is able to provide good results. However, outside the forest, that is, for one antenna

or both the antennas outside the dielectric slab, it does not seem to work properly [140]. An attempt to deal with these shortcomings can be found in [14]. An important circumstance with the model by Tamir is that, in some examples, the used complex index of refraction for the vegetation is close to unity. If one can assume this, it would be possible to model wave propagation in a forest using the parabolic wave equation technique. This can be done by treating leaves and branches as a collection of randomly oriented scatterers, and trees can be modelled by complex refractive index [143]. To analyse propagation in the presence of vegetation, trees are modelled as dissipative slabs having refractive indices of the form [77]:

$$n^2 = \varepsilon + j60\lambda\sigma \tag{5.1}$$

where ε is the dielectric constant, σ is the conductivity of the trees and λ is the wavelength of radio frequency. Above the air canopy boundary standard atmospheric conditions as defined in ITU [1] were assumed. To model trees accurately Tamir has considered the following ranges of ε and σ:

$$1.01 \leq \varepsilon \leq 1.5 \tag{5.2}$$

$$10^{-5} \leq \sigma \leq 10^{-3} \tag{5.3}$$

The PE model has already been tested against propagation measurements in a fir-forest environment near Östersund, in the northern part of Sweden in 2000 with good results [141]. The parabolic equation method is a full wave method used for the resolution of several continuous-wave propagation problems in electromagnetism

like in particular ground propagation over irregular terrain as discussed in chapter 4. For details of wide angle formulation of the parabolic equation method, refer to chapter 2.

When applying the parabolic equation technique, the forest is assimilated to multi-layered lossy dielectric continous medium that can eventually be height and range dependent and located upon irregular ground as shown in figure 5.1. The PE algorithm treats the vegetation bulk like an absorbing atmospheric layer characterised by complex refractivity index profiles.

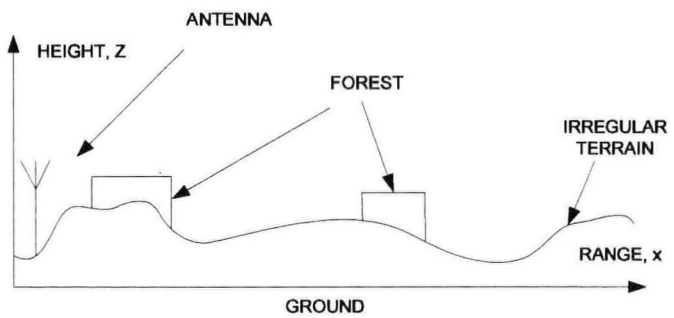

Figure 5.1: Example of using PE technique in vegetation

From chapter 2, the wide angle parabolic equation is given as:

$$\frac{\partial^2 u(x,z)}{\partial x^2} + j2k\frac{\partial u(x,z)}{\partial x} + \frac{\partial^2 u(x,z)}{\partial z^2} + k^2(n^2(x,z) - 1)u(x,z) = 0 \qquad (5.4)$$

It should be noted that in equation (5.4), refractive index $n(x,z)$ is a strong function of both height z and range x. Similar types of boundary conditions and initial field are used as describe in section 4.3.3 and 4.3.4 respectively.

The finite element formulation of equation (5.4) is similar to that described in section

4.4. So the final propagation algorithm can be written as,

$$\Big\{-j4k_0[\tilde{M}] - Dx\big\{[K] - k_0^2[M]\big\}\Big\}\{u\}^{x+Dx} = \Big\{-j4k_0[\tilde{M}] + Dx\big\{[K] - k_0^2[M]\big\}\Big\}\{u\}^{x} \tag{5.5}$$

where matrices $[K]$, $[M]$ and $[\tilde{M}]$ are defined in equations (4.27), (4.28) and (4.41) respectively.

5.3 Results and Discussion

To analyse wave propagation in a forest environment using the finite element approach, path loss as computed by the proposed method is compared with the well known Tamir results. Propagation loss of a transmitting antenna gain of G_t by the application of the parabolic equation method may be obtained by the expression [27],

$$L = -20\log|u(x,z)| + 20\log(4\pi) + 10\log(x) - 30\log(\lambda) - G_t \tag{5.6}$$

where x is the propagation direction and λ is the wavelength of radio waves.

Tamir showed that in the case of transmitter and receiving antennas inside a forest, the dominant propagating mode is a lateral wave at the boundary of air-forest canopy [76]. Forest height is assumed to be 18.75m while the transmitting antenna is at 16.75m with a transmitting gain of 24.57dB. Different models of forest are considered by varying complex refractive indices for comparison purposes. Frequency is assumed to be 100MHz in all simulations unless stated otherwise.

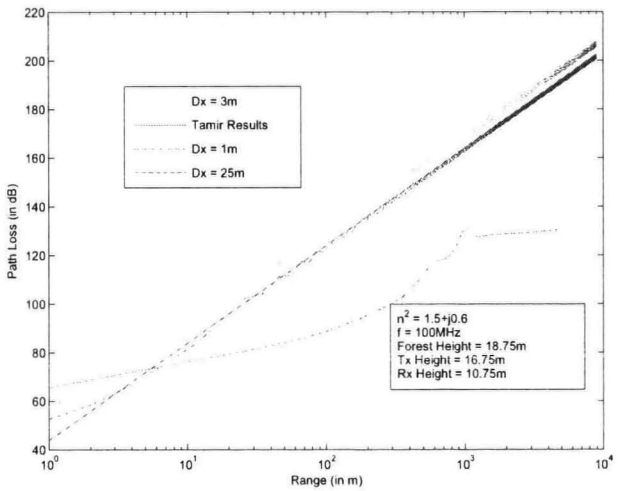

Figure 5.2: Comparison of Propagation Loss calculated by FEM with Tamir Results at 100MHZ

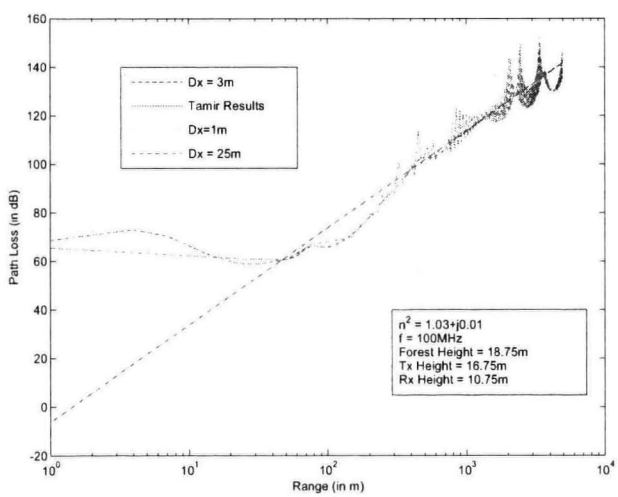

Figure 5.3: Comparison of Propagation Loss calculated by FEM with Tamir Results at 100MHZ

Path loss is computed for various refractive indices in an area with a vegetation canopy, by using two different methods. Figure 5.2 to 5.4 indicates that the parabolic equation method is in good agreement with Tamir's method, especially in the far field of the transmitter. In figure 5.2, trees are modelled by using $\epsilon = 1.5$ and $\sigma = 10^{-3}$ while in figure 5.3 and 5.4, plants are modelled using lower values of ϵ and σ. By comparing figure 5.2 and 5.3, it is clear that for large values of ϵ and σ, the range step should be small. For example, for $Dx = 25m$, the error rate is high with refractive index $n^2 = 1.5 + j0.6$ as compared to other values of refractive index like $n^2 = 1.03 + j0.01$ and $n^2 = 1.01 + j0.01$. For vegetation with smaller refractive index and the same range step, the error in propagation loss decreases. So for an acceptable error, range step should be decreased.

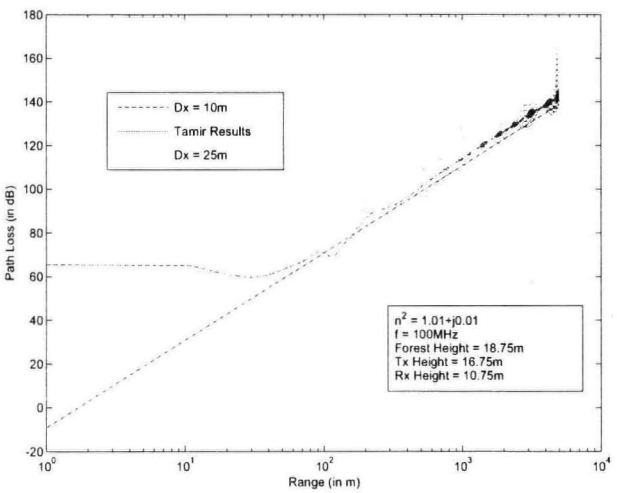

Figure 5.4: Comparison of Propagation Loss calculated by FEM with Tamir Results at 100MHZ

Figures 5.3 to 5.4 shows that in short ranges from the transmitter parabolic equation

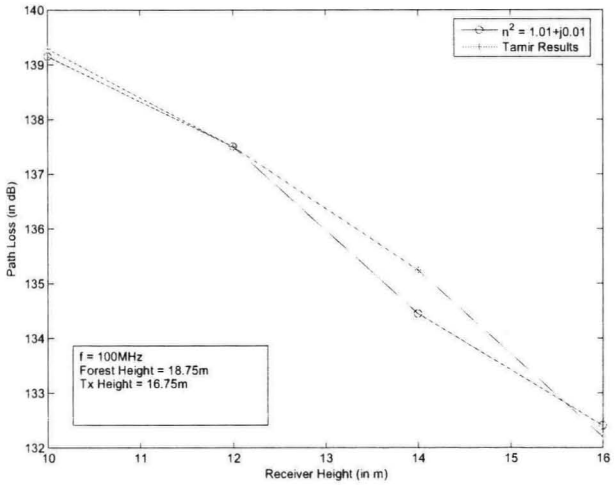

Figure 5.5: Plot of Path Loss variations with Receiver Height at 1000m range

method and Tamir results do not agree well. Tamir's theory is specifically focused on the case of transmitting and receiving antennas inside the vegetation [14]. One obvious reason is that near the transmitter, dominant waves are geometric waves rather than lateral waves, and Tamir calculations of path loss are based on lateral waves. Infact, from figure 5.3 and 5.4, a range can be calculated for different models of trees within which geometric waves are dominant. This range depends on the loss tangent of vegetation [45].

Figure 5.5 to 5.7 shows the basic transmission loss versus the receiver height inside the forest. An agreement in the general behavior of the curve between the Tamir results and parabolic equation method can be seen at values of refractive index close to unity. Three different values of refractive index have been choosen and it is finally concluded that as refractive index increases the difference between Tamir results and

the parabolic equation method results also increases.

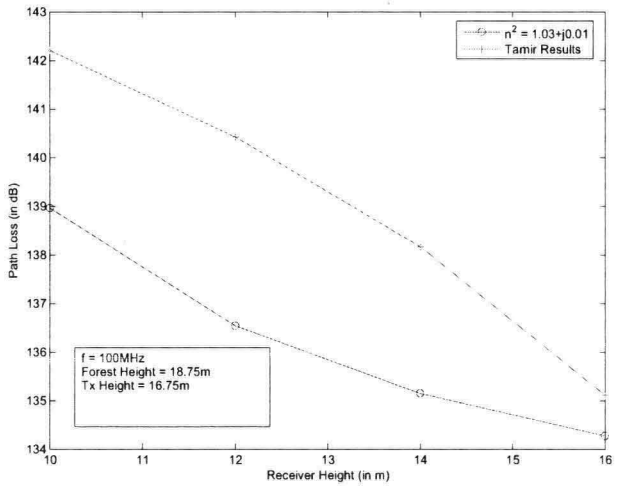

Figure 5.6: Plot of Path Loss variations with Receiver Height at 1000m range

5.4 Summary

In this chapter, applications of the finite element method for analysing radio wave propagation in a forest has been presented. It has been shown that a finite element solution of the parabolic equation can handle the problem of propagation in a forest similar to the troposphere. Finite element formulation of the parabolic equation gives a more reliable and efficient solution as compare to the split-step Fourier method, which is computationally difficult because of computation of IFFT and FFT algorithms in every range step. Further, it has been shown here that for better results refractive index should be close to unity. However at large refractive indices range step size should be decreased.

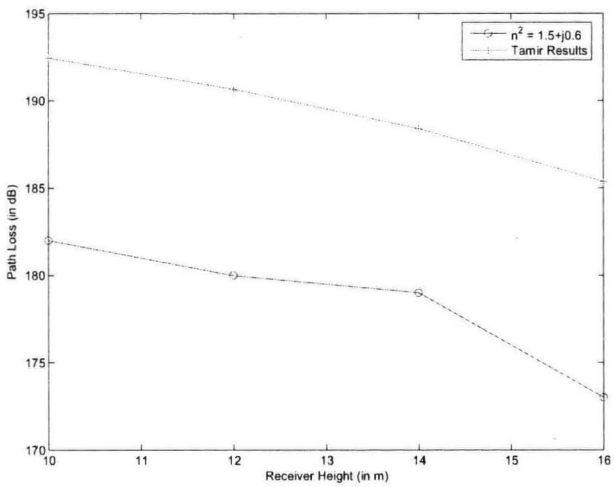

Figure 5.7: Plot of Path Loss variations with Receiver Height at 1000m range

Chapter 6

Wave Propagation Modelling inside Tunnels

6.1 Introduction

The popularity of cellular mobile systems led to extensive work with special reference to radio channel modelling but most of this work mainly focused on urban and suburban environments [144]. Mobile and wireless service users are growing very fast in large cities especially in the past decade. Mobile operators have deployed a greater capacity of infrastructure in order to satisfy the demand and achieve more complete coverage. Mobile and wireless service providers aim to provide users excellent communications without time and space constraints. It is obvious that radio network coverage is needed for daily and emergency conditions. Development of

such networks requires thorough knowledge of radio wave propagation characteristics. Tunnels play an important role in the transportation of materials and people. Current communication systems are not designed to operate reliably in tunnels and signal quality is severely degraded due to lossy surfaces of the tunnel. Designing of reliable communication systems that provide total coverage requires knowledge of wave propagation in tunnels. Thus wave propagation analysis in tunnel environments is therefore essential.

Interest in analysing tunnel wave propagation in Europe emerged in the early 1970's, and initially the mining industry sponsored much of the work. Later on the topic became of interest to the military and homeland security communications. Military interest is obvious while the later interest is because of two reasons. First there is a need of personnel communication in tunnels especially in an emergency while second is the potential use of RF links for sensors. If the propagation of the signal inside tunnels could be characterised then a more robust communication system could be designed specifically for operation in tunnels. Coverage in tunnels should be optimised in order to minimise infrastructure cost. Recent interest in this area arose after advances in the field of mobile communication systems.

Tunnels form a major part of the transport infrastructure in most modern metropolitan cities. A mountainous country like Austria for example, has 10% of its transport in high priority roads made up of tunnels. Further, many large cities like London have a vast network of underground trains where all communication needs to be wire-

less. It is a common observation that signals cannot be heard in tunnels. Therefore, there is a need to develop accurate techniques to model the propagation of radio waves in tunnels. Tunnel environments are quite different and having special wave propagation characteristics. In general, tunnels may be considered as hollow waveguides surrounded with some lossy materials. Many researchers have therefore been focusing their attention on radio propagation in tunnels [145]. An extensive review of the literature has been provided in chapter 2.

In modern mobile networks, quality of service is mainly determined by radio coverage. In designing cellular mobile radio systems, the mean signal strength or received power is an essential factor that must be determined and a number of approaches have been developed for both urban environment and terrain profiles [146]. Coverage in tunnels would be of high interest for mobile cellular radio and personal communication services for daily and emergency services. To solve for the field distribution in tunnels a number of factors must be taken into account such as size and shape of tunnel, frequency, direction of polarisation, electrical parameters of the surrounding material and obstructions in the tunnel [147].

A simple rectangular waveguide model was used in the past to model wave propagation in tunnels [70]. Computing RF propagation in waveguides has a long history ranging from older works using analytical solutions to modern work using numerical methods [100]. For circular or elliptical but constant cross sectional area geometries, numerical techniques can be used to find propagating modes and eigenvalues,

while rectangular cross section curved tunnels were treated analytically in [148]. Maxwell's equations contain the basic physics of wave propagation in tunnels but finding the efficient solution is a big challenge. Analytical solutions are limited to simple geometries and idealised wall properties.

The parabolic equation method resulted a wide variety of solutions to numerous diffraction and propagation problems [149]. However the potential of PE was not completely realised until its computational advantages had been demonstrated. The first finite-difference solutions of the parabolic equation method applied to diffraction theory was published in [150]. This approach became dominant in ocean acoustics when the well known works by Tappert [30] were published. Many further improvements proposed during the last decade made it one of the most powerful and versatile computational tools in modern electromagnetic theory. The computational efficiency of the vectorial parabolic equation method has been demonstrated in [151],[152] where realistic problems of wave propagation and scattering were solved on a desktop machine.

The parabolic equation method was successfully applied to guided wave propagation in electromagnetic ducts of different nature [25] and was proposed in [102] as a suitable way for analytical modelling of wave propagation in tunnels. The parabolic equation method has been suggested as an adequate mathematical model of wave propagation in tunnels due to selective wall absorption filtering out higher Brillouin angles thereby forming a paraxial wave packet even if the tunnel has a curved

axis [102]. The computational efficiencies of the PE method allow calculations to be performed in minutes on a high-end laptop computer. Effects of tunnel curvature and vehicles are included in the characterisation.

In this chapter the finite element method (FEM) is applied to analyse radio wave propagation in straight and curved tunnels of varying crossections. In previous chapters, finite element formulation has been developed for tropospheric wave propagation and propagation in the presence of vegetation canopies. In this chapter, applications of the finite element method as well as the Crank-Nicolson scheme are used to convert a vectorial parabolic equation into a discretized one. Solving the resulting sparse matrix equation stepwise along the tunnel axis results in the field distribution in the entire tunnel. In contrast to other methods, like sparse matrix solver [152] or FD splitting techniques [153], FEM gives the field in the whole domain and complex types of tunnel structures can easily be modelled.

6.2 Parabolic Equation Modelling for Curved Tunnel

To model radio wave propagation in tunnels the parabolic equation method seems to be the most promising choice as mentioned in introduction and in chapter 2. However, long tunnels are normally curved and some modification in the vectorial parabolic equation method is required. A reliable way to modify this is by using adi-

abatic mode theory for oversised waveguides [101]. This yields a parabolic equation based model describing diffraction, attenuation and depolarisation of electromagnetic waves in nonuniform oversised waveguides.

Consider a curved tunnel shown in figure 6.1, where y and z are the transverse dimensions and $\rho(s)$ denotes the curvature radius; thus for straight tunnels $\rho(s) = \infty$. It is assumed that wavelength λ is small compared with tunnel diameter D (oversised waveguide) and the ratio between the diameter D and curvature radius $\rho(s)$ is very small. These assumptions can be mathematically formulated by introducing a new parameter ν:

$$\nu = \sqrt{\frac{D}{L}} \ll 1 \tag{6.1}$$

and these relationships which allow a simple description in terms of the parabolic equation,

$$\sigma = \sqrt{\frac{k^2 D^3}{L}} \sim 1 \tag{6.2}$$

Maxwell equations are solved by using the following scaled coordinate variables,

$$\xi = \frac{s}{L}, \quad \eta = \frac{y}{D}, \quad \zeta = \frac{z}{D}, \quad \kappa = \frac{L}{\rho} \tag{6.3}$$

and to calculate the asymptotic solution one has to determine the unknown amplitude functions $u_i(\xi, \eta, \zeta)$ and $v_i(\xi, \eta, \zeta)$ for $i = 0, 1$ which satisfies the following

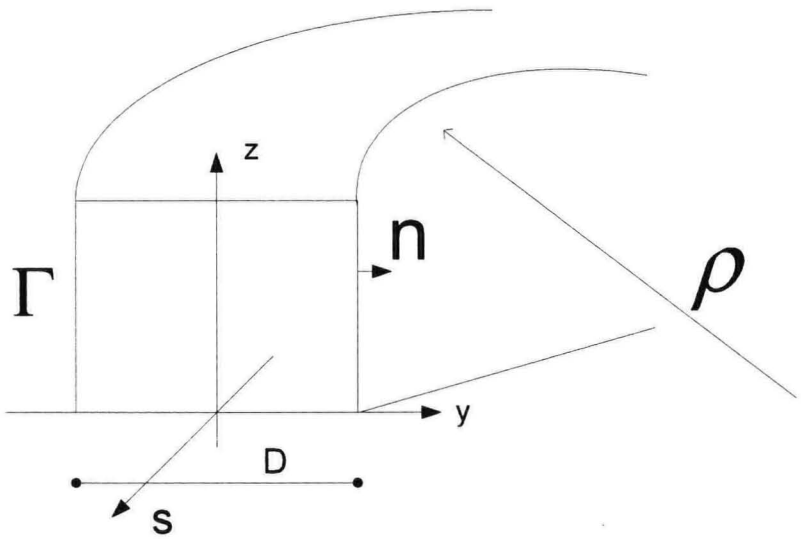

Figure 6.1: Cross section of a curved Tunnel with radius of curvature ρ

differential equation [154]:

$$\frac{\partial^2 w_i}{\partial \eta^2} + \frac{\partial^2 w_i}{\partial \zeta^2} - 2\sigma^2 \kappa \left[\eta \cos\theta + \zeta \sin\theta\right] w_i = j2\sigma \frac{\partial w_{i-1}}{\partial \xi} \tag{6.4}$$

where $w_i = (u_i, v_i)^T$. It is implied that $w_{-1} = 0$ so the zero order PDE defined in equation (6.4) is homogenous. Equation (6.4) is a recursive two dimensional partial differential equation, however a vectorial parabolic equation can be derived by assuming:

$$w = w_0 + \nu w_1 \tag{6.5}$$

So from equation (6.4) for $i = 0, 1$ two independent equations can be obtained:

$$\frac{\partial^2 w_0}{\partial \eta^2} + \frac{\partial^2 w_0}{\partial \zeta^2} - 2\sigma^2 \kappa \left[\eta \cos\theta + \zeta \sin\theta\right] w_0 = j2\sigma \frac{\partial w_{-1}}{\partial \xi} \tag{6.6}$$

$$\frac{\partial^2 w_1}{\partial \eta^2} + \frac{\partial^2 w_1}{\partial \zeta^2} - 2\sigma^2 \kappa \left[\eta \cos\theta + \zeta \sin\theta\right] w_1 = j2\sigma \frac{\partial w_0}{\partial \xi} \tag{6.7}$$

Multiply equation (6.7) by ν and add in equation (6.6) and by using a modified function $\mathbf{W} = (U, V) = e^{-j\sigma\nu^{-1}}$, a governing equation of $\mathbf{W}$ comes up as:

$$\frac{\partial^2 \mathbf{W}}{\partial \eta^2} + \frac{\partial^2 \mathbf{W}}{\partial \zeta^2} - 2\sigma^2 \kappa \left[\eta \cos\theta + \zeta \sin\theta\right] \mathbf{W} = j2\sigma\nu \frac{\partial \mathbf{W}}{\partial \xi} \tag{6.8}$$

Equation (6.8) is a vectorial parabolic equation model of wave propagation in an oversised waveguide and can be used directly with tunnels. The vector function $\mathbf{W}(\xi, \eta, \zeta)$ is like an attenuation function and describes the amplitude of a plane wave along the tunnel axis. Equation (6.8) is the vectorial parabolic equation for a curved tunnel in scaled coordinate systems, which can be returned back to normal coordinates by using equations (6.1)-(6.3).

$$D^2 \left[\frac{\partial^2 \mathbf{W}}{\partial y^2} + \frac{\partial^2 \mathbf{W}}{\partial z^2}\right] - 2\frac{k^2 D^3}{L}\frac{L}{\rho}\left[\frac{y}{D}\cos\theta + \frac{z}{D}\sin\theta\right] \mathbf{W} = j2\frac{D}{L}\frac{k^2 D^3}{L}\frac{\partial \mathbf{W}}{\partial s}.L \tag{6.9}$$

which can be simplified further,

$$D^2 \left[\frac{\partial^2 \mathbf{W}}{\partial y^2} + \frac{\partial^2 \mathbf{W}}{\partial z^2}\right] - 2k^2 D^2 \left[\frac{y}{\rho}\cos\theta + \frac{z}{\rho}\sin\theta\right] \mathbf{W} = j2kD^2 \frac{\partial \mathbf{W}}{\partial s} \tag{6.10}$$

and finally the vectorial parabolic equation for curved tunnel in cartesian coordinates is given as,

$$\frac{\partial^2 \mathbf{W}}{\partial y^2} + \frac{\partial^2 \mathbf{W}}{\partial z^2} - 2k^2 \left[\frac{y\cos\theta + z\sin\theta}{\rho}\right] \mathbf{W} = j2k \frac{\partial \mathbf{W}}{\partial s} \tag{6.11}$$

where θ is the rotational angle [denoting a tunnel that is possibly curved in more then one dimension] and k is the wave number.

At the boundary contour Γ of the tunnel cross section, Leontovich impedance boundary conditions can be implemented as an approximation of the wall electrical properties [102].

$$\mathbf{W} = \frac{j}{k}\tilde{\mathbf{A}}\tilde{\mathbf{B}}\tilde{\mathbf{A}}\frac{\partial \mathbf{W}}{\partial n} \tag{6.12}$$

with,

$$\begin{aligned} \tilde{\mathbf{A}} &= \begin{bmatrix} n_y & n_z \\ n_z & -n_y \end{bmatrix} \\ \tilde{\mathbf{B}} &= \begin{bmatrix} 1/Z & 0 \\ 0 & Z \end{bmatrix} \end{aligned} \tag{6.13}$$

Here $n = (n_y, n_z)$ is the unit normal to Γ and $Z_0 Z$ is the impedance of the tunnel walls. For a wall material with relative permittivity ϵ_r and conductivity σ, Z can be approximated as $Z = \frac{1}{\sqrt{\epsilon_r - j60\lambda\sigma}}$ [132] and Z_0 is the impedance of free space which can be defined as $Z_0 = \mu_0 c$ where $\mu_0 = 4\pi.10^{-7}$ Henry/m and c is the speed of light. Equation (6.11) is the vectorial version of the scalar parabolic equation describing creeping and whispering gallery waves and accounts for transversal diffusion of wave amplitude $\mathbf{W}(s, y, z)$. The matrix boundary condition defined in equation (6.12) governs the effects of grazing angle reflection, selective mode absorption and depolarisation in the tunnel walls.

6.3 Finite Element Formulation of Vectorial Parabolic Equation Model

Applying the Galerkin formulation of the finite element method (FEM) over the domain $y_{min} \leq y \leq y_{max}$ and $z_{min} \leq z \leq z_{max}$ to equation (6.11). Let $\Omega \subset \Re^2$ be a bounded domain with boundary Γ while $\bar{\Omega} \subseteq \Omega$ denotes domain over each element i.e. $\Omega = \sum_{i=1}^{\alpha} \bar{\Omega}$ where α denotes total number of elements. From equation (6.11),

$$2kj\frac{\partial \mathbf{W}}{\partial s} - \frac{\partial^2 \mathbf{W}}{\partial y^2} - \frac{\partial^2 \mathbf{W}}{\partial z^2} + 2k^2\frac{y\cos\theta(s) + z\sin\theta(s)}{\rho(s)}\mathbf{W} = 0 \tag{6.14}$$

Assume,

$$\psi(s,y,z) = \frac{y\cos\theta(s) + z\sin\theta(s)}{\rho(s)}$$

So equation (6.14) becomes,

$$2kj\frac{\partial \mathbf{W}}{\partial s} - \frac{\partial^2 \mathbf{W}}{\partial y^2} - \frac{\partial^2 \mathbf{W}}{\partial z^2} + 2k^2\psi(s,y,z)\mathbf{W} = 0 \tag{6.15}$$

For the sake of simplicity, ψ is used instead of $\psi(s,y,z)$. If $\phi(y,z)$ is assumed to be a trial function then the weak formulation of equation (6.15) over an element is given as:

$$\begin{aligned}\int_{\bar{\Omega}} \phi.2kj\frac{\partial \mathbf{W}}{\partial s}\partial\bar{\Omega} - \int_{\bar{\Omega}} \phi.\frac{\partial^2 \mathbf{W}}{\partial y^2}\partial\bar{\Omega} - \int_{\bar{\Omega}} \phi.\frac{\partial^2 \mathbf{W}}{\partial z^2}\partial\bar{\Omega} \\ + \int_{\bar{\Omega}} \phi.2k^2\psi(s,y,z)\mathbf{W}\partial\bar{\Omega} + \int_{\bar{\Omega}} \phi.gdS = 0\end{aligned} \tag{6.16}$$

Where g is the boundary condition function of W. Now by using integration by parts,

$$\int_{\bar{\Omega}} j2k\frac{\partial \mathbf{W}}{\partial s}\phi\partial\bar{\Omega} + \int_{\bar{\Omega}} \frac{\partial \mathbf{W}}{\partial y}.\frac{\partial \phi}{\partial y}\partial\bar{\Omega} + \int_{\bar{\Omega}} \frac{\partial \mathbf{W}}{\partial z}.\frac{\partial \phi}{\partial z}\partial\bar{\Omega} + \int_{\bar{\Omega}} 2k^2\psi(s,y,z)\phi\mathbf{W}\partial\bar{\Omega} + \int_{\bar{\Omega}} \phi.gdS = 0 \tag{6.17}$$

If $\{N\}$ is the shape function vector and by using the Galerkin method an approximate solution $\mathbf{W}$ can be approximated on each element by,

$$\mathbf{W} = \{N\}\{W\}, \qquad \phi = \{N\}^T \tag{6.18}$$

So from equation (6.17),

$$j2k\int_{\bar{\Omega}} \{N\}\{N\}^T\frac{\partial\{W\}}{\partial s}\partial\bar{\Omega} + \int_{\bar{\Omega}} \frac{\partial\{N\}}{\partial y}.\frac{\partial\{N\}^T}{\partial y}\{W\}\partial\bar{\Omega} + \int_{\bar{\Omega}} \frac{\partial\{N\}}{\partial z}.\frac{\partial\{N\}^T}{\partial z}\{W\}\partial\bar{\Omega} + 2k^2\int_{\bar{\Omega}} \psi\{N\}\{N\}^T\partial\bar{\Omega} + \int_{\bar{\Omega}} \phi.gdS = 0 \tag{6.19}$$

Assume,

$$[\mathbf{M}] = \Sigma_e \int_{\bar{\Omega}} \{N\}\{N\}^T\partial\bar{\Omega} \tag{6.20}$$

$$[\mathbf{K}] = \Sigma_e \int_{\bar{\Omega}} [2k^2(\psi-1)\{N\}\{N\}^T - \frac{\partial\{N\}}{\partial y}.\frac{\partial\{N\}^T}{\partial y} - \frac{\partial\{N\}}{\partial z}.\frac{\partial\{N\}^T}{\partial z}]\partial\bar{\Omega} \tag{6.21}$$

Where $\sum_e$ represents summation over all elements for the whole domain Ω. So for domain Ω,

$$j2k[\mathbf{M}]\frac{\partial\{W\}}{\partial s} + k^2[\mathbf{M}]\{W\} - [\tilde{\mathbf{K}}]\{W\} + 2k^2\psi[\mathbf{M}]\{W\} = 0 \tag{6.22}$$

where,

$$[\tilde{\mathbf{K}}] = [\mathbf{K}] + [\mathbf{K}]_\Gamma$$

where $[\mathbf{K}]_\Gamma$ is the matrix defined on boundary Γ. From equation (6.22),

$$j2k[\mathbf{M}]\{\dot{W}\} + 2k^2[\mathbf{M}]\{W\} - [\tilde{\mathbf{K}}]\{W\} = 0 \tag{6.23}$$

where,

$$\{\dot{W}\} = \frac{\partial\{W\}}{\partial s}$$

So from equation (6.23),

$$j2k[\mathbf{M}]\{\dot{W}\} - \{[\tilde{\mathbf{K}}] - 2k^2[\mathbf{M}]\}\{W\} = 0 \tag{6.24}$$

Apply a Crank-Nicholson algorithm to equation (6.24) in propagation direction s by assuming:

$$\{\dot{W}\}^{s+\frac{\Delta s}{2}} = \frac{\{W\}^{s+\Delta s} - \{W\}^s}{\Delta s} \tag{6.25}$$

$$\{W\}^{s+\frac{\Delta s}{2}} = \frac{\{W\}^{s+\Delta s} + \{W\}^s}{2} \tag{6.26}$$

Consider equation (6.24) at step $s+\frac{\Delta s}{2}$, and substituting equation (6.25) and (6.26) in equation (6.24) yields,

$$j4k[\mathbf{M}][\{W\}^{s+\Delta s} - \{W\}^s] = \Delta s[[\tilde{\mathbf{K}}] - 2k^2[\mathbf{M}]][\{W\}^{s+\Delta s} + \{W\}^s]$$

or,

$$\begin{aligned}[j4k[\mathbf{M}] - \Delta s[[\tilde{\mathbf{K}}] - 2k^2[\mathbf{M}]]]\{W\}^{s+\Delta s} \\ = [j4k[\mathbf{M}] + \Delta s[[\tilde{\mathbf{K}}] - 2k^2[\mathbf{M}]]]\{W\}^{s+\Delta s}\end{aligned} \tag{6.27}$$

or, in simplified notation it can be written as,

$$[A]\{W\}^{s+\Delta s} = [B]\{W\}^{s+\Delta s} \tag{6.28}$$

with,

$$[A] = j4k[\mathbf{M}] - \Delta s[[\tilde{\mathbf{K}}] - 2k^2[\mathbf{M}]]$$

$$[B] = j4k[\mathbf{M}] + \Delta s[[\tilde{\mathbf{K}}] - 2k^2[\mathbf{M}]]$$

6.4 Results and Discussions

6.4.1 Simulation Parameters

Most of the commonly used tunnels are rectangular or arched shaped tunnels. The choice of the tunnel shape is made after careful consideration of the geological and mechanical conditions of the tunnel ambient media. To analyse radio wave propagation and attenuation in tunnels, two different types are considered, a rectangular tunnel of cross section 10m x 5m and an arch tunnel. An arch tunnel cross section consists of a half-circle of radius 4.8m and a trapezoid of widths 9.6m and 8.8m and of height 2.5m. These tunnel dimensions are choosen just for illustration purposes and different tunnel dimensions may be choosen. The tunnels are modelled as a straight or curved waveguide surrounded by lossy random wall. A transmitting antenna is placed at the start of tunnel operating at different frequencies, while receiving antenna moves along the length of tunnel. The cross sectional geometry of a

curved rectangular tunnel is shown in figure 6.2. The length of the tunnel is assumed to be 300m. A mesh is generated using the Delaunay algorithm [155] in Matlab and the total number of elements is 32224 with 384 boundary elements. The number of elements vary for different frequencies. For better accuracy, Lagrange quadratic type elements are used [52].

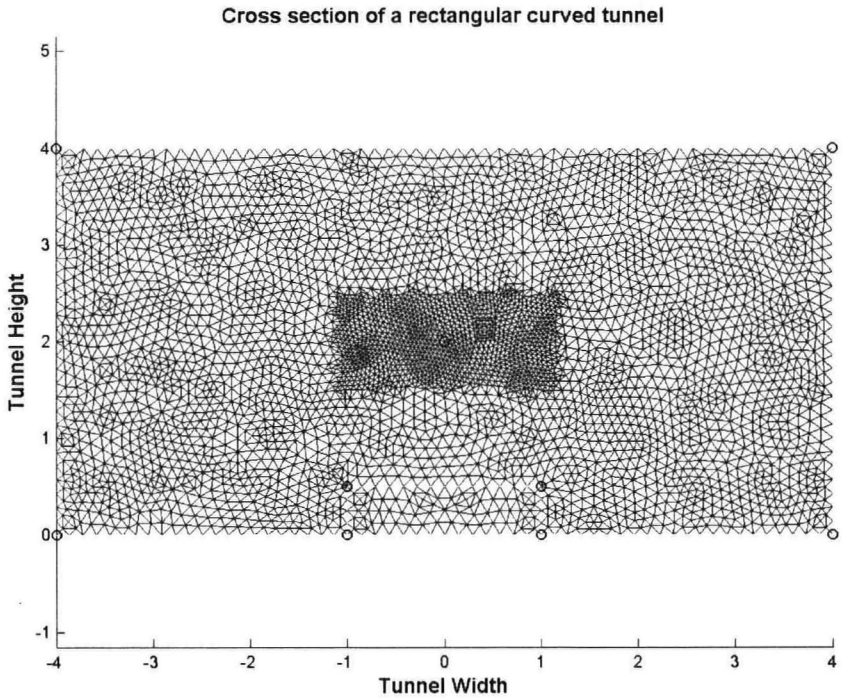

Figure 6.2: Mesh of cross section of tunnel (all dimensions are in meters)

The transmitting antenna is centered in the middle of the tunnel. A normalized gaussian pattern is used in which the initial field $u(0, z)$ can be written as [134],

$$u(0, z) = [A(z - H_0) - \bar{A}(z + H_0)] \tag{6.29}$$

where H_0 represents the antenna height and bar denotes complex conjugate. The

Fourier transform of $A(z)$ is given as,

$$a(\zeta) = e^{-\zeta^2 w^2/4}, \tag{6.30}$$

where w is defined as,

$$w = \frac{\sqrt{2\ln 2}}{k_0 \sin\frac{\theta_{bw}}{2}} \tag{6.31}$$

In equation (6.31), $\sin\frac{\theta_{bw}}{2}$ is the sine of the 3dB beamwidth.

The rotational angle θ as defined in equation (6.14) is assumed to be 0 in all simulations. Various radio frequencies in the VHF and UHF range were used in the analysis. The walls of the tunnel are characterised by a relative permittivity of $\epsilon_r = 4.0$ and conductivity $\sigma = 0.01$S/m while at vehicle boundaries $\epsilon_r = 1$ and $\sigma = 4$ x 10^6S/m is assumed, until stated otherwise. Three different types of the vehicles have been used: small van, bus and a large truck. Typical dimensions of vehicles are shown in Table 6.1.

Type	length(m)	width(m)	height(m)
Small Van	10	0.5	2
Bus	13	1.5	2
Truck	17	2	3

Table 6.1: Different Vehicles dimensions used in simulations

6.4.2 Geometry of Tunnel

The configuration of the tunnel plays a crucial role in determining the radio coverage. The geometry of tunnel can be characterised by its shape, cross-section and

curvature. Straight tunnels are modelled by using infinite radius of curvature i.e. $\rho = \infty$ while for curved tunnels $\rho = 800$m is used in simulations. If the tunnel is straight and the antenna is located in the tunnel, the signal's primary component will be the result of line of sight transmission. As the tunnel changes direction, the signal experiences more loss due to reflections and scattering. The more abruptly the tunnel changes direction, the greater the loss is and lower the signal level will be. Figure 6.3 to 6.5 represents electric field distribution at 300m from the entrance of the tunnel for straight and curved rectangular tunnel, while figure 6.6 to 6.8 represents signal intensity distribution in an arch shaped tunnel. Further results shows that propagation performance is almost identical in rectangular and arch shaped tunnels.

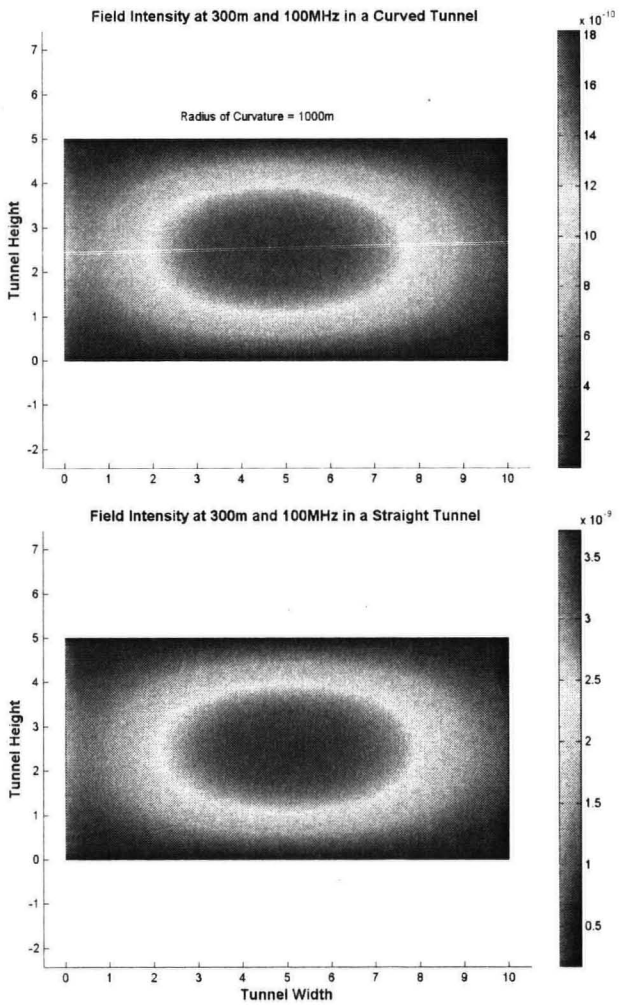

Figure 6.3: Signal Intensity at the end of rectangular tunnel at 100MHz (all dimensions are in meters)

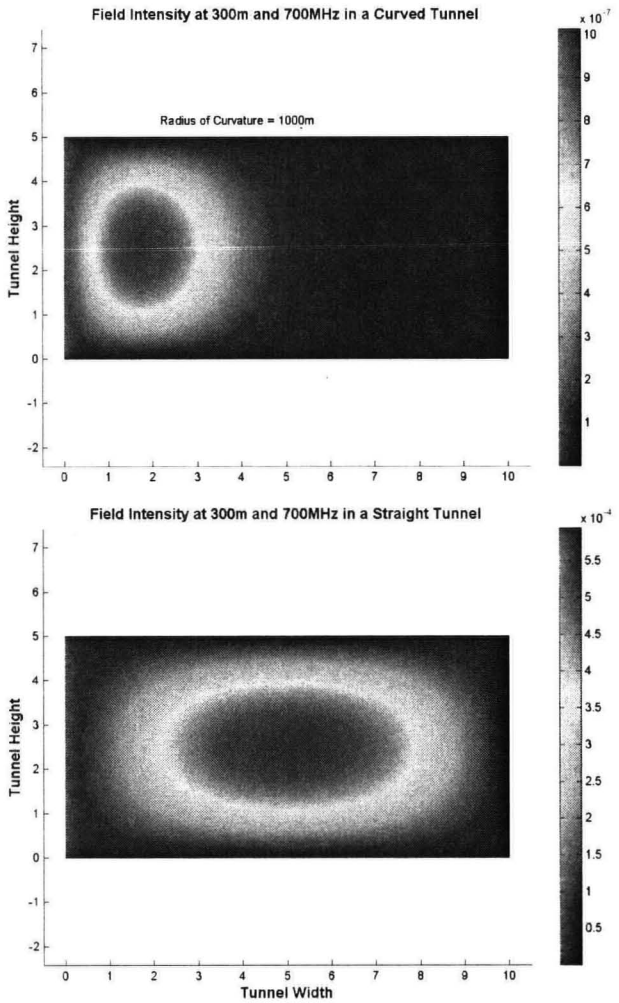

Figure 6.4: Signal Intensity at the end of rectangular tunnel at 700MHz (all dimensions are in meters)

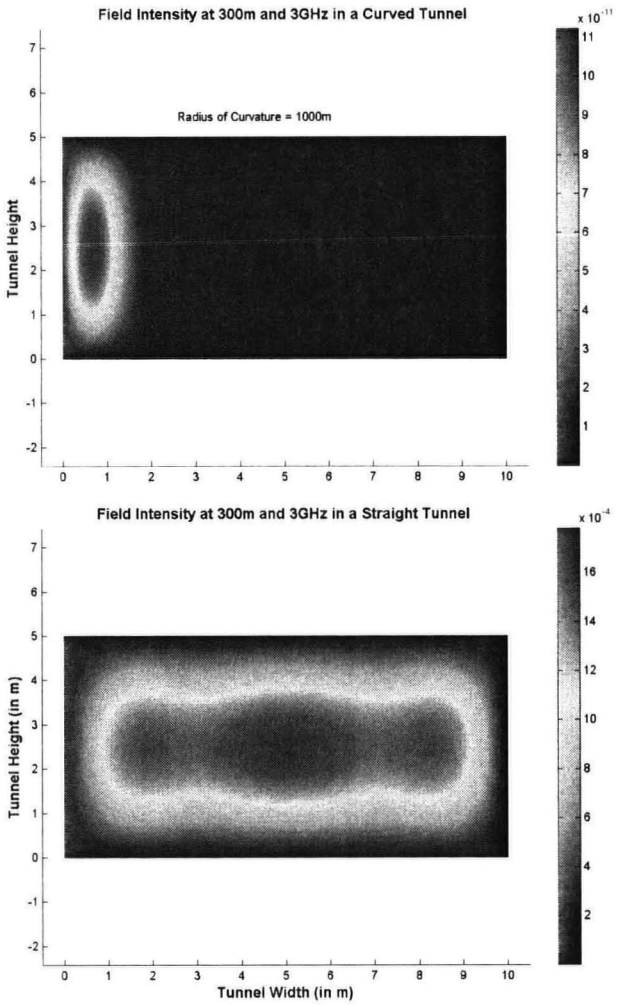

Figure 6.5: Signal Intensity at the end of rectangular tunnel at 3GHz (all dimensions are in meters)

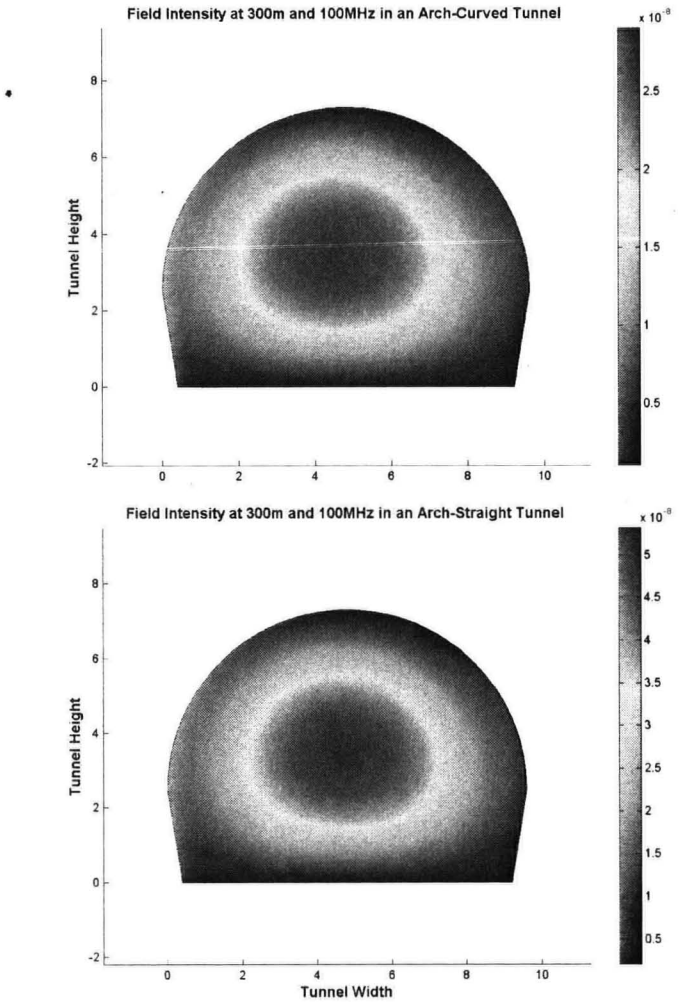

Figure 6.6: Signal Intensity at the end of arch tunnel at 100MHz (all dimensions are in meters)

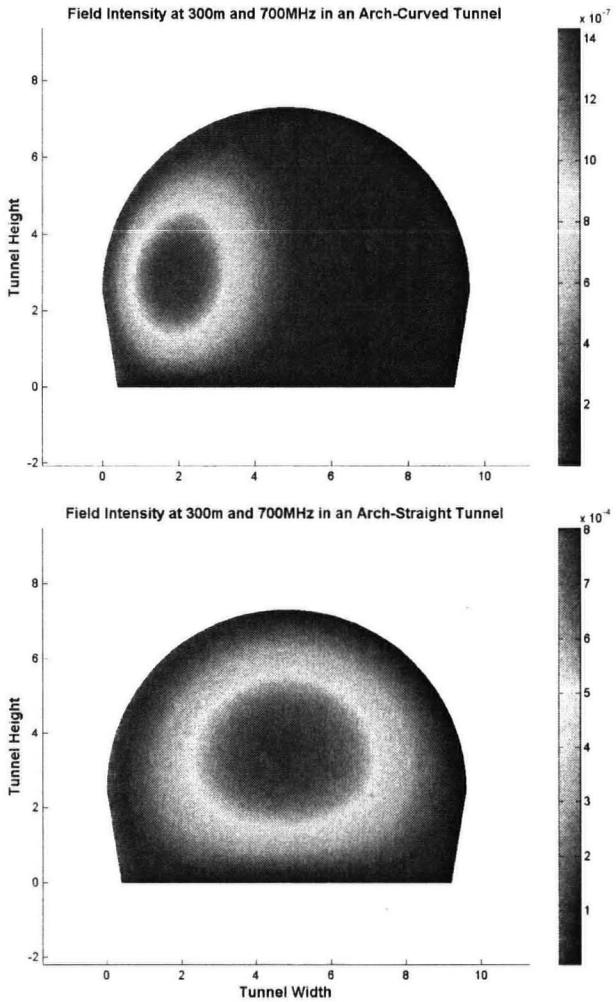

Figure 6.7: Signal Intensity at the end of arch tunnel at 700MHz (all dimensions are in meters)

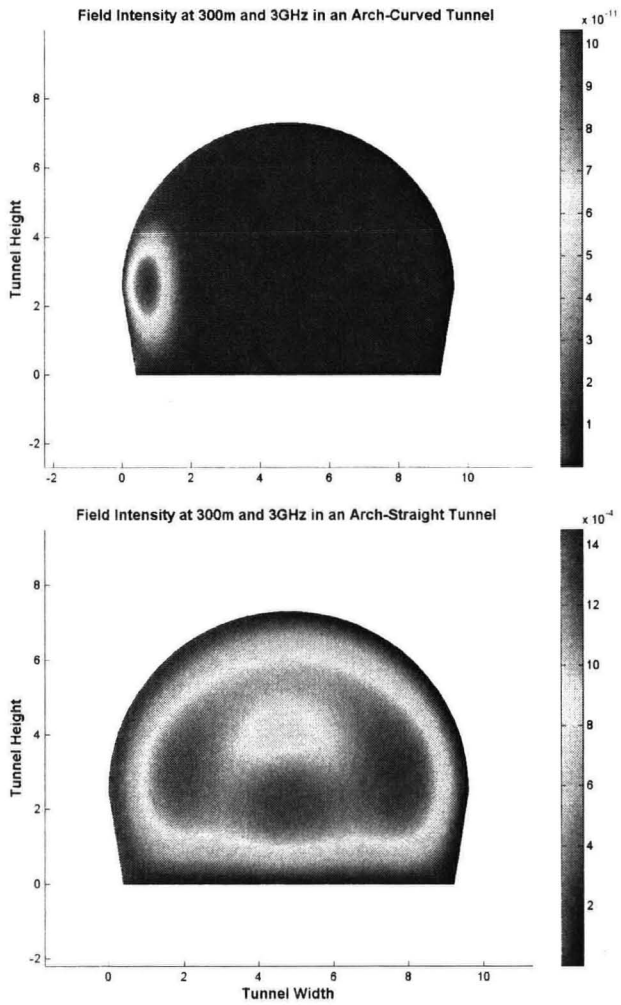

Figure 6.8: Signal Intensity at the end of arch tunnel at 3GHz (all dimensions are in meters)

For gaussian excitation defined by (6.22), one mode is dominant as shown in figures 6.3 to 6.5. Signals propagating through curved tunnels experience a dramatic decrease in signal strength compared with that in straight tunnel for both types of tunnels. It is well known that the tunnel axis of curvature causes a field concentration near the concave side wall as is clear from figures 6.3 to 6.8. These results are in good agreement with the experimental results in [148]. For simple tunnel profiles like straight rectangular tunnels, it is possible to calculate the field analytically based on separation of variables, but straightforward numerical solution of the vectorial PEM is more efficient and effective [102].

Simulations were carried out at $\sigma = 0.01$mho/m and $\epsilon_r = 4.0$. Figure 6.9-6.12 shows received signal power level calculated across tunnel cross sections at various range steps in straight/curved rectangular and arch shaped tunnel. In figure 6.9 and 6.10, power level is calculated at 300m from the tunnel entrance and plotted versus distance between transmitter and receiver at different frequencies in straight and curve rectangular tunnels respectively. Results show that the difference in power at the end of a tunnel for 100MHz and 3GHz is much higher for straight tunnels as compare to curved tunnels. Similarly, average power at the middle of the tunnel is plotted for straight and curved arch shaped tunnels. Comparing results for rectangular and arch tunnels, it can be deduced that the shape of the tunnel has little influence on received power. However power plots for straight and curved tunnels (either rectangular or arch) confirm this fact that the frequency dependance of attenuation in

curved tunnels is much less important then in a straight tunnel. A similar conclusion was drawn by Lienard in [95] after performing a series of experiments in straight and curved tunnels.

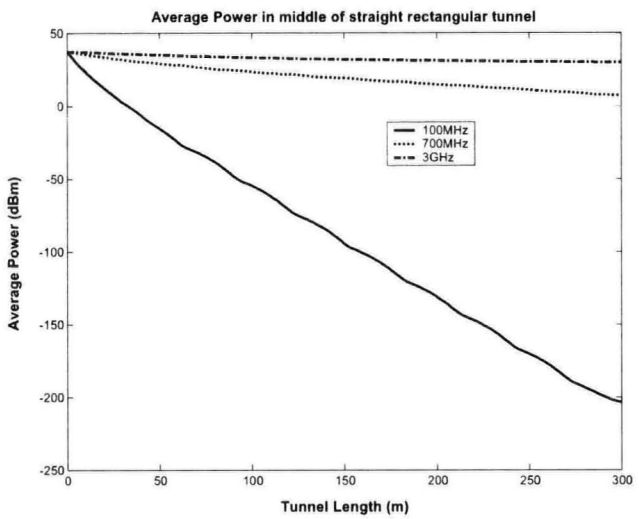

Figure 6.9: Average Signal Power across straight rectangular tunnel cross section versus tunnel length

Results indicated that in straight rectangular and arch shaped tunnels, more power is lost at low frequencies like 100MHz. In curved tunnels most of the energy is concentrated on one side of the tunnel rather than in the middle. So for curved tunnels, the power level in the middle of the tunnel is low at high frequencies e.g. 3GHz as compare to frequency like 700MHz. This phenomenon can be explained by the reflection and absorption properties of tunnel walls. At smaller wavelengths, the waves are more likely to be reflected in the environment. Rather then being reflected,

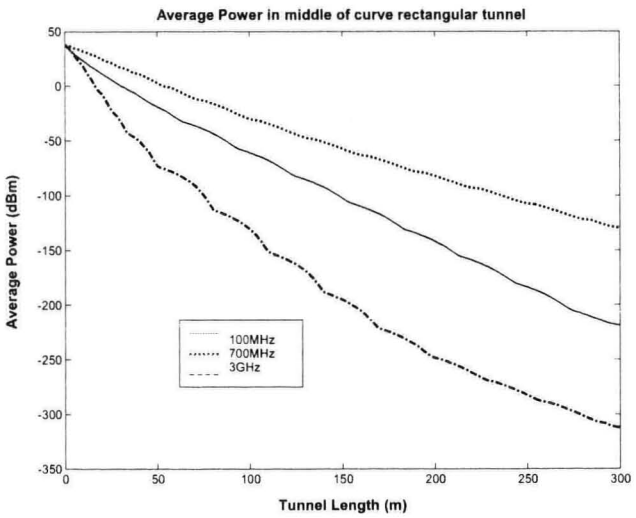

Figure 6.10: Average Signal Power across curved rectangular tunnel cross section versus tunnel length

the low frequency waves tends to be absorbed in the tunnel walls as compared to high frequency waves. These results are in good agreement with the experimental results presented in the Public Safety Wireless Network (PSWN) report [145].

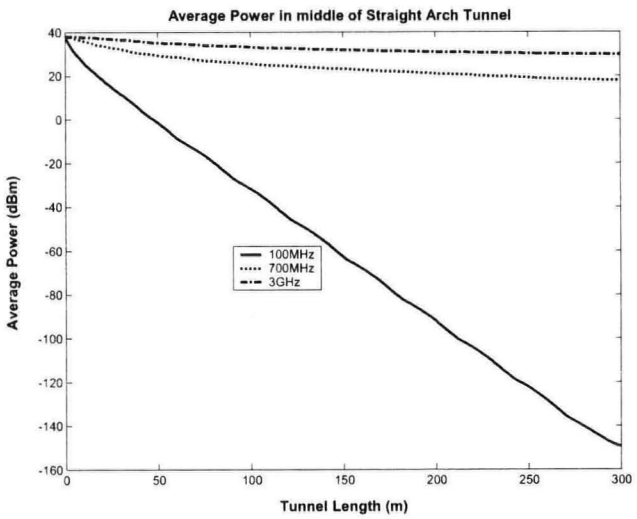

Figure 6.11: Average Signal Power across straight arch tunnel cross section versus tunnel length

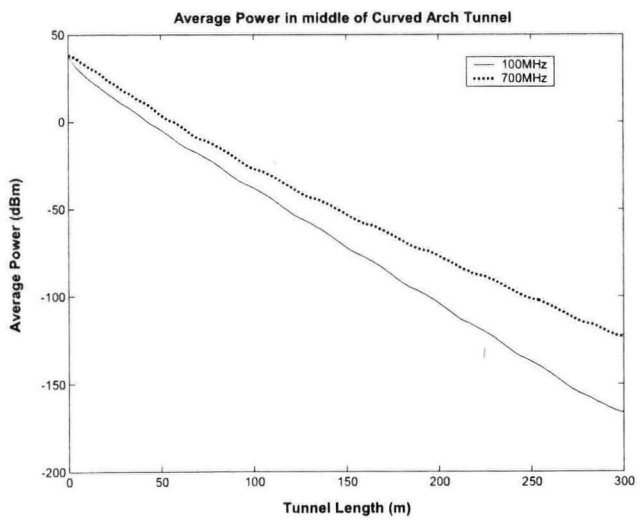

Figure 6.12: Average Signal Power across curved arch tunnel cross section versus tunnel length

6.4.3 Electrical Parameters and Wall Properties

Tunnel walls are usually made from concrete and metal net. Electromagnetic properties of concrete or metal are well known i.e. permittivity, conductivity and permeability and they normally remain static. In this chapter, relative permittivity and conductivity is varying and permeability is assumed to be constant. A signal leaving the transmitter is partially absorbed and partially reflected by the tunnel walls. Due to the electrical properties of the tunnel walls, a signal may propagate more efficiently so analysis is carried out by choosing different values of conductivity and relative permittivity in a curved rectangular and arch tunnel. Figure 6.13 shows

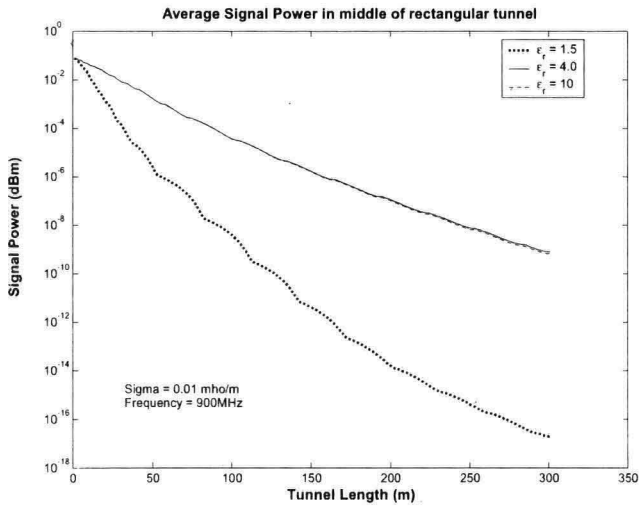

Figure 6.13: Average Signal Power at 900MHz for different ϵ_r in rectangular tunnel

received power versus tunnel length for different values of relative permittivity ϵ_r in a rectangular tunnel. From figure 6.13, it is obvious that received power depends on relative permittivity for lower values of ϵ_r and for higher values of ϵ_r received power

is independent of ϵ_r. Figure 6.14 shows average power distribution across rectangular tunnel versus tunnel length at 900MHz for different values of conductivity σ. Effect of tunnel wall conductivity is almost negligible as evident from figure 6.14, however one need to be consider effect of conductivity for higher values of conductivities. These results are in good agreement with [105] where analysis was carried out by using ray tracing techniques. Figure 6.15 and 6.16 shows power versus ϵ_r and

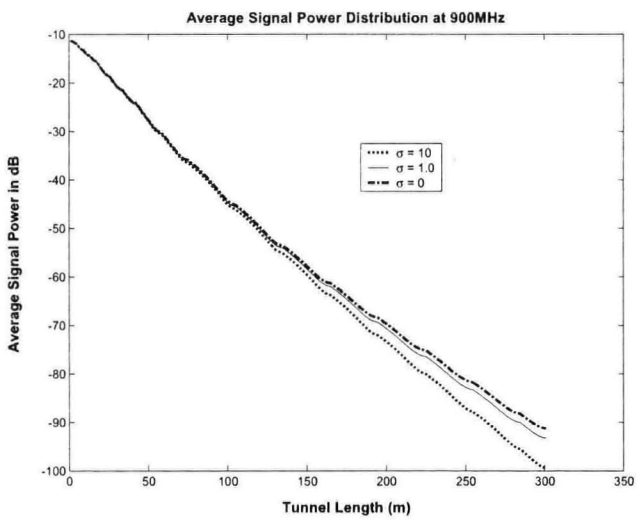

Figure 6.14: Average Signal Power at 900MHz for different σ in rectangular tunnel

σ at 900MHz at the end of an arch tunnel. Results shows in arch tunnels, power decreases with increasing ϵ_r and σ. From these plots, a threshold for the relative permittivity and conductivity can be calculated for arch tunnels. However, pattern of received power dependence on electrical properties of tunnel walls is similar in both types of tunnels.

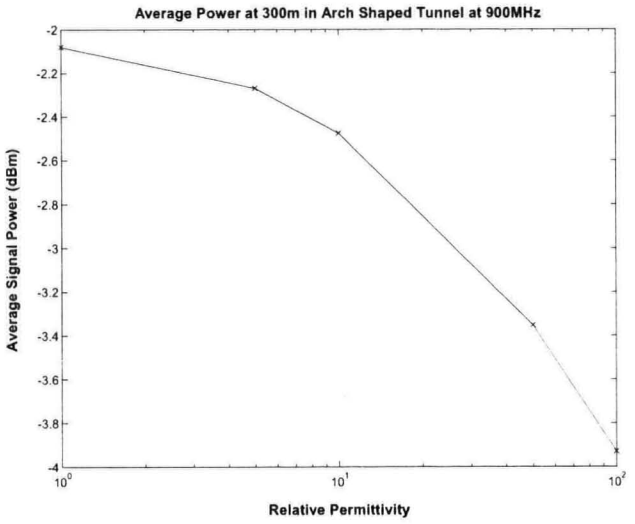

Figure 6.15: Average Signal Power at the end of arch tunnel at 900MHz versus ϵ_r

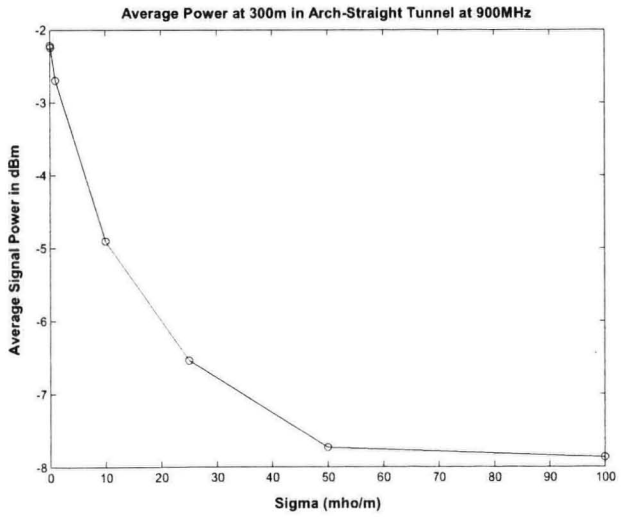

Figure 6.16: Average Signal Power at the end of arch tunnel at 900MHz versus σ

6.4.4 Transmitter Antenna Position

Figure 6.17 represents the power distance variation for three different positions of the transmit antenna, left corner, middle and right most corner of the tunnel. Simulations were carried out at 900MHz and $\epsilon_r = 4.0$, $\sigma = 0.01$mho/m in a curved rectangular tunnel. Power loss for the case of left and middle position is almost the same while for the right position there is more power loss. This effect depends on which direction tunnel is turning, if the tunnel is bending towards the left, suitable positions of the transmitting antenna are center or right. Similarly, if the tunnel is bending in the right direction the transmitting antenna should be placed in the middle or left. Thus the mobile antenna position should be considered carefully in order to maximize the received signal power and is dependant on tunnel geometry.

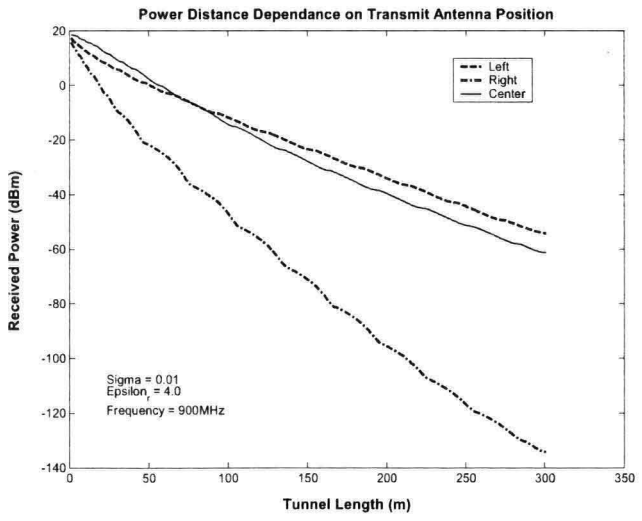

Figure 6.17: Plot of power distance dependence on transmit antenna positions

6.4.5 Effect of Curvature

The curvature in the tunnel causes large reflection angles, therefore radio wave propagation characteristics in any tunnel for different curvatures are not equal. Figure 6.18 shows average power distribution in an arch tunnel for different radius of curvatures at 900MHz. ϵ_r and σ is assumed to be 4.0 and 0.01mho/m respectively. The curvature is purely horizontal in these simulations i.e. θ is zero. It can be seen that average power decreases with increase in radius of curvature. For large radius of curvatures ρ reflections inside the tunnel are more and hence more power is lost inside the tunnel. A similar effect can be observed in case of rectangular tunnels.

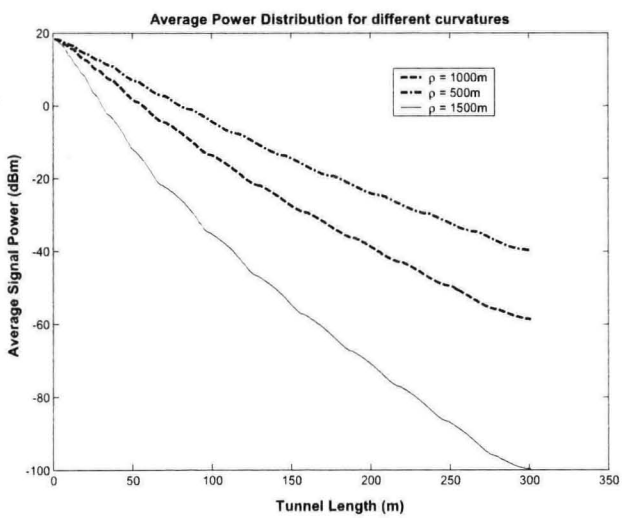

Figure 6.18: Average Power Distribution in an arch tunnel at 900MHz for different curvature radius

6.4.6 Effect of Vehicles

Propagation loss inside a tunnel is affected by a number of parameters including, frequency of transmission, size of tunnel, shape of tunnel, electrical properties of tunnel wall, polarisation, size of vehicle, number of vehicles, location of vehicles inside tunnel etc. Propagation loss inside a tunnel is loss due to the tunnel itself and losses due to the presence of obstructions. In this section, propagation loss because of number, size and location of vehicles in a rectangular straight and curved tunnel is examined.

Size of Vehicles

It is well know that the scattering properties of a scatterer depends on the size of scatterer. So different sizes of obstructions (vehicles) are expected to produce different propagation losses. Different vehicles (small van, bus and truck) of dimensions mentioned in Table 6.1 were placed at 40m from the entrance of tunnel. Results are shown in figure 6.19 for a rectangular straight tunnel and in figure 6.20 for a curved rectangular tunnel at 950MHz. The power level is measured along the length of the tunnel at the center line of the cross section. The presence of vehicles produces an additional loss behind the vehicle in each case. As expected, large vehicles produces more loss than small vehicles both in straight and curved tunnels.

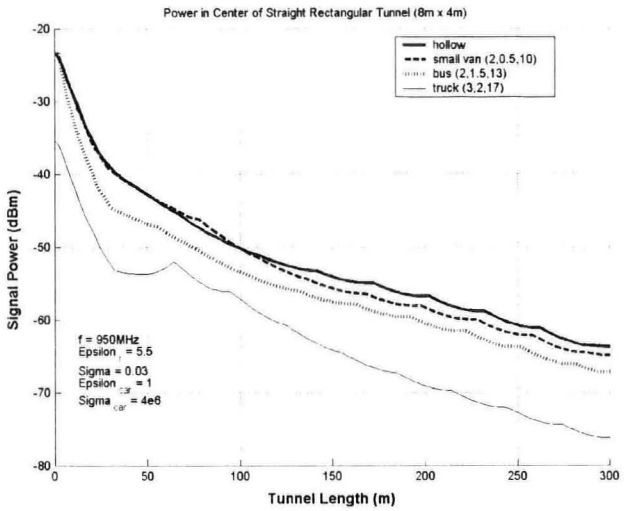

Figure 6.19: Received power level vs. tunnel length in Straight tunnel

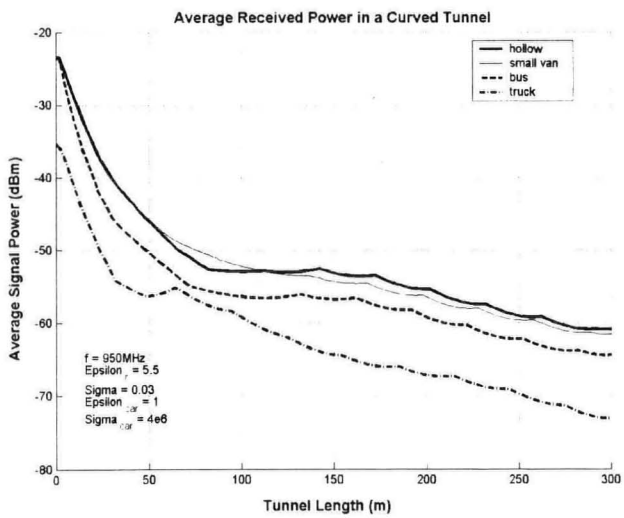

Figure 6.20: Received power level vs. tunnel length in Curved tunnel

Location of Vehicles

To examine propagation loss due to the location of vehicles inside tunnel, a bus of dimensions shown in Table 6.1 is placed at various locations in straight and curved tunnel. The power level in dBm versus tunnel length is shown in figures 6.21 and 6.22. It can be seen from the diagram that power level remains the same in a stable region and is independent on the location of vehicle for a straight tunnel. In a curved tunnel, power level in the stable region depends on the location of vehicle. This is because of the curvature effect of tunnel. If the bus is far from the transmitter, power loss is more as compared to one close to transmitter.

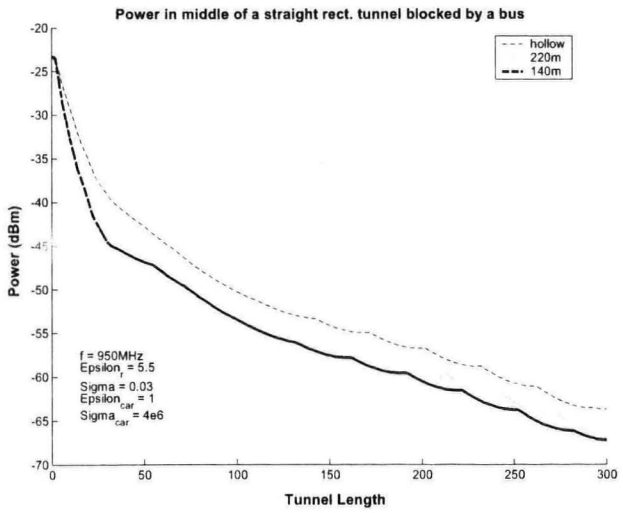

Figure 6.21: Received power level vs. tunnel length in Straight tunnel

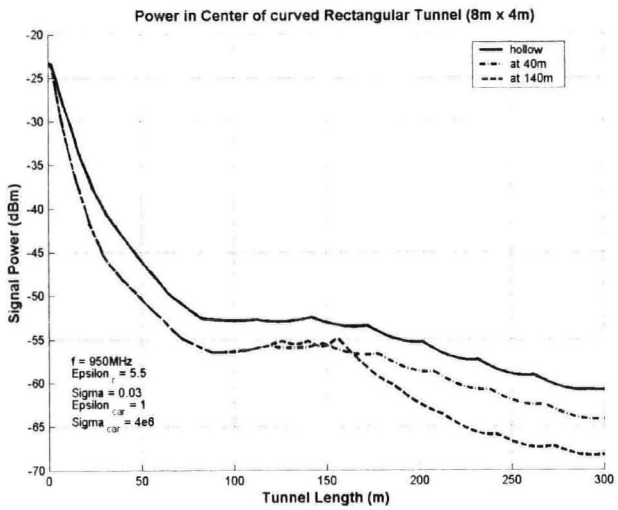

Figure 6.22: Received power level vs. tunnel length in Curved tunnel

Number of Vehicles

Next, how the propagation loss changes due to the number of vehicles is examined. Power level is calculated for a hollow tunnel, with one bus and with three buses all placed at 40m away from the entrance of the tunnel. From figure 6.23 and 6.24 it is clear that power level changes because of the number of vehicles and produces additional loss which is quite prominent in the stable region. The value of propagation loss depends on many factors, but it almost increases in linear proportion, provided identical vehicles are used.

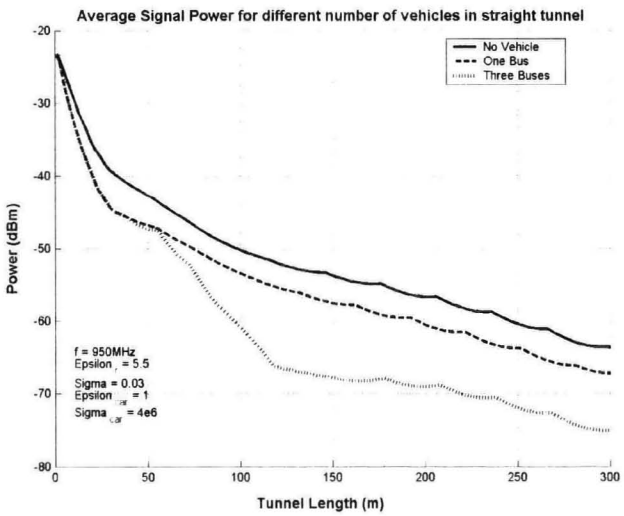

Figure 6.23: Received power level vs. tunnel length in Straight tunnel

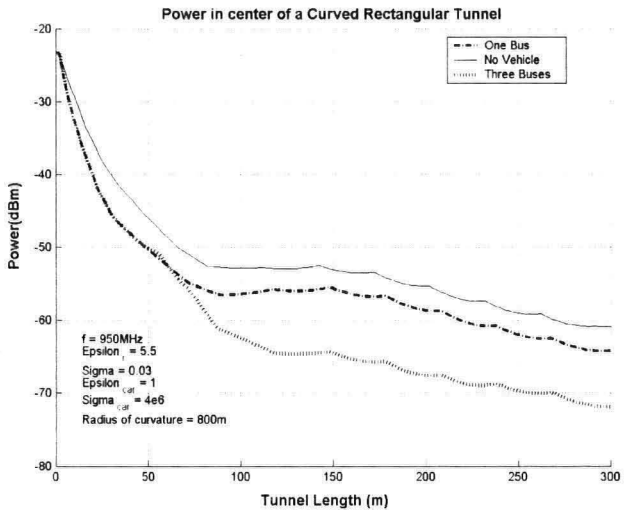

Figure 6.24: Received power level vs. tunnel length in Curved tunnel

6.5 Summary

The finite element based vectorial parabolic equation method is capable of modelling radio communications in tunnels of different cross sections. This approach can take into account the tunnel geometry, frequency of waves, electrical or mechanical properties of tunnel walls and tunnel curvature in both dimensions. This approach can easily be adapted to complex tunnel structures and different propagation scenarios. Different radiation patterns or antenna structures can be easily integrated with this method. Computational advantages of the parabolic equation method have already been demonstrated and can be used to model obstructions in tunnels without much additional computational burden. 3D field distributions and power loss diagrams obtained by the FE solution of V-PEM help to provide deeper insight into the physical effects of radio wave propagation inside tunnels. Effects of

curvature and electrical parameters such as conductivity and relative permittivity is analysed. The finite element method along with the parabolic equation method provide a fast and accurate solution of radio wave propagation in realistic tunnels and can be used to enhance future communication systems.

Chapter 7

Conclusion and Further Work

7.1 Conclusions

Different radio wave propagation models based on the parabolic equation method have been proposed and simulated efficient solutions were developed using the finite element method . The primary aim of this research was to develop finite element formulations of radio wave propagation in different environments. The different propagation scenarios considered in this thesis were the troposphere, urban areas, vegetation and tunnels. The finite element method is used because of its accuracy and versatility. The most attractive feature of the finite element method is its ability to handle complex geometries and boundaries with relative ease. It was shown in this thesis that the proposed finite element formulation provided an accurate modelling of wave propagation in the environments considered.

Advantages of high speed computing allows new approaches for the precise modelling of radio wave propagation in the troposphere to satisfy new demands. A method to accurately model tropospheric wave propagation in the presence of height dependant refractivity using the finite element method was presented. The finite element solution was computed at some range and then the solution advances using a marching algorithm. The main advantage of using the finite element analysis is that this approach can handle a highly varying environment by using smaller elements and different environmental properties can be assigned to each element. The model allows specification of the frequency, polarisation, earth shape, antenna pattern, antenna altitude and elevation angle.

Simulation results for the 2D and 3D finite element solution of the parabolic equation method were presented in chapter 4. Finite element formulation of narrow and wide angle versions of the parabolic approximation were described. It was shown that wide angle finite element formulation of the parabolic equation method successfully model large propagation angles in contrast to the narrow angle model.

Coverage diagrams and path loss contours were shown at different frequencies and for the case of flat earth and irregular terrain. Different abnormal environmental conditions have been investigated and ducting phenomena in the troposphere were studied. In microwave communications, refractivity variations in the lower part of the troposphere are usually important and are considered in this thesis. However, the simulations made and described in this thesis can easily take into account a

larger vertical extent depending on the relevant terrain profile. It has been shown that the proposed method can model radio wave propagation over irregular terrain, urban streets or any complex geometry easily.

The method is capable of taking account of the vertical and horizontal distribution of tropospheric refractivity of a real terrain profile hence can model highly varying atmosphere easily, and the electrical properties of the ground. The refractive index of the troposphere is independent between consecutive range steps and can be entered easily in successive range steps. Moreover, measured environmental data can be entered at each range in the program and between range steps data can be obtained by interpolation. Aside from slight differences due to the extra interpolations required between profiles, the complexity of the environment has no impact on the time required for calculations.

Accurate modelling of wave propagation behaviour over a forested environment is of great interest for civilian and military communication since the forest affects communication channel significantly. The finite element method has been applied to model wave propagation in the presence of vegetation using a wide angle formulation of the parabolic equation method. It has been shown that the proposed approach can handle wave propagation in vegetation similar to the troposphere. Different types of vegetation have been analysed and results were compared with the well know Tamir results. It has been shown that for accurate results, the refractive index of a forest should be close to unity with this approach.

The theory of oversised nonuniform waveguides has a number of applications in electromagnetics ranging from radio communications in tunnels to light propagation in optical fibers. By using the theory of oversised waveguides a vectorial parabolic wave equation can be derived and solved efficiently and accurately using the finite element method . Field components in the vectorial parabolic equation coupled on the tunnel walls via a Leontovich-type matrix impedance boundary condition. The model is described along with its finite element formulation for curved and straight tunnels. Different obstructions were considered and it was demonstrated that this method provides a suitable approach for modelling wave propagation in empty and blocked tunnels.

Radio wave characteristics inside tunnels were influenced by different factors like shape of a tunnel, its curvature, frequency of propagation, electrical properties of tunnel walls, different size and type of obstructions, etc. These factors were analysed separately and some conclusions were made. It was shown that for straight tunnels more power is lost at low frequencies rather than high frequencies. For curved tunnels of any cross section, power is mainly concentrated on one side of the tunnel if the transmitting antenna is placed at the center of the tunnel. Tunnel shape (rectangular or arch) has little influence on the propagation of waves.

Average powers were plotted versus electrical parameters; conductivity σ and relative permittivity ϵ_r. Threshold values of σ and ϵ_r can be calculated for different tunnel geometries and shapes. The effect of curvature and transmitter antenna posi-

tion were also analysed in chapter 6. Real tunnels always carry vehicles, so vehicles of different sizes were considered. Propagation loss inside a tunnel is loss due to the tunnel itself and losses due to obstructions like vehicles. Propagation losses due to size, number and location of vehicles were examined. It was shown that large vehicles produces more loss than small vehicles both in straight and curve tunnels.

7.2 Further Work

There are few suggestions regarding the future work. The proposed type of analysis is not suitable for ultra high frequencies because of high computational requirements. The finite element analysis is accurate if the element size is about $\lambda/10$ and generation of such a mesh is computationally inefficient at very high frequencies. Some meshing algorithms or matrix analysis can be proposed to deal with such cases. Further, finite element based models can be tested in real cases by performing experiments and comparing results.

Backscatter is a process that can often be disregarded in rural areas but not in built-up areas. That's the reason the parabolic equation method is a doubtful method to use in urban areas. So in future it might be conceivable to devise schemes where the paraxial direction in PEM is changed after reflections at building surfaces, which is obviously complicated in urban areas because of the large number of multipath signals. Another suggestion is to combine the parabolic equation method with ray

tracing techniques and propose some hybrid models. Similarly for the case of the troposphere, the possibility of utilisation of meteorological techniques to obtain real spatial distribution of atmospheric refractivity may be studied.

In future, a complete model including urban houses/buildings and forest needs to be produced. The proposed method presented in this thesis needs to be modified to include the absorbing and diffracting properties of houses and trees. Perhaps, one need to leave parabolic approximation and find a solution that can be formulated by direct solution of the Helmholtz equation. In future the effects of scattering by forest leaves can be added in the model, and a more accurate but complex model for propagation in vegetation can be obtained.

Appendix 1

Method of Weighted Residual

In this appendix the method of weighted residuals for obtaining approximate solutions to differential equations is introduced. Weak formulation of the residual in the weighted residual method is also described. Weighted residual methods are another way to develop approximate solutions. As described in chapter 2, in the finite difference method an approximation to the differential equation at a point is formed. In contrast, in weighted residual methods, form of the global solution and then adjust parameters to obtain the best global fit to the actual solution is assumed.

In weighted residual methods the requirement is that the approximate function must satisfy both the essential and natural boundary conditions. In the weighted residual method the weak form of the differential equation can be used to develop methods that loosen this requirement, so that only the essential boundary conditions must be satisfied by our approximating function as described later in this section. The basic step in weighted residual methods is to assume a solution of the form:

$$u_n = \sum_{j=1}^{n} a_j u_j \tag{A1-1}$$

The main task is to solve for the coefficients a_j that give a best approximation (by some measure) to the exact solution. To understand the method of the weighted residual, consider a partial differential equation of second order along with boundary

conditions as,

$$\frac{\partial^2 u}{\partial x^2} + b = 0, \quad \text{for} \quad 0 \leq x \leq x_{max} \tag{A1-2}$$

$$u\,|_{x=0} = 0 \tag{A1-3}$$

$$\left.\frac{\partial u}{\partial x}\right|_{x=x_{max}} = P \tag{A1-4}$$

Equation (A1-2) along with the boundary conditions in (A1-3) and (A1-4), forms the mathematical description of the problem at hand. They can be solved by direct integration for the exact solution.

For the weighted residual formulation, first choose a weighting function $w(x)$ then multiply (A1-2) with the weighting function:

$$w\left[\frac{\partial^2 u}{\partial x^2} + b\right] = 0 \tag{A1-5}$$

and than integrate over the whole domain.

$$\int_0^{x_{max}} w\left\{\frac{\partial^2 u}{\partial x^2} + b\right\} dx \tag{A1-6}$$

This is called the weighted residual formulation. It is called this because if a trial function u_n (that satisfies all boundary conditions) is assumed then,

$$\frac{\partial^2 u_n}{\partial x^2} + b = R(x) \neq 0 \tag{A1-7}$$

Instead, there is an error (residual) that is a function of x . Thus (A1-7) is really a weighting of the residual over the domain $0 \leq x \leq x_{max}$, which must be zero for the approximate solution, so,

$$\int_0^{x_{max}} w(x)R(x)\,dx = 0 \tag{A1-8}$$

Now pick a trial function which satisfies all boundary conditions,

$$u_n = Px + a_1 \sin\left(\frac{\pi x}{2x_{max}}\right) \tag{A1-9}$$

Clearly, this function satisfies the essential boundary condition (A1-3). In addition, the first term satisfies the natural boundary condition (A1-4). The second term is zero at the essential condition and has zero slope at the natural condition, so it does not add additional terms at the boundaries. Taking the derivatives and substituting in equation (A1-7).

$$-a_1\left(\frac{\pi}{2x_{max}}\right)^2 \sin\left(\frac{\pi x}{2x_{max}}\right) + b = R(x) \tag{A1-10}$$

For simplicity assume $P = b = 1$ and plot th residual for different values of a_1. The residual is a function of x and from figure A1-1 it is clear why the residual is integrated. The residual can be weighted in any way over the interval and for the integral to be zero. Depending on how the residual is weighted different solutions can be obtained. Different methods that can be used to weight the residual are summarised below:

Collection Method

In this case, the residual is forced to be zero at a specific location (nail-down method). That is,

$$R(x_i) = 0 \tag{A1-11}$$

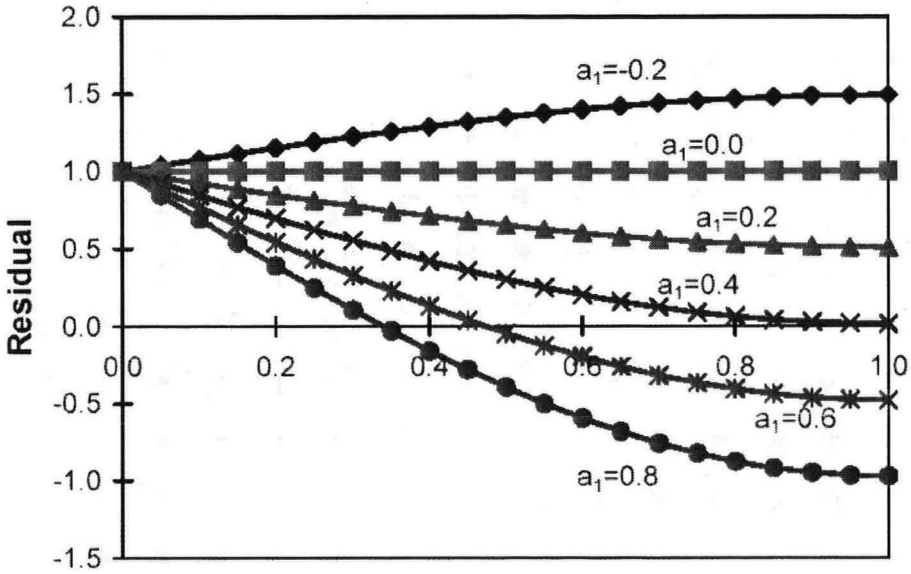

Figure A1-1: Residual over domain of interest

This is equivalent to selecting the Dirac delta function as the weighting function.

$$w(x) = \delta(x - x_i) = \begin{cases} \infty & \text{when } x = x_i \\ 0 & \text{when } x \neq x_i \end{cases}$$

and for any function $f(x)$,

$$\int_{-\infty}^{\infty} f(x)\delta(x - x_i)\, dx = f(x_i)$$

That is the weighted residual according to equation (A1-8) is,

$$\int_0^1 \delta(x - x_i) R\, dx = 0 \tag{A1-12}$$

Pick a value of x_i, e.g., $x_i = 0.5$, that is, the residual is a force to equal zero at the midpoint, solving equation (A1-12) gives a value of $a_1 \approx 0.6$.

Subdomain Method

Alternately, let us weight the residual uniformly over the interval (glue method). That is,

$$w(x) = 1$$

Then from equation (A1-8),

$$\int_0^1 1.R\,dx = 0 \tag{A1-13}$$

Putting the value of the residual from (A1-10) and solving to obtain value of $a_1 \approx 0.637$.

Least Square Method

In least squares, it is required that the squared residual be minimized with respect to the adjusting parameter, i.e.,

$$\text{Minimize}\left(\int_0^1 R^2\,dx\right)$$

or

$$\int_0^1 R\frac{\partial R}{\partial a_1}\,dx = 0 \tag{A1-14}$$

This is equivalent to selecting $\frac{\partial R}{\partial a_1}$ as the weighting function. From equation (A1-7) calculate $\frac{\partial R}{\partial a_1}$ and put it in equation (A1-14) to solve for a_1. The value of a_1 calculated by the least square method is 0.516.

Galerkin Method

Finally, if the same function is used for the weighting function as is used for the approximating function (except that the term in the approximating function that satisfies the essential boundary conditions is not included) then:

$$w(x) = a_1 \sin \frac{\pi x}{2} \tag{A1-15}$$

Substitute equation (A1-15) in (A1-7) and obtain the value of $a_1 \approx 0.516$. Note that for this particular example, the least-squares method and Galerkin's method yield identical results. In general, however, the two methods may give different answers. In order to improve the approximate solution more terms can be added in the trial function defined in equation (A1-7). The most widely used trial functions are polynomial functions.

Weak Formulation The Galerkin formulation described in this appendix is called the strong formulation of the weighted residual method. The strong formulation requires evaluation of the term $\int_{x_{min}}^{x_{max}} w \left(\frac{\partial^2 u_n}{\partial x^2} \right) dx$, which includes the highest order of the derivative term in the differential equation. The integral must have a non-zero finite value to yield a meaningful approximate solution to the differential equation. This means a trial function should be differentiable twice and its second derivative should not vanish. In order to reduce the requirement for a trial function in terms of differentiability, integration by parts is applied to the strong formulation.

Consider the second order term,

$$\int_{x_{min}}^{x_{max}} w \left[\frac{\partial^2 u_n}{\partial x^2}\right] dx$$

Now by applying integration by parts,

$$\int_{x_{min}}^{x_{max}} w \left[\frac{\partial^2 u_n}{\partial x^2}\right] dx = \int_{x_{min}}^{x_{max}} \left[-\frac{\partial w}{\partial x}\frac{\partial u}{\partial x}\right] dx + \left[w\frac{\partial u_n}{\partial x}\right]_{x_{min}}^{x_{max}} \qquad \text{(A1-16)}$$

As seen from equation (A1-16) the trial function needs the first order differentiation instead of the second order differentiation. As a result, the requirement for the trial function is reduced. This formulation is called the weak formulation.

Appendix 2

Linear Quadratic Elements

In this appendix Linear Quadratic Elements for Galerkin based Finite Element formulation are described. Other than linear elements or first order elements, quadratic or higher order elements can be used for Galerkin based finite element formulation. The main advantage of using first order or linear elements is simplicity of formulation and narrow bandwidth of the system of equations. However, the disadvantage is poor accuracy and slow convergence of solution with respect to the number of nodes or elements. One approach to obtain a high accuracy without increasing the number of nodes is to employ higher order interpolation function. This approach has proven to be very cost-effective [127].

Quadratic elements have three nodes one at each of the two endpoints and a third usually placed at the center of the element as shown in figure A2-1. Within each

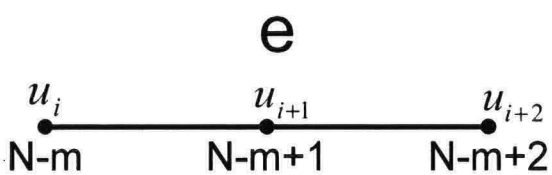

Figure A2-1: Quadratic element with local node numbers

element the interpolation function is approximated as,

$$u^e(x) = a + bx + cx^2 \tag{A2-1}$$

Now enforce equation (A2-1) at the three nodes of element e as shown in figure A2-1

yields,

$$\begin{aligned} u_i^e\ (x) &= a + bx_i + cx_i^2 \\ u_{i+1}^e(x) &= a + bx_{i+1} + cx_{i+1}^2 \\ u_{i+2}^e(x) &= a + bx_{i+2} + cx_{i+2}^2 \end{aligned} \tag{A2-2}$$

Solving for a, b and c and substituting in (A2-1),

$$u^e(x) = \sum_{j=1}^{3} N_j^e(x) u_j^e \tag{A2-3}$$

where the interpolation functions are given by,

$$\begin{aligned} N_i^e &= \frac{(x - x_{i+1})(x - x_{i+2})}{(x_i - x_{i+1})(x_i - x_{i+2})} \\ N_{i+1}^e &= \frac{(x - x_i)(x - x_{i+2})}{(x_{i+1} - x_i)(x_{i+1} - x_{i+2})} \\ N_{i+2}^e &= \frac{(x - x_i)(x - x_{i+1})}{(x_{i+2} - x_i)(x_{i+2} - x_{i+1})} \end{aligned} \tag{A2-4}$$

Appendix 3

List of Publications

1. "Modelling of Wave Propagation over Irregular Terrain using Finite Element Method", Kamran Arshad, Ferdinand Katsriku and Aboubaker Lasebae, Accepted for publication in SPRINGER VERLAG Special Issue "Advances in Scientific Computing" (Book Chapter).

2. "An Investigation of Tropospheric Wave Propagation using Finite Elements", Kamran Arshad, Ferdinand Katsriku and Aboubaker Lasebae, WSEAS Transactions in Communications, Issue 11, Volume 4, ISSN: 1109-2742, November 2005.

3. "Effect of different parameters on attenuation rates in circular and arch tunnels", Kamran Arshad, Ferdinand Katsriku and Aboubaker Lasebae, Progress in Electromagnetics Research Symposium, Beijing China, 26-30 March 2007.

4. "An investigation of Tropospheric wave propagation over irregular terrain and urban streets using finite elements", Kamran Arshad, Ferdinand Katsriku and Aboubaker Lasebae, 7th WSEAS Conference on Telecommunications and Informatics, Dallas USA, 22-24 March 2007 (RECEIVED BEST STUDENT PAPER AWARD).

5. "Finite Element formulation of Radio Wave Propagation in Tunnels", Kamran Arshad, Ferdinand Katsriku and Aboubaker Lasebae, 2006 International

Symposium on Antennas and Propagation, Singapore, 1-4 November 2006.

6. "Radiowave VHF Propagation modelling in forest using finite elements", Kamran Arshad, Ferdinand Katsriku and Aboubaker Lasebae, 2nd IEEE Conference in Information and Communication Technologies: From Theory to Applications, Syria, 24-28 April 2006.

7. "Finite Element based beam propagation method for 3D Wave Propagation in troposphere", Kamran Arshad, Ferdinand Katsriku and Aboubaker Lasebae, 8th International Conference on Advanced Communication Technology, Republic of Korea, 20-22 February 2006.

8. "Propagation modelling in troposphere using paraxial form of Helmholtz equation", Kamran Arshad, Ferdinand Katsriku and Aboubaker Lasebae, IEEE Asia Pacific Microwave Conference, China, 4-7 December 2005.

9. "A new approach in modelling EM Wave Propagation in Troposphere using Finite Elements", Kamran Arshad, Ferdinand Katsriku and Aboubaker Lasebae, WSEAS Conference on Information Technology, Greece, August 2005 (RECEIVED BEST STUDENT PAPER AWARD).

References

[1] ITU-R. The radio refractive index: its formula and refractivity data. *International Telecommunication Union, Recommendation*, pages 453–459, 2003.

[2] N. Chandarn and M. C. Valenti. Three generations of cellular wireless systems. *IEEE Potentials*, 20(1):32–35, March 2001.

[3] J. M. Periera. Balancing public and private in fourth generation. *The 12th IEEE International Symposium, Indoor and Mobile radio Communications*, 12:125–132, September/October 2001.

[4] Kamran Arshad and A. U. H. Sheikh. Performance of wireless ofdm system channel estimation with different pilot patterns. *8th IEEE international symposium on spread spectrum techniques and applications*, pages 179–183, 30 Aug - 2 Sept 2004.

[5] J. Takada, Jiye Fu, Z. Houtao, and T. Kobayashi. Spatio-temporal chan-

nel characterization in a suburban non-line-of-sight microcellular environment. *IEEE J. Select. Areas Commun.*, 20:532–538, April 2002.

[6] R. S. Awadallah, J. Z. Gehman, J. R. Kuttler, and M. H. Newkirk. Modeling radar propagation in three-dimensional environments. *Johns Hopkins Apl. Technical Digest*, 25(2):101–111, 2004.

[7] http://www.mobilemastinfo.com/information/history.htm.

[8] B. H. Fleury and P. E. Leuthold. Radiowave propagation in mobile communications: an overview of european research. *IEEE Communication Mag.*, 50(3):662–673, March 2002.

[9] Y. Zhang, Y. Hwang, and R. G. Kouyoumjian. Ray-optical prediction of radiowave propagation characterstics in tunnel environments - part 2. *IEEE Transactions on Antennas and Propagation*, 46(3):1337–1345, September 1998.

[10] In-building/in-tunnel user considerations. Report, Public Safety PSWN Wireless Network, August 2002.

[11] S. Y. Seidel and T. S. Rappaport. Site-specific program prediction for wireless in-personal communication system design. *IEEE Trans. Veh. Technol.*, 43:879–891, November 1994.

[12] M. A. Leontovich and V. A. Fock. Solution of propagation of electromagnetic

waves along the earth's surface by the method of parabolic equations. *J. Phys. USSR*, 10:13–23, 1965.

[13] F. A. Katsriku, B. M. A. Rahman, and K. T. V. Grattan. Numerical modelling of second harmonic generation in optical waveguides using the finite element method. *IEEE Journal of Quantum Electronics*, 33:1727–1733, 1997.

[14] T. Tamir. Radiowave propagation along mixed path in forest environment. *IEEE Transactions on Antennas and Propagation*, 25(4):471–477, November 1977.

[15] D. C. Livingston. *The Physics of Microwave Propagation.* 1970.

[16] R. Heddergott, B. H. Fleury, and U. P. Bernhard. Stochastic radio channel model for advanced indoor mobile communication systems,. *IEEE Transactions On Vehicular Technology*, 51(5), September 2002.

[17] R. Janaswamy. *Radiowave Propagation and Smart Antennas for Wireless Communications.* Kluwer Academic Publishers, Massachusetts, 2000.

[18] K. J. Gladstone and J. P. McGeehan. Computer simulation of multipath fading in the land mobile radio environment. *IEE Proceedings G. Electronic Circuits and Systems*, 127:323–330, December 1980.

[19] J. W. McKown and Jr. R. L. Hamilton. Ray tracing as a design tool for radio networks. *IEEE Network Magazine*, 5(6):27–30, November 1991.

[20] W. Honcharenko, H. L. Bertoni, J. L. Dailing, J. Qian, and H. D. Yee. Mechanisms governing uhf propagation on single floors in modern office buildings. *IEEE Transactions on Vehicular Technology*, 41(4):496–504, November 1992.

[21] M. Lebherz, W. Wiesbeck, and W. Krank. A versaitle wave propagation model for the vhf/uhf range considering three-dimensional terrain. *IEEE Transactions on Antennas and Propagation*, 40(10):1121–1131, October 1992.

[22] R. Gollreiter. Channel models. *RACE Advanced TDMA Mobile Access (ATDMA)*, Rep. R2084/ESG/CC3/DS/P/029/b1, May 1994.

[23] G. E. Athanasiadou, A. R. Nix, and J. P. McGeehan. A new 3-d indoor ray tracing propagation model with particular reference to the prediction of power and delay spread. *Sixth IEEE International Symposium on Personal, Indoor and Mobile Radio Communications, PIMRC'95*, 3:1161–1165, 27-29 September 1995.

[24] COST-207. Cost 207: Digital land mobile radio communications. Technical report, Commission of the European Communities, 1989.

[25] R. S. Awadallah and G. S. Brown. Low-grazing angle scattering from rough surfaces in a duct formed by a linear-square refractive index profile. *IEEE Trans. Antennas Propag.*, 48:1461–1474, 2000.

[26] G. D. Dockery. Modeling electromagnetic wave propagation in the troposphere

using the parabolic equation. *IEEE Trans. Antennas Propagat.*, 36:1464–1470, October 1988.

[27] M. Levy. *Parabolic Equation Methods for Electromagnetic Wave Propagation.* IEE Publisher, 2005.

[28] K. H. Craig and M. F. Levy. Parabolic equation modelling of the effects of multipath and ducting on radar systems. *IEE Proceedings of Radar and Signal Processing*, 138(2):153–162, May 1991.

[29] S. T. McDaniel. Propagation of a normal mode in the parabolic approximation. *J. Acoust. Soc. Am.*, 57(2):307–311, 1975.

[30] F. D. Tappert. The parabolic approximation method. *in Wave Propagation and Underwater Acoustics Vol 70 (Lectures Notes in Physics)*, 1977.

[31] S. W. Marcus. A hybrid (finite difference-surface greens function) method for computing transmission losses in an inhomogeneous atmosphere over irregular terrain. *IEEE Trans. Antennas Propagation*, 40(12):1451–1458, December 1992.

[32] F. J. Ryan. Analysis of electromagnetic propagation over variable terrain using the parabolic wave equation. *Rep. NOSC Tr 1453*, October 1991.

[33] K. H. Craig. Propagation modelling in the troposphere: Parabolic equation method. *IEEE Electronics Letters*, 24(18):1136–1139, 1988.

[34] V. A. Fock. *Electromagnetic Diffraction and Propagation Problems.* Pergamon Press, 1965.

[35] R. S. Awadllah. *Rough Surface Scattering and Propagation over Rough Terrain in Ducting Environments.* Phd dissertation, Virginia Polytechnic Institute and State University, USA, April 1998.

[36] T. A. Spencer, R. A. Walker, and R. M. Hawkes. Inverse diffraction parabolic wave equation localisation system (idpels). *Journal of Global Positioning Systems*, 4(1-2):245–257, 2005.

[37] R. M. Hawkes, T. A. Spencer, and R. A. Walker. Tropospheric propagation model using huygen's principle. *Proceedings of the second IASTED Conference, Antennas, Radar and Wave Propagation*, 19-21, July 2005.

[38] G. N. Watson. The diffraction of radiowaves by the earth. *Proc. Roy. Soc. London*, 95:83–99, 1918.

[39] B. Van der Pol and H. Bremmer. The propagation of radiowaves over a finitely conductin earth. *Philos. Magazine*, 27:261–275, 1937.

[40] G. D. Malyuzhinets. Progress in understanding diffraction phenomena. *Sov. Phys. Usp.*, 69:321–334, 1959.

[41] J. F. Claerbout. *Fundamentals of Geophysical Data Processing.* Blackwell, Oxford, UK, 1985.

[42] M. D. Collins. Applications and time-domain solution of higher-order parabolic equations in underwater acoustics. *Journal of the Acoustical Society of America*, 86:1097–1102, 1989.

[43] F. B. Jensen, W. A. Kuperman, M. B. Porter, and H. Schmidt. Computational ocean acoustics. *American Institute of Physics*, 1994.

[44] L. M. Brekhovskikh. *Waves in Layered Media.* New York: Academic Press, 1980.

[45] H. Oraizi and S. Hosseinzadeh. Determination of the effect of vegetation on radiowave propagation by the parabolic equation method. *International Symposiom on Telecomunication, Isfahan, Iran*, pages 340–344, August 2003.

[46] M. D. Collings. A split-step pade solution for the parabolic equation method. *J. Acoust. Soc. Am.*, 94:1736–1742, 1993.

[47] J. F. Claerbout. *Fundamentals of Geophysical Data Processing with Applications to Petroleum Prospect.* McGraw-Hill, New York, 1976.

[48] R. J. McArthur. Propagation modelling over irregular terrain using the split-step parabolic equation method. *International Conference: Radar 92*, (365):54–57, October 1992.

[49] A. E. Barrios. A terrain parabolic equation model for propagation in the

troposphere. *IEEE Transactions on Antennas and Propagation*, 42(1):90–98, January 1994.

[50] R. Cocciolo, T. Itoh, G. Pelosi, and P. P. Silvester. Finite-element methods in microwaves: A selected bibliography. *IEEE Antennas and Propagation Magazine*, 38(6):34–48, 1996.

[51] å. Waern, P. Johansson, B. Lundborg, E. Löfsved, and P. Sakari. The communication channel in urban operations - a first survey. *FOI Linköping, FOI-R–0884–SE*, June 2003.

[52] P. P. Silvester and R. L. Ferrari. *Finite Elements for Electrical Engineers.* Cambridge University Press, Cambridge, 1990.

[53] R. F. Harrington. *Field Computation by Moment Methods.* The Macmillan Co., New York, 1968.

[54] G. J. Burke and A. J. Poggio. Numerical electromagnetic code (nec) - method of moments. *Naval Ocean Syst. Center San Diego, CA, NOSC Tech. Document*, January 1981.

[55] K. S. Lee. Numerical solution of initial boundary value problems involving maxwells equations in isotropic media. *IEEE Transactions on Antennas and Propagation*, AP-14(4):302–207, 1966.

[56] D. Lee and S. T. McDaniel. Ocean acoustics propagation by finite difference methods. *comput. Math. Applic.*, 14:305–423, 1987.

[57] G. D. Smith. *Numerical Solution of Partial Differential Equations: Finite Difference Methods,*. Clarendon Press, Oxford, 3rd edition, 1985.

[58] J. R. Wolfgang. The transmission-line matrix method, theory and applications. *IEEE Transaction on microwave theory and techniques*, 33(10):882–893, October 1985.

[59] T. Wriedt. *The Generalized Multipole Technique for Electromagnetic and Light Scattering.* Amterdam Elsevier, 1999.

[60] Y. Leviatan and A. Boag. Analysis of electromagnetic scattering from dielectric cylinders using a multifilament current model. *IEEE Trans. Antennas Prop.*, AP-35:1119–1127, October 1987.

[61] Y. Leviatan, P. G. Li, A. J. Adams, and J. Perini. Single post inductive obstacle in rectangular waveguide. *IEEE Trans. Microwave Theorey Tech.*, MTT-31:806–1812, October 1983.

[62] A. C. Ludwig. A comparison of spherical wave boundary value matching versus integral equation scattering solutions for a perfectly conducting body. *IEEE Trans. Antennas Prop.*, AP-34, July 1986.

[63] D. M. Young and K. C. Jea. Generalized conjugate gradient acceleration of nonsymmetrizable iterative methods. *Linear Algebra and its Applications*, 34:159–194, 1980.

[64] T. K. Sarkar. From reaction concept to conjugate gradient: Have we made any progress. *IEEE Trans. Antennas Prop. Society Newsletter*, 31:6–12, August 1989.

[65] M. P. M. Hall, L. W. Barclay, and M. T. Hewitt. *Propagation of radiowaves.* The Institution of Electrical Engineers, London, 1996.

[66] G. B. Baumgartner, H. V. Hitney, and R. A. Pappert. Duct propagation modelling for the integrated-refractive-effects prediction programs. *IEEE Proc., Pt. F*, 130:630–642, 1983.

[67] C. H. Shellman. A new version of modesrch using interpolated values of the magnetoionic reflection coefficients,. *Interim technical report NOSC/TR-1143, Naval Ocean Systems Cneter, ADA179094*, 1986.

[68] H. V. Hitney. Refractive effects from vhf to ehf, part a: Propagation mechanism. *AGARD-LS-196, 4A-1-4A-13*, 1994.

[69] P. L. Slingsbay. Modelling tropospheric ducting effects on vhf/uhf propagation. *IEEE Transaction on Braodcasting*, 37:25–34, 1991.

[70] J. R. Wait. Coupled mode analysis for a non-uniform troposphere wave guide,. *Radio Sri.,*, 15(3):667–673, 1980.

[71] L. B. Felsen. Hybrid ray-mode fields in inhomogeneous waveguides and ducts,. *J. Acoust. Soc. Am.,*, 69(2):352–361, 1981.

[72] J. A. Stratton. *Electromagnetic Theory.* McGraw-Hill, 1941.

[73] R. F. Graham. *Identification of Suitable Carrier Frequency for Mobile Terrestrial Communication Systems with low Antenna Height.* http:argreenhouse.com/society/TacCom/milcom_98_paper.html, 1998.

[74] N. Blaunstein. Radiowave propagation in cellular networks,. *Artech House mobile communication Library*, 1999.

[75] R. F. S. Caldeirinha. Radio characterisation of single trees at micro- and millimetre wave frequencies,. *PhD thesis, University of Glamorgan*, 2001.

[76] T. Tamir. On radio-wave propagation in forest environments. *IEEE Transactions on Antennas and Propagation*, 15(6):806–817, November 1967.

[77] K. Sarabandi and I. S. Koh. Effect of air-canopy interface roughness on hf-vhf wave propagation in forest. *IEEE Trans. Antennas Propagation.*, 50(2), 2002.

[78] R. B. L. Stephens. A study and modelling of the propagation effects of vege-

tation on radiowaves at cm-wavelength frequencies. *PhD thesis, University of Glamorgan*, 1998.

[79] A. Sville. Vegetation attenuation: Modelling and measurements at millimetric frequencies. *10th International Conference on Antennas and Propagation*, (436):14–17, 1997.

[80] COST-235. Radiowave propagation effects on next generation fixed services terrestrial telecommunications systems. Final Report 92-827-8023-6, Commission of the European Union, 1996.

[81] A. Paulseen and A. Seville. Attenuation and distortion of millimeter radio wave propagation through vegetation. *Millennium conference on Antennas and Propagation (AP 2000)*, April 2000.

[82] R. Matschek and B. Linot. Model for wave propagation in presence of vegetation based on the utd associating transmitted and lateral waves. *National Conference on Antenna and Propagation*, (461), 1999.

[83] M. O. AL-Nuaimi and A. M. Hammoudeh. Measurements and predictions of attenuation and scatter of microwave signals by trees. *IEE Proceeding on Antennas and Propagation*, 141(2), 1994.

[84] D. Didascalou. Millimeter-wave scattering and penetration in isolated vegeta-

tion structures. *IEEE trans Geoscience and Remote Sensing*, 38(5), September 2000.

[85] R. Caldeirinha and M. Al-Nuaimi. Analysis of the re-radiation functions of single trees and idealised structures at 20ghz. *AP2000 Millennium Conference on Antennas and Propagation*, Pap. 460:11–15, April 2000.

[86] D. Dence and T. Tamir. Radio loss of lateral waves in forest environments. *Radio Science*, 4:307, 1969.

[87] G. P. S. Cavalcante, D. A. Rogers, and A. J. Giardola. Raido lost in forest using a model with four layer media. *Radio Science*, 18:691–695, 1983.

[88] S. S. Seker. Radio pulse transmission along mixed paths in a stratified forest. *IEEE Proc. Microwave, Antennas and Propagation*, 136:13–18, 1989.

[89] S. S. Seker. Vhf/uhf radiowave propagation through forests: Modeling and experimental observations. *Proceedings-H*, 139(1), Feburary 1992.

[90] G. P. S. Cavalcante, D. A. Rogers, and A. J. Giardola. Analysis of the electromagnetic wave propagation in multilayered media using dyadic green's function. *Radio Science*, 17:503–508, 1982.

[91] C. T. Tai. *Dyadi Green's Functions in Electromagnetic Theory.* IEEE Press, Piscataway, New Jersey, 2nd edition, 1994.

[92] Le-Wei Li, Jin-Hou Koh, Tat-Soon Yeo, Mook-Seng Leong, and Pang-Shyan Kooi. Analysis of radiowave propagation in four-layered anisotropic forest environment. *IEEE Transactions on Geoscience and Remote Sensing*, 37:1967–1979, July 1999.

[93] P. Delogne. *Leaky feeders and Subsurface Radio Communications.* Stevage, United Kingdom, 1982.

[94] P. Degauque. *Leaky Feeders and Subsurface Radio Communications.* IEE Electromagnetic Wave Series. Peregrinus Series, 1982., London, 1982.

[95] M. Lienard, S. Baranowski, and P. Degauque. Theoritical and experimental study of radio coverage in tunnels using radiated cables. *Annales Telecom.*, 49(3-4):143–153, March 1999.

[96] T. Klemenschits and E. Bonek;. Radio coverage of road tunnels at 900 and 1800 mhz by discrete antennas. *5th IEEE Intl. Symposium on Mobile Future*, 2(18-23):411–415, September 1994.

[97] Y. Yamaguchi, T. ABE, T. Sekiguchi, and J. Chiba. Attenuation constants of uhf radio waves in arhced tunnels. *IEEE Trans.*, MTT-33:714–718, 1985.

[98] S. F. Mahmoud and J. R. Wait. Geometrical optiacl approach for electromagnetic wave propagation in rectangular mine tunnels. *Radio Sci.*, 9:1147–1158, 1974.

[99] S. F. Mahmoud and J. R. Wait. Guided electromagnetic waves in a curved rectangular mine tunnel. *Radio Sci.*, 9:567–572, 1974.

[100] A. G. Emslie, R. L. Lagace, and P. F. Strong. Theory of propagation of uhf radio waves in coal mine tunnels. *IEEE Transaction Antennas Propagat.*, AP-23:192–205, 1975.

[101] V. A. Baranov and A. V. Popov. Adiabatic modes of curved em waveguides of arbitrary cross section. *Proc. 13th ACES*, pages 1036–1041, March 1997.

[102] A. V. Popov, V. A. Vinogradov, N. Y. Zhu, and F. M. Landstorfer. 3-d parabolic equation model of em wave propagation in tunnels. *Electronic Letters*, 35(11):880–882, 1999.

[103] J. Lee and H. Bertoni. Coupling at cross, t, and l junctions in tunnels and urban street canyons. *IEEE Transactions on Antennas and Propagation*, 15(5):926–935, 2003.

[104] C. Cerasoli. Rf propagation in tunnel environments. *IEEE Military Communication Conference*, 1:363–369, November 2004.

[105] J. S. Lamminmaki and J. J. A. Lempiainen. Radio propagation charaterstics in curved tunnels. *Inst. Elect. Eng. Proc. Microwave Antennas Propagation*, 145:327–331, 1998.

[106] P. Mariage, L. Leonard, and P. Degauque. Theoritical and experimental approach of the propagation of high frequency waves in road tunnels. *IEEE Transactions on Antennas and Propagation*, 42:75–81, 1994.

[107] M. Nilsson, J. Slettenmark, and C. Beckman. Wave propagation in a curved tunnel. *Proc. IEEE AP-S Intl. Symposium*, pages 1976–1979, 1998.

[108] M. Lienard and P. Degauque. Natural wave propagation in mine environments. *IEEE Trans. Antennas and Propagation*, 48:1326–1339, 2000.

[109] D. Didascalou, J. Maurer, and W. Wiesbeck. Subway tunnel guided electromagnetic wave propagation at mobile communications frequencies. *IEEE Transactions on Antennas and Propagation*, 49:1590–1595, 2001.

[110] Shen Zhang. Researches on the structure of coal mine underground integrated service digital network and the key technique of its wireless access. *CUMT, Xuzhou China*, 2001.

[111] Enjie Ding and Bingyu Li. Algorithm for calculating multi-path distances in rectangular tunnels. *IEEE*, 03, 2003.

[112] D. G. Dudley. Wireless propagation in circular tunnels. *IEEE Transactions on Antennas and Propagation*, 53(1):435–441, 2005.

[113] H-Y. Pao. Proability density function for total fields in a straight pec rough wall tunnel. *Microwave and Optical Tech. Letters*, 46(2):128–132, 2005.

[114] P. Deqauque, M. Lienard, and P. Laly:. Combining radar sensor and data transmission between vehicles in tunnels. *AICT-ICIW*, 19:83–83, Feburary 2006.

[115] F. J. Schaefer. 850 mhz measurements in the brookelyn/battery tunnel. *Proc. of the 35th IEEE Veh. Tech. Conf.*, pages 93–96, 1985.

[116] N. Noori, Safavi-Saeini, and H. Oraizi. A new three-dimensional vector parabolic equation approach for modeling radio wave propagation in tunnels. *IEEE Intl. Symposium on Antenna and Propagation*, 4B(3-8):314–317, July 2005.

[117] R. L. Courant. Variational methods for the solution of problems of equilibrium and vibration. *Bulletin of the American Mathematical Society*, 5:1–23, 1943.

[118] P. P. Silvester. Finite-element solution of homogenous waveguide problems. *Alta Frequenza*, 38:313–317, 1969.

[119] D. S. Burnett. *Finite Element Analysis.* Addison-Wesley, 1987.

[120] K. J. Binns, P. J. Lawrenson, and C. W. Trowbridge. *The Analytical and Numerical Solution of Electric and Magnetic Fields.* John Wiley, 1992.

[121] MSC/EMAS. *Finite Element Software available from MacNeal-Schwendler Corporation.* 9076 North Deerbrook Trail, Milwaukee, WI 53223-2434.

[122] MAXWELL. *Finite Element Software available from Ansoft Corporation.* 4516 Hnery Street, Pittsburgh, PA 15213.

[123] J. P. Webb. *Developments in a Finite Element Method for Three Dimensional Electromagnetic Problems.* PhD dissertation, University of Cambridge, 1981.

[124] G. L. Maile. *Three dimensional analysis of Electromagnetic problems by Finite Element Methods.* PhD dissertation, University of Cambridge, 1979.

[125] www.ath-it.edu/ persson/mesh.

[126] J. N. Reddy. *Introduction to the Finite Element Method.* Singapore: McGraw-Hill, Inc, 1993.

[127] J. Jin. The finite element method in electromagnetics. *John Wiley & Sons*, New York 2002.

[128] W. L. Flock. Propagation effects on satellite systems at frequencies below 10 ghz,. *A Handbook for Satellite System Design,Second edition, NASA Reference Publication*, 1108 (02), 1987.

[129] F. A. Katsriku, B. M. A. Rahman, and K. T. V. Grattan. Finite element analysis of second harmonic generation in algaas waveguides. *IEEE Journal of Quantum Electronics*, 36:282–289, 2000.

[130] D. E. Kerr. *Propagation of Short Radio Waves.* Los Altos, CA: Penisula Publishing, 1988.

[131] A. Holstad and I. Lie. Radar path loss computations over irregular terrain. Technical report, Storm Weather Center, June 2005.

[132] T. B. A. Senior and J. L. Volakis. *Approximate Boundary Conditions in Electromagnetics*, volume 41. Inst. Electrical Engineers, London, UK, 1995.

[133] J. Fang and Zhonghua Wu. Generalized perfectly matched layer for the absorption of propagating and evanescent waves in lossless and lossy media. *Microwave Theory and Techniques, IEEE Transactions on*, 44(1):2216–2222, December 1996.

[134] J. D. Jackson. *Classical Electrodynamics.* Wiley, New York, 1999.

[135] um-AREPS-30, http://sunspot.spawar.navy.mil. *Users Manual for Advanced Refractive Effects Prediction System*, 3 edition, August 2003.

[136] AREPS, TEMPER Similarities, and Differences. E. brookner. Technical report, The RAytheon Company, 2006.

[137] J. Deygout. Correction factor for multiple knife-edge diffraction. *IEEE Trans. Antennas Propagation*, 39:1256–1258, 1991.

[138] J. T. Hviid, J. Bach Anderson, J. Toftgård, and J. Bøger. Terrain-based

propagation model for rural area - an integral equation approach. *IEEE Trans. Anteena Propagat.*, 43:41–46, 1995.

[139] COST-231. Digital mobile radio: Cost 231 view on the evolution towards 3rd generation systems. *COST-231 TD(96)042-A*, 1996.

[140] M. L. Palud. Propagation modeling of vhf radio channel in forest environments. *MILCOM 2004 - IEEE Military Communication Conference*, 2004.

[141] Peter Holm and Asa Waern. Wave propagation over a forest edge, parabolic equation modelling vs gtd modelling. *IEEE Conference*, 03, 2003.

[142] D. A. Mcnamara, C. W. I. Pistorius, and J. A. G. Malherbe. Introduction to the uniform geometrical theory of diffraction. *Artech House, Norwood, MA*, 1990.

[143] S. A. Torrico, H. L. Bertoni, and R. H. Lang. Modeling tree effects on path loss in a residential environment,. *IEEE Trans. Antennas Propagation.*, 46:872–880, 1998.

[144] J. D. Parsons. *The Mobile Radio Propagation Channel.* Pentech, London, U.K., 1992.

[145] Public Safety Wireless Network Program. Public safety wireless network program. Technical report, In-Building/In-tunnel User Considerations, August 2002.

[146] R. Pattuelli and V. Zingarelli. Precision of the estimation of area coverage by planning tools in cellular systems. *IEEE Personal Communications*, 7(3):50–53, June 2000.

[147] Sun Jiping, Cheng Lingfei, and Liu Xiaoyang. Influence of electrical parameters on uhf radio propagation in tunnels. *10th Asia-Pacific Conference on Communications and 5th International Symposium on Multi-Dimensional Mobile Communications*, 2004.

[148] S. F. Mahoud and J. R. Wait. Guided electromagnetic waves in a curved rectangular tunnel. *Radio Science*, 9(5):567–572, 1974.

[149] V. M. Babic and V. S. Buldyrev. *Short-wavelength diffraction theory: Asymptotic methods.* Springer-Verlag, Berlin, 1991.

[150] A. V. Popov. Numerical solution of the wedge diffraction problem by the transversal diffusion method. *Sov. Physics Accoustics*, 15(2):226–233, 1969.

[151] A. A. Zaporozhets and M. F. Levy. Radar cross-section calculations with marching methods. *Electron. Lett.*, 34(20):1971–1972, 1998.

[152] A. A. Zaporozhets. Application of vector parabolic equation method to urban radiowave propagation problems. *Inst. Elect. Eng. Proc. Microwave Antenna Propagation*, 146(4):253–256, 1999.

[153] C. A. J. Fletcher. Computational technqiues for fluid dynamics. *Springer Ser. Computat. Phys.*, I, 1997.

[154] A. V. Popov and N. Y. Zhu. Modeling radio wave propagation in tunnels with a vectorial parabolic equation. *IEEE Transactions on Antennas and Propagation*, 48(9):1403–1412, 2000.

[155] http://goanna.cs.rmit.edu.au/research/compgeom/delaunay/delaunay.html.